PECVD OF SILICON AND TITANIUM BASED COATINGS TO ENHANCE THE BIOCOMPATIBILITY OF BLOOD CONTACTING BIOMEDICAL DEVICES

A THESIS FOR THE DEGREE OF DOCTOR OF PHILOSOPHY

Presented to

Dublin City University (DCU)

by

Ram Prasad Gandhiraman
B. Sc., M. Sc.,

School of Electronic Engineering
Dublin City University

Research Supervisors

Dr. Stephen Daniels and Prof. David Cameron

March 2007

DECLARATION

I hereby certify that this material, which I now submit for assessment on the programme of study leading to the award of Doctor of Philosophy is entirely my own work and has not been taken from the work of others save and to the extent that such work has been cited and acknowledged within the text of my work.

ID No.: 52143287

Signed: [signature]

Date: 30-04-2007

DEDICATED TO

PREFACE

The major portion of the work included in this thesis was completely carried out by me, however I wish to acknowledge the contribution of several collaborators.

The fibrinogen adsorption measurements, in chapter 5, were carried out in collaboration with Mr. Mohan Kumar, National Institute of Cellular Biotechnology, Dublin City University and Mr. Paul Barham, Archport Limited, Dublin City University.

The cell proliferation and cytotoxicity tests, in chapter 5, were solely carried out by Ms. Elizabeth Tully, School of Biotechnology, Dublin City University.

ABSTRACT

The clinical success of a surgical implantation depends on various factors including the design and biocompatibility of the biomaterial, surgical procedure adopted, injuries made during implantation and health and condition of the patient. The success of a biomaterial depends on the interaction and the progressive reaction between the blood components and the surface of the implant. Proteins present in the blood will be the first components to become adsorbed on the surface of the biomaterial. Studies show that the protein fibrinogen present in the blood plasma is the major initiator of inflammatory reactions and involved in blood clotting. By minimizing the fibrinogen adsorption it is possible to reduce the contribution of the biomaterial surface characteristics to thrombosis and inflammatory reactions.

In this work, silicon and titanium based thin film coatings with four different surface characteristics were deposited by PECVD on 316L stainless steel substrates. Polymer-like $SiO_xC_yH_z$, silica-like SiO_x, titanium oxide TiO_x and silicon-titanium mixed oxide coatings were deposited by plasma decomposition of organic molecules. An extensive study was done on silicon based coatings deposited from hexamethyl disiloxane (HMDSO) to analyze the influence of plasma process parameters like RF power, precursor flow ratio and flow rate on the surface chemical and mechanical characteristics of the film. Titanium dioxide coatings deposited from titanium tetraisopropoxide (TIP) were also analyzed for the effect of plasma process parameters on their surface characteristics. Silicon - titanium mixed oxide coatings were deposited to obtain intermediate characteristics between silicon oxide and titanium oxide films and the process was optimized to get a hydrophilic surface with wettability lower than SiO_x and a bandgap higher than that of titanium dioxide. It was concluded, from the fibrinogen adsorption studies, that both the film wettability and bandgap has to be optimized in order to minimize the fibrinogen adsorption.

ACKNOWLEDGEMENTS

I would like to express my heartfelt gratitude to Prof. David Cameron and Dr. Stephen Daniels, my academic supervisors. They both have always been very supportive and encouraging throughout the process of this accomplishment, with all their constructive remarks and good scientific discussions. It is a great pleasure to have worked with both of them.

My thanks are always there for my parents, brother and sister who keep providing me all the moral supports necessary for a successful career and a peaceful life.

Interdisciplinary research always involves efforts of specialists with different scientific backgrounds. The experimental works included in this thesis were carried out in various research centres and universities. I am indebted to my friends from various research centres and universities, who helped me to carry out some of the experimental work in their laboratories and for their fruitful discussions.

My sincere thanks to our technician Billy Roarty, who got involved in the project with lots of interest and help build the control box for mass flow controller. In addition to this, I would like to thank him for his assistance in maintenance of the deposition system.

At this stage, I would like to whole heartedly thank my friend Mohan Kumar, for all the collaborative assistance to carry out the fibrinogen adsorption measurement. My sincere thanks also go to Paul Barham, Archport ltd., for his help and advice to carry out the fibrinogen adsorption measurements.

I wish to thank Rahamath for her constant support to finish my writing up.

My sincere thanks to Gowri and Mari Tanttari for their help in carrying out EDAX analysis and other fruitful discussion.

The contact angle measurements were all carried out in the surface engineering laboratory in University College Dublin (UCD). I should thank Prof. Denis Dowling, Dr. Fergal O'Reilly and Dr. Paul Duggan for their support in doing the wettability and surface energy measurements.

I would like to thank Elizabeth Tully for her help in doing the cytotoxicity and cell proliferation studies

I would like to thank all my friends in Dublin including Arul, Prince, Ola, Chiara, Justina, Ahmed, Saman, Shekar, Ramesh, Jai, Sweta, kishore, Sundar, and Gomathi for their help in various ways during my stay in Dublin.

TABLE OF CONTENTS

LIST OF FIGURES

1. INTRODUCTION

1.1 Blood contacting biomedical devices

Man made metallic and polymeric materials are widely used in producing vascular prosthesis, artificial heart valves, stents and haemodialysis, where the human blood comes in direct contact with the surface of the implant. The clinical success of implantation depends on many factors like, the design of the implant, mechanical and biocompatible properties of the biomaterial, surgical procedure and the injuries made during the implantation, health and condition of the patient. The success of a biomaterial depends on the interaction and the progressive reaction between the blood components and the surface of the implant. Immune response of the body tends to defend against pathogens (infectious agents) and other foreign invasion to the host by responding immediately after the implantation process.

Two major problems associated with respect to biocompatible transplant devices are, triggering inflammatory reaction resulting in over growth of cells (mostly phagocytes which includes macrophages and neutrophils) on the implant surface and secondly blood clotting called thrombosis. In the case of arterial stents, the metallic foreign body and vascular injury activates circulating neutrophils and tissue macrophages resulting in a cascade of events leading to uncontrolled proliferation of smooth muscle cells called neointimal hyperplasia. The early interaction between transplant and inflammatory cells is mediated by the accumulation of host proteins on to the surface of materials [1,2]. Platelets present in the blood are passive and are circulating throughout the body. When the platelets are activated it triggers blood clotting by releasing different coagulation factors leading to haemostasis. In order to make the implantation a success, the immune system's natural defence against aliens has to be overcome. The biological system should no longer see the implant as an alien by not provoking the passive platelets.

Studies show that fibrinogen is the major initiator of inflammatory response and is involved in blood clotting through the activation of platelets resulting in thrombosis [3] and hence the fibrinogen adsorption has to be minimised to prevent platelet adhesion and activation.

1.2 Blood-biomaterial interaction

Human serum albumin, immunoglobulin and fibrinogen are the three major proteins present in the blood plasma. When a blood contacting biomedical device is implanted into the body, the proteins present in the blood plasma will come in contact with the implant. Then the proteins will get adsorbed immediately to the surface of the implant. Protein adsorption is the first thing that takes place after implantation. The cells will attach on the proteins on the implant surface [4,5].

The nature and composition of the first adsorbed protein layer is of major importance for the subsequent cellular response in blood or other tissues [6,7]. The protein adsorption process is complex involving complicated and dynamic processes such as (i) competitive adsorption, where proteins are sequentially exchanged over time and (ii) associative adsorption, where the adsorbed proteins favours the adsorption of other proteins in the blood [8,9]. Depending on the type, amount and the conformational state of the adsorbed proteins the platelet will be activated and then trigger inflammatory reaction and/or thrombosis through coagulation related cascades. Some surfaces may preferentially absorb albumin, whereas others will tie fibrinogen. The former may promote passivation of the implant surface while the latter may lead to thrombus accumulation [10-13]. Adsorbed fibrinogen proteins are known to promote excessive adhesion and activation of platelets, whereas preferential adsorption of albumin reduces platelet adhesion [14,15].

Adsorbed fibrinogen proteins undergo conformational changes after getting adsorbed on the implant surface. Fibrinogen conformational change takes place on hydrophobic surfaces, where the adsorbed fibrinogen takes up an extended conformation to facilitate exposure of its hydrophobic components, thus enabling more protein adsorption on hydrophobic surfaces [16,17]. The adsorption of proteins

on hydrophilic and hydrophobic surfaces depends on the nature of proteins. Some will get adsorbed on hydrophilic and some on hydrophobic surfaces [18-20]. However, fibrinogen is found to get adsorbed more on hydrophobic surfaces than on hydrophilic surfaces [21-23].

Biomaterial thrombogenicity is related to the denaturation of fibrinogen into fibrin monomers and fibrinopeptides. The denaturation depends on electron exchange from fibrinogen to the surface of the biomaterial [24-26]. Prevention of fibrinogen denaturation can improve the haemocompatibility of the implant [27-29].

Issues with blood contacting device surfaces

Endovascular coronary stenting is a proven technique to increase the luminal diameter beyond that achieved with balloon angioplasty and has reduced the restenosis rate to a significant extent [30-32]. Clinical experience suggests that the mechanisms of restenosis involve the combination of three components: vessel recoil and remodelling, thrombus formation, and neointimal hyperplasia [33-36]. Though the vessel recoil has been limited by mechanically stiff metallic stenting, the inherent thrombogenicity of the metallic stents leading to thrombus formation is still a problem.

The clinical outcome data showed that stainless steel stents are prone to occlusion due to sub-acute thrombosis and restenosis. Clinical studies with tantalum and nitinol stents also showed a similar behaviour, thrombotic closure and restenosis (re-narrowing of a blood vessel after it has been treated with stenting) are observed with all type of metallic stents [37-41] and hence a severe anticoagulation therapy is needed with bare metallic stenting to prevent thrombosis [42-44]. The use of anti-thrombogenic coatings on the metallic stents along with the anti-platelet therapy has decreased the sub-acute stent thrombosis to a significant extent [45-47], but late stent restenosis that occurs over a period of time through neointimal hyperplasia (thickening of the inner layer of the blood vessel through abnormal multiplication of cells, which could ultimately result in closing of the blood vessel) is still a major issue. There are many other factors that are not under the control of engineers and

scientists have to be taken into consideration. For example, there is a high probability to injure the blood vessel during deployment and hence the injured location is vulnerable to overgrowth of tissues [48,49]. The possibility for injuring the vessel wall during deployment, use of under sized stent, over expansion, stent design can all contribute to neointimal hyperplasia [50-52]. There are three major stent related factors influencing the neointimal hyperplasia, they are

(i) stent design,

(ii) stent material and

(iii) degree of vascular injury.

The factors corresponding to stent material that trigger neointimal hyperplastic response are thrombus formation, inflammatory reaction and smooth muscle cell proliferation [53,54]. Fibrinogen, the major protein involved in thrombosis (blood coagulation) is well known to promote excessive adhesion and activation of platelets when adsorbed and denatured onto a foreign surface [55-57]. The activated platelets in turn trigger inflammatory reaction and smooth muscle cell proliferation leading to neointimal hyperplasia. Studies suggest that stainless steel and all other metallic stents made of tantalum and cobalt-chromium have more affinity towards fibrinogen and promote excess binding of fibrinogen. Hence there is a need to modify the surface characteristics of metallic stents while retaining the bulk material characteristics.

Necessity of metallic implant materials

Stenting provides mechanical scaffolding to the artery to prevent vessel recoil associated with balloon angioplasty [58,59]. Stents are normally fabricated from stainless steel, cobalt-chromium, tantalum, nitinol etc. 316 L stainless steel is the most commonly used material for stent manufacturing. To determine the correct delineation of the edges of restenotic lesion, the radiopacity characteristic of the stent material is used. Metallic Stents are preferred to polymeric stents because of the competitive structural characteristics of the metallic stents with high radial hoop strength and radiopacity. Biocompatible coating on metal stents would provide the mechanical advantages of stenting, including reduction in early elastic recoil and the

elimination of unfavourable late remodelling, and at the same time provide antithrombogenicity and inhibit platelet activation [60,61].

1.3 Surface characteristics that contribute for fibrinogen adsorption

- **Surface energy - Wettability and surface hydrophobicity of the film**

  The surface hydrophobicity strongly influences the adsorption properties of human serum albumin (HSA), Immunoglobulin (IgG) and fibrinogen [62,63]. Surfaces of different wettability result in different biological responses [64,65]. Studies show that fibrinogen adsorption is higher in hydrophobic surfaces than on hydrophilic surfaces [66,67]. The hydrophobic component of the protein interacts with the hydrophobic surface through the hydrophobic interaction [68]. Fibrinogen takes up an extended conformation when it gets adsorbed on hydrophobic surfaces resulting in an irreversible structural change.

- **Energy band gap**

  Fibrinogen, the protein responsible for blood clotting, has an energy band gap of 1.8 eV. Denaturing of adsorbed fibrinogen, which causes thrombosis rely on the electron exchange from occupied valence band states of the fibrinogen to the surface of the stent [69,70]. Denaturing (decomposition) of fibrinogen causes inflammatory reactions and can be prevented if the charge transfer is inhibited. A surface with a band gap much higher than fibrinogen will inhibit the charge transfer [71-73].

- **Surface charge**

  Charge interactions also play a role in protein adsorption. Attraction or repulsion of the protein is dependent on the surface charge. At a pH of 7.2 – 7.3, human serum albumin (HSA) has a net negative charge of 4.7 to 5.3e and fibrinogen 5.5e. However, proteins are found to adsorb at surfaces of both

charge signs irrespective of the charge of the protein. If, for example, the hydrophobic interaction overcomes the electrostatic interaction then the surface charge effect is less significant. Yongli et al., suggested that electrostatic force was dominant in the case of fibrinogen binding on TiO_2 surface [74], Cai et al., suggested that the electrostatic interaction is a dominant force in deciding the protein binding [75]. However, Vinuesa et al., Wahlgren et al., Lassen and Malsmsten et al., have all demonstrated that a higher amount of albumin and fibrinogen adsorption took place irrespective of the repulsive electrostatic force [76-78] and they suggested that the electrostatic force only slowed down, rather than prevent, the adsorption kinetics, and hence the effect of surface charge is not taken into consideration in this study.

- **Surface roughness**

  Fibrinogen has a mass of 340 kD and an elongated shape with dimensions of 45 nm X 9 nm X 6 nm. Surfaces with roughness ranging in micrometers influence the fibrinogen adsorption to a significant extent due to the increase in surface area and the scale of roughness being larger the size of the protein [79]. Investigation on the influence of nano scale topography of titanium surfaces on fibrinogen adsorption has been studied by various groups and it has been reported that no statistically significant difference were found for films with different topographies [80,81]. Hasebe et al., demonstrated that nano order surface roughness <100nm has no effect on thrombogenicity [82]. However, Walivaara et al., studied the influence of nanometer scale surface roughness of titanium oxide coating on fibrinogen adsorption and proved that surface roughness greater than 5 nm do affect the fibrinogen adsorption [83]. Rechendorff et al., in their recent publication proved that surface roughness in nanometer scale increases the binding of strongly anisotropic proteins like fibrinogen since the anisotropic nature could lead to binding in different orientation [84].

1.4 Surface engineering by Plasma Enhanced Chemical Vapor Deposition (PECVD)

By manipulating (engineering) the surface of the implanted device the preferential absorption of fibrinogen can be controlled. Plasma-surface modification is an effective and economical surface treatment technique for many materials and of growing interest in biomedical engineering. The unique advantage of plasma modification is that surface properties and biocompatibility can be engineered selectively while bulk properties of the material remain unchanged. Plasma enhanced chemical vapour deposition (PECVD) has been used to produce thin layers of polymeric and inorganic coatings with properties completely different from those of conventional materials. This process, known conventionally as plasma polymerization, is a procedure in which gaseous polymers, stimulated through plasma, condense on a substrate as highly cross-linked layers.

In general, with a thrombo-resistant, non-inflammatory and biocompatible film which can serve as a base coating for a porous functional coating with the ability to hold the immunosuppressive drug and elute with slow release, it is possible to prevent late stent thrombosis, reduce the restenosis rate and hence increase the efficacy of the implant for long term clinical success of cardiovascular stents.

Thin films produced by PECVD tend to have advantages for biomedical applications:

- Modification of the surface can be achieved without altering the bulk characteristics of the substrate material
- Very precise control over the thickness from nanometre to micron range depending on the requirement
- Excellent control over the physical and chemical structure of the coating, and possibility to tailor the structure according to the needs by controlling the plasma process parameters
- Film characteristics like wettability, bandgap, refractive index, hardness, adhesion can all be tailored by carefully controlling the plasma and process parameters

- Ability to do layered coatings and in-situ surface preparation for enhanced adhesion
- Ability to have conformal coating on complex three dimensional substrates
- Coating can be applied in such a way that the chemical nature of the surface can be modified without affecting the overall surface topography

The biocompatible coating for cardiovascular device applications should have an excellent barrier property that prevents direct contact of the blood with thrombogenic stainless steel surface and also offer imperturbable surface characteristics in a harsh biological environment

1.5 Survey of stent coatings

The use of bare metallic stents has minimized the elastic recoil and geometric remodelling of the vessel wall and has reduced the restenosis rate to a significant extent when compared to balloon angioplasty [85,86]. But the acute and sub-acute thrombosis and neointimal hyperplasia remain a major problem associated with all types of metallic stents [37-41,87]. Severe anticoagulant and anti-platelet therapies had to be taken to alleniate the thrombotic issue [88-90].

To overcome the disadvantages of metallic stents, a number of materials were investigated and also surface engineering of metallic stents has been proposed [61,91-96]. Several polymeric coatings were also applied to metallic stents to study its effect on thrombogenicity and neointimal hyperplasia. However, polymer biocompatibility remains a concern, as polymers often induce an exaggerated inflammatory reaction [52,97,98].

Amorphous silicon carbide coating was used as an anti-thrombogenic coating on metallic stents [99,100]. Several studies have been carried out on these coatings, Özbek et al., and Kalnins et al., in their separate clinical studies showed that the silicon carbide coating decreased the stent thrombosis by a significant level and Kalnins observed that the silicon carbide coating attenuated the progression of

endothelial growth [101,102]. Hanekamp et al., and Unverdorben et al.,on the other hand, in their clinical studies observed that the silicon carbide coating was safe to use but did not have much beneficial effect on the restenosis rate [103,104]. Murphy et al.,[105] deployed polyethylene terephthalate (PET) polymeric stents percutaneously in porcine coronary arteries and found that the PET stents were associated with intense proliferative neointimal response that resulted in complete vessel occlusion. Alvarado et al.[106] implanted the metallic and silicone coated metallic stents in bile ducts and found no inflammatory reaction of silicone coated stent but mucosal hyperplasia was observed on both metallic and silicone coated stents. A decrease of 20-60% in luminal diameter was seen with all types at 24 weeks.

Gold, being a biocompatible material, the stainless stents were coated with gold to overcome the thrombogenicity of steel stents. Animal studies showed that gold coating can be beneficial to the performance of bare stainless steel stents [107,108]. However, the human clinical investigation yielded negative results showing increased restenosis rate with gold coated stents [109,110].

Giessen et al., used five different biodegradable polymers (polyglycolic acid/polylactic acid [PLGA], polycaprolactone [PCL], polyhydroxybutyrate valerate [PHBV], polyorthoester [POE], and polyethyleneoxide/polybutylene terephthalate [PEO/PBT]) and three non-biodegradable polymers (polyurethane [PUR], silicone [SIL], and polyethylene terephthalate [PET]) coated on metallic stents to study the inflammatory response after implantation and found that all the polymers induced a marked inflammatory reaction within the coronary artery [98]. Tim Fischell, investigated all the biodegradable and non-biodegradable polymers used by Giessen et al., [98] and found that all of the implanted polymer coatings were associated with a significant inflammatory and exaggerated neointimal proliferative response [93].

Geremia et al., implanted the silicone coated metallic stents in dog carotid arteries and found that the silicone coating led to thrombus aggregation and fibroproliferative tissue response [111]. Scheerder et al.,[112] deposited two different polymeric coatings on stainless steel stents and found that both the polymers induce neointimal

proliferation. In their study, a biodegradable poly (organo)phosphazene and biostable polyurethane coatings were deposited on metallic stents, and it was found that the degree of neointimal proliferation induced by polyurethane was comparable to that of bare metal stents whereas, the polyphosphazene coatings induced severe inflammatory response. Owing to its anticoagulant property and inhibitory effect on smooth muscle cell proliferation, heparin was considered for coating on metallic stents to reduce the complications of bare metallic stents [113-115]. Hårdhammar et al., showed that heparin coating of metal stents reduces the immediate effects of thrombotic events associated with their deployment in normal porcine coronary arteries [116]. Scheerder et al., in their animal study made clear that the heparin coating reduced thrombotic events but did not influence the neointimal hyperplasia [117]. Human clinical studies by Wohrle et al., on heparin coated stents suggested that the heparin coating did not have a significant impact on the longer term in-stent restenosis after 6 months and reasoned it to be the presence of low heparin activity on the stent [118]. Verweire et al., considered fluorinated polyphosphazenes and polymethacrylates for evaluation as coronary stent coating and observed that both the polymers induced a slight neointimal response [119].

Hyaluronic acid (HA) coating reduced platelet thrombus formation on stainless steel stents and improved the thrombo-resistance of endovascular devices [120]. Phosphorylcholine coating reduced the neointimal hyperplasia in canine carotid arteries [121]. Fischell and Fischell patented their invention of using phosphorylcholine coating as a anti-thrombogenic as well as radioactive coating on metallic intravascular stents [122]. Lewis et al., in their study showed that the phosphorylcholine coated metal stents implanted on porcine coronary arteries were biocompatible and did not cause inflammatory reaction by itself. Phosphorylcholine reduces irreversible protein adsorption at their surface and are effective at reducing the adhesion of platelets, fibroblasts and macrophages [123].

In-vitro biocompatibility tests showed that DLC coatings have higher albumin/fibrinogen ratio and hence lower platelet adhesion [124]. Clinical studies of carbon coated stainless steel stent carried out by Antoniucci et al., [125] showed that the carbon coating reduced the restenosis rate to a significant extent and the

proliferative response was non-significant resulting in a very high clinical success rate, but clinical results from Emin et al., showed that after implantation of carbon coated stent the C-reactive protein, fibrinogen and leukocyte concentrations increased but carbon coating did not affect this inflammatory reaction [126]. Maguire et al., deposited amorphous diamond-like carbon coatings with and without Si doping on metallic stents and guide wires, and observed that the Si doped coatings were less inflammatory with reduced platelet attachments than the undoped DLC coatings [127]. Polyphoshazene passive coating has decreased the restenosis rate significantly compared to other passive coatings [128].

1.6 Local drug delivery

To provide a high concentration of drugs at the site of vascular injury, the concept of local drug delivery was adopted so that the drug can be eluted from the implant after implantation. Drug eluting stents coated with anti-proliferative agents like rapamycin and paclitaxel have decreased the restenosis rate to a significant extent. The polymer matrix carrying the drug that is coated on the metallic stent, should be non-inflammatory and should not cause any consequences after all the drug has been eluted. The polymer toxicity results in enhanced neointimal hyperplasia. Therefore, the success of local drug delivery in cardiovascular implants depends on the biocompatibility of the polymer matrix. Attempts have been undertaken to investigate the drug elution potential of porous passive silicon-carbide coating [129,130]. By having a thrombo-resistant, non-inflammatory and biocompatible coating, which can serve as a base coating for a porous functional coating, it is possible to prevent late stent thrombosis, reduce the restenosis rate and hence increase the efficacy of the implant

1.7 Contribution of this thesis

The ideas and hypothesis

The ultimate goal of this work is to study how the surface chemistry and structure of silicon and titanium based coatings can be used to control the biological reactivity of the proteins with the surface. Polymer-like ($SiO_xC_yH_z$), silica-like (SiO_x), titanium dioxide (TiO_x) and silicon-titanium mixed oxide (SiO-TiO) coatings have been deposited by PECVD to get a range of surface properties. Previous works have shown that fibrinogen is the major protein involved in adhesion and activation of platelets leading to several biological cascades of events resulting in unwanted consequences. To minimise the fibrinogen adsorption on to a biomaterial surface it is essential to understand the factors that influence it. The major factors influencing the fibrinogen adsorption on to the biomaterial surface are film wettability, energy bandgap, surface charge and pH of the solution.

Earlier studies on fibrinogen adsorption onto a biomaterial surface suggest that hydrophobic surfaces adsorb more than hydrophilic surfaces [131]. Fibrinogen adsorption studies carried out on hydrophilic silica and hydrophobic methylated silica shows that the hydrophobic methylated silica adsorbs more than the hydrophilic silica [62]. A similar behaviour was observed on hydrophilic titanium dioxide and hydrophobic methylated titanium dioxide.

The optical bandgap of the surface with which the fibrinogen comes in contact influences the adsorption to a significant extent. The bandgap of fibrinogen is 1.8 eV. When the fibrinogen comes in contact with any biomaterial that has a bandgap closer to that of fibrinogen then charge transfer takes place between the biomaterial and fibrinogen resulting in adsorption of fibrinogen on the biomaterial surface. The fibrinogen adsorption on titanium dioxide with a bandgap of 3.2 eV had been minimised by doping tantalum into titanium dioxide thereby increasing the optical bandgap of the film [132]. Silicon carbide semiconductor films with a bandgap higher than that of fibrinogen showed good haemocompatibility and reduced the thrombus formation [133]. In conclusion, hydrophobic, conducting and low bandgap

surfaces adsorb more fibrinogen. The influence of surface roughness on the fibrinogen adsorption will also be investigated.

Hypothesis :-

Previous studies suggest that hydrophobic $SiO_xC_yH_z$ and low bandgap TiO_x surfaces adsorb higher amount of fibrinogen than that of hydrophilic and high bandgap surfaces. Inspite of its hydrophilicity the TiO_x surface adsorb more fibrinogen due to its low bandgap. SiO_x should exhibit low fibrinogen adsorption due to its high bandgap and moderate hydrophilicity. By having an intermediate bandgap, the influence of biomaterial bandgap on fibrinogen adsorption could be studied. Silicon-titanium mixed oxide coatings is hypothesised to have lower fibrinogen adsorption owing to its lower contact angle than SiO_x and higher bandgap than TiO_x.

1.8 The approach to implement the ideas and hypothesis

The objective of this work is to deposit a biocompatible coating, on 316L stainless steel, with a bandgap higher than that of fibrinogen and low contact angle to minimise the fibrinogen adsorption. To achieve the objective, the films with a range of water contact angle and optical bandgap are deposited. Films with varying surface characteristics, including wettability and bandgap are deposited by plasma enhanced chemical vapour deposition that enables the tailoring of film properties by controlling the plasma process parameters. The major requirements of the coatings are controlled surface characteristics and good mechanical properties.

The tailored surface characteristics and improved mechanical properties can only be obtained through proper understanding of the plasma process parameters that govern the film properties. The first step is to analyse the influence of process parameters such as RF power, operating pressure and precursor flow ratios on film characteristics. By knowing the influence of process parameters on the surface characteristics, the chemical structure can be controlled and modified according to the need through careful control over the process parameters. After gaining a

thorough understanding of the chemistry of the film, the film adhesion to medical grade stainless steel is analysed. Then the suitability of the film for autoclave and its stability in biological media was tested by immersing the samples in dulbecco's modified eagle medium (DMEM) media and also in acidic, basic and physiological pH solutions. The conformality of the coating on complex three dimensional substrates was also studied. Fibrinogen adsorption characteristics of the films are studied.

A very sophisticated method of altering the surface texture and chemistry that was used for this work was Plasma Enhanced Chemical Vapour Deposition [PECVD], the process that enhances and enables deposition of biocompatible chemical compounds under low substrate temperatures and high deposition rates on to bio-transplant devices [134,135]. Hexamethyldisiloxane (HMDSO) and titanium isopropoxide (TIP), organic precursors used in this work, had been widely used as monomers in plasma polymerization because of their high deposition rate and the ability to tailor the physical and chemical properties by controlling the process parameters [136-139]. Previous studies suggest that the HMDSO deposited films substantially improve the biomedical behaviour of the implants [140-142].

Work overview

a) To study the influence of process parameters on surface characteristics

b) To tailor the surface characteristics, by varying the process parameters, to achieve a wide range of surface properties

c) Optimise the process parameters to have a high band gap and moderate wettability film which will minimise fibrinogen adsorption

d) Improve the adhesion strength of the film to 316 L stainless steel and the film stability in biological media

e) Measure the surface roughness of the untreated and coated 316L stainless steel samples

f) Study the uniformity of the coating on complex three dimensional steel substrates

g) Test the preliminary biocompatible characteristics of the film – cell toxicity, growth and viability studies

h) Study the protein adsorption behaviour of the films with varying wettability and band gap

2 DESCRIPTION OF THE WORK

2.1 Plasma

Plasma is a partially ionized gas consisting of equal numbers of positive and negative charges, and a different number of un-ionized neutral molecules. A glow discharge is achieved by applying a potential between two electrodes in a gas. The electrons (or other charged particles) present in the gas, due to the background cosmic rays, are accelerated by the electric field between the electrodes. If the energy gained by the electron is sufficiently high, an inelastic collision with a gas atom may result in excitation or ionisation of the gas atom. If ionisation takes place, a second electron is released into the gas. Subsequently both electrons will be accelerated again, creating a condition known as gas breakdown.

2.1.1 Collisions in plasma

The four major inelastic processes that take place in a glow discharge are –ionization and recombination, excitation and relaxation [143]. Ionisation is the process in which a primary electron removes an electron from the atom, producing a positive ion and two electrons. The two electrons produced by the ionizing collisions will then be accelerated by the electric field resulting in further ionization that maintains the glow discharge. The minimum energy required to remove the most weakly bound electron from the atom is called the ionization potential. Recombination is the inverse of ionization wherein an electron coalesces with a positive ion to form a neutral atom. If the energy transfer during an electron collision with an atom is less than the ionization potential then the bound electron would jump to a higher energy level resulting in excitation. Relaxation is an inverse of excitation, the excited states are unstable and the electron configuration returns to stable lower energy states. The transition from higher energy state to lower energy state is accompanied by the emission of a photon of very specific energy corresponding to the difference in energy between the relevant quantum levels. The glow in the plasma is due to this emission of energy during the transition from higher to lower energy state.

Other types of inelastic collisions that take place in plasma are dissociation, electron attachment, ion-neutral collisions and metastable collision. The process of dissociation is the breaking apart of a molecule. An electron with energy higher than the bond strength of a molecule can dissociate it either resulting in ionized products or a free radicals without causing any ionisation. The products of dissociation are more reactive than the parent molecule and hence the dissociation results in an enhanced chemical activity. Electron attachment is the process in which the colliding electron may join the atom to form a negative ion. Ions and neutrals can collide with each other elastically or inelastically to either exchange charges or cause further ionization. Excited atoms with long lifetimes are known as metastable excited atoms. The probability of collisions involving excited atoms depends on the density and the lifetime of the excited atoms.

The applied electric field to generate plasma accelerates electrons and the electrons receive energy from the field resulting in heating up to extremely higher temperatures. The reason that the electrons are hotter than any other particles is that they absorb energy from the field but they cannot share it efficiently with the heavier particles. When a fast moving electron collides with a slow atom, only a very small part of the electron energy is transferred to the atom. This makes heat conduction from the electrons to the ions and neutrals very poor. The electrons stay hot and the ions and neutrals remain at roughly room temperature.

The mean thermal velocity of the particle is given by [144]

$$\bar{c} = \sqrt{\frac{8kT}{\pi m}}$$

Raising the temperature increases the velocities of the particles. The velocities depend on the mass, so at a given temperature lighter particles will move faster than heavier particles. In an RF glow discharge, the typical electron temperature varies from 1 to 3 eV (1 eV=11600 K) and the ion temperature is less than 0.05 eV (580 K). The electrons with higher temperature moves much faster than the ions.

Electrons are much lighter than the ions. The equation shows that the mass is inversely proportional to the velocity, since the electrons are lighter than the ions they move much faster than the ions. The combination of high temperature and low mass contributes for the high velocity of the electrons.

2.1.2 Debye Shielding

A fundamental characteristic of plasma is its ability to shield out an externally applied electric field. If an electric field is applied to the plasma by inserting two electrodes, the electrodes attract charge carriers of opposite charge and a cloud of electrons and ions will surround each electrode. For very cold plasma with no thermal motion of the charge carriers, the electric field of the electrodes would be totally shielded. No electric field would be present inside the plasma body. If the temperature is finite, some of the ions and electrons at the edge of the cloud could escape the attractive force of the electrode. In this case, some of the electric field will penetrate into the plasma. The region where the electric field penetrates the plasma is called a sheath. The thickness of a sheath is of the order of the Debye length λ_D given by the equation [145]

$$\lambda_D = \sqrt{\frac{\varepsilon_o k T_e}{n_e e^2}}$$

where, ε_o is the permittivity of free space, k is Boltzmann's constant, e is the electron charge, T_e is the electron temperature, n_e is the electron density.

The Debye length is an important parameter in processing plasmas since it describes behaviour of the plasma around the objects present in the plasma chamber.

Ions and electrons reaching the solid surface recombine and are lost from the plasma system. The current densities of electrons and ions to the substrate is given by

$$j_e = \frac{e n_e \overline{c_e}}{4}$$

$$j_i = \frac{en_i \bar{c}_i}{4}$$

Where j is the current density, n is the particle density and $\bar{c}$ is the average velocity.

Due to their smaller mass, the average velocity of electrons is much larger than that of the ions and hence $j_e >> j_i$. The substrate immediately starts to build up a negative charge and the plasma becomes positive charge in the vicinity of the surface.

An electric field that retards the electrons and accelerates the ions develops near the surface in such a way that the surface is at a negative self-bias relative to the plasma.

The plasma is therefore always at a positive potential relative to any surface in contact with it. Because of the Debye shielding effect, the potential developed between the surface and the plasma bulk is confined to a layer of thickness of several Debye lengths. This layer of positive space charge that exists around all surfaces in contact with the plasma is called the plasma sheath. The thickness of the plasma sheath is defined as the thickness of the region where the electron density is negligible and where the potential drop V_s occurs. Since the glow intensity depends on the number density and energy of the exciting electrons, the sheath surrounding any object in contact with the plasma looks comparatively dark due to the less electron density in the sheath.

2.1.3 Floating potential and powered electrode

The sheath potential is the electrical potential developed across the plasma sheath. Only electrons having sufficiently high thermal energy will penetrate through the sheath and reach the surface, which, being negative relative to the plasma tends to repel the electrons [146].

$$Vs = \frac{kT_e}{2e} \ln(\frac{\pi m_e}{2.3 m_i})$$

In the case of RF discharge, a floating substrate immersed in the discharge will also have a sheath and will be biased negatively with respect to the plasma. When the bias

develops on the floating substrate it will be subject to ion bombardment from the plasma. On the powered electrode, the voltage depends on the RF power source. The bias on the powered electrode will be the summation of self induced bias (similar to floating electrode) and the voltage determined by the RF source. This high biasing on the powered electrode can be a very influential parameter in determining the properties of the growing film since the ions are accelerated across the sheath to an energy which depends on the sheath potential.

2.2 Process adopted

Plasma enhanced chemical vapor deposition (PECVD) is a well known low temperature deposition technique widely used for surface modification of metals and polymers at low temperatures. In a PECVD process, the plasma is generated and controlled by ionizing a gas with a RF electromagnetic field of sufficient power, although dc and microwave fields have also been used. The primary role of the plasma is to break up the monomers and promote chemical reactions. Charged species (free electrons and ions) present in the chamber are accelerated by the electric field and collide with molecules of the source gases. In this way, the source gas molecules are excited to higher energy states, primarily by inelastic collisions with the energetic electrons, and dissociate into a variety of radicals, ions, atoms and more electrons. Since the energy required for excitation and dissociation is lower than that of ionization, the plasma will produce a large supply of excited and dissociated molecules and thus reactive radicals, even for a modest fraction of ionization. Radicals and atoms, generated in the plasma, travel to the growing film surface through a gas phase diffusion process. They are then adsorbed onto the surface and form chemical bonds at favorable sites to form an amorphous network. In order to ensure the high quality and the reproducibility of a given plasma process, many parameters must be controlled with care, such as the flow rate and ratio of the gas mixtures, the RF power and pressure.

The computer controlled CD 300 plasma system used for the deposition reported in this thesis consists of 1) vacuum chamber, 2) RF generator and automatic matching unit, 3) Rotary and mechanical booster pump, 4) Liquid precursor container, 5) MFCs and manifold

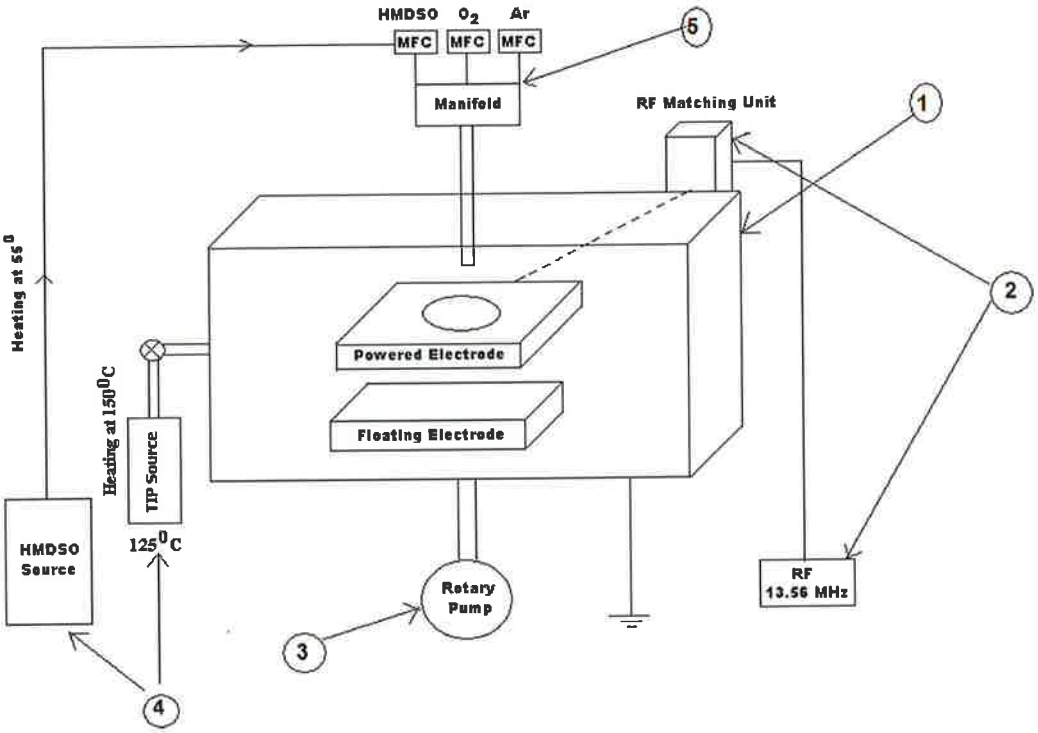

(a)

(b)

Figure 1 (a) Schematic diagram and (b) photograph of 13.56 MHz RF PECVD reactor

Figure 1(a) show the schematic diagram of the 13.56 MHz RF power driven capacitively coupled plasma device used for depositions in this work. The vacuum chamber was an aluminium based container. Edwards EH mechanical booster pump backed by an Edwards E1M40 rotary pump was used to pump down the chamber. The live (powered) electrode, hereafter named as powered electrode (PE) was separated from the ground chamber by ceramic spacers and a floating potential (FP) electrode was placed under the powered electrode. During the process, electrical energy from the RF generator was applied to the powered electrode, which in turn excited the gases present in the chamber to a plasma state. The RF generator was connected to the chamber through an automated matching box which was connected at the rear side of the chamber. The operating frequency of the RF generator was 13.56 MHz. The power distribution rack consisted of main switch, fuses, relays, electronic interfaces and boards. The PC rack contained the industrial computer and a printer. The measuring equipment consisted of MKS baratron type pirani gauge, thermocouple, process timer, flow meters. The pressure in the chamber was measured using a Granville-Phillips gauge. The real time clock of the computer was used to control the process. However manual mode of operation was also possible. The mass flow controllers (MFC) were used to control the flow of gases. Before each MFC, a shut off valve was installed to avoid leakage of any gas that was not used during the process. The rotary pump was connected through a port at the bottom of the chamber. The powered electrode whose area was 450 square centimetres, with a hole in the middle, was placed slightly below the top of the chamber and the chamber wall was grounded.

The precursors were hexamethyl disiloxane (HMDSO), titanium isopropoxide (TIP) and oxygen. The argon, oxygen and HMDSO supply to the chamber were through mass flow controllers connected to a manifold that was connected at the top of the chamber. Liquid HMDSO was stored in a container and connected to the MFC through stainless steel tubes. Liquid titanium isopropoxide was stored in a container and connected to the chamber through a needle valve attached to a side port of the chamber. As the vapour pressure of titanium isopropoxide was much lower 0.9 torr than that of HMDSO with a vapour pressure of 33 torr, the TIP source was heated at 125°C to increase the vapour pressure. To prevent condensation of HMDSO and TIP

in the pipelines, the stainless steel supply lines from source to manifold and chamber wall were heated at 55°C and 150°C respectively through a temperature controlled heating tape. The RF power varied from 50 to 450 W and the working pressure ranged from 80 mTorr for a oxygen to HMDSO ratio of 0:1 to 227 mTorr for a oxygen: HMDSO flow ratio of 15:1. The maximum temperature on the floating potential substrate holder was less than 55°C and that on the powered electrode was around 95°C with water cooling. A nitrogen purge line was connected to the MFC, which lets HMDSO into the system, enabling purging the MFC after deposition. The substrate holder was at the plasma floating potential. The films were also deposited on the powered electrode. Both the powered and the floating electrode were water cooled. A stainless steel plate was placed on the powered electrode to act as an alternative substrate holder.

Why 13.56 MHz?

It is very common for an excitation frequency of 13.56 MHz to be employed in plasma processing. This frequency, and some of its harmonics, are reserved for industrial, scientific and medical applications. While there is no underlying physical reason to prefer 13.56 MHz, the powerful influence of the economics of scale has made power supplies and matching networks more widely available at lower cost for this standard frequency. The various RF frequencies include relatively narrow bands centered at 125/134 kHz or low frequency (LF), 13.56 MHz and its harmonics or high frequency (HF), 433/869/915 MHz or ultra high frequency (UHF), and 2.45/5.8 GHz or micro-wave.

2.3 Plasma process parameters

2.3.1 Precursors

The precursors used were, silicon containing organic liquid hexamethyldisiloxane (HMDSO), titanium containing organic liquid titanium isopropoxide (TIP), and oxygen that was used as a reactive gas. HMDSO is a clear colourless organic liquid with a chemical formula of $(CH_3)_3$- Si-O-Si-$(CH_3)_3$., vapor pressure of 33 torr at 20°C and with a boiling point of 101°C at 760 torr (1 atm)

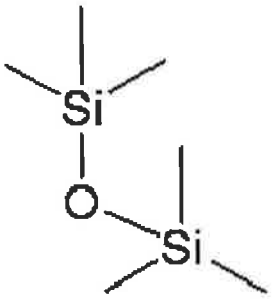

HMDSO

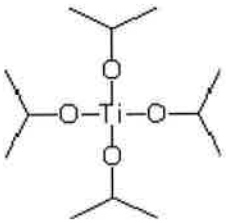

TIP

TIP is a clear pale yellow organic liquid with a molecular formula of $TiC_{12}H_{28}O_4$, vapour pressure of 0.9 torr at 50°C and with a boiling point of 58°C at 1 Torr

Since the methyl groups were predominant, oxygen had to be used to oxidise and remove the hydrocarbons from the film if an oxide coating had to be deposited. Both the precursors had oxygen in them, but using the precursors as such to create a plasma without any extra oxygen would give a SiO_x or TiO_x surface but with a significant amount of undissociated methyl groups present in the film. Hence the oxygen flow had to be controlled and optimised to get the required surface chemistry.

2.3.2 Substrates

316L (medical grade) stainless steel was used as the substrate material. For FTIR, ellipsometry and density measurements, single side polished Si wafer supplied by Wafer world Inc., was used. In ellipsometry measurements, a good match between the experimental data and the theoretical model could be obtained when silicon wafer with a known, fixed refractive index is used as the substrate material. Quartz substrate was used for measuring the bandgap through UV-Visible spectroscopy, since glass slides have the adsorption edge close to that of titanium dioxide, quartz was used. For adhesion strength measurement, stability in biological media, cell culture and fibrinogen adsorption tests 316L stainless steel substrates from Goodfellows were used.

2.3.3 Process parameters

The Objective was achieved by

a) Studying the effect of process parameters on surface characteristics of the film

b) Tailoring the surface characteristics, by varying the process parameters, to achieve a wide range of surface properties

The process parameters considered are

i) Oxygen to HMDSO to TIP flow ratio

In HMDSO, each silicon atom was bonded to three methyl groups and two silicon atoms were bonded to one oxygen atom. In the case of titanium isopropoxide with a molecular formula of $[(CH_3)_2CHO]_4Ti$, each titanium atom was bonded to four oxygen atoms and each of those oxygen atoms were again bonded to 3 methyl groups. Hence the amount of hydrocarbons in the precursor was significantly higher than the amount of oxygen in it. In order to get an oxide film, either silicon oxide or titanium oxide, from these precursors, there had to be an additional oxygen flow into the chamber for oxidising the hydrocarbon contents from the precursor and hence an external oxygen flow was maintained to reduce the amount of hydrocarbon content in the film. In order to get a right proportion of silicon, titanium, oxygen and hydrocarbon content in the film, the oxygen to HMDSO, oxygen to TIP and oxygen to HMDSO to TIP flow ratios had to be optimised.

The oxygen to HMDSO flow ratio was varied from 0:1 to 33:1 at a fixed RF power of 250 W. The titanium isopropoxide flow was kept as an unknown constant (n) and the oxygen to TIP flow ratio was varied from 250: n up to 1000: n, where the TIP flow was fixed through a needle valve.

ii) RF Power

The RF power plays a significant role in PECVD. The fragmentation of precursor molecules depends on the nature of the plasma, which in turn depends on the RF power. As the RF power is increased, the amount of energy supplied to the plasma increases and hence the fragmentation increase with increase in RF power. To study the influence of RF power on the film characteristics, the oxygen to HMDSO flow ratio was fixed at 10:1 (250 sccm: 25 sccm) and the RF power varied from 50 W to 450 W. In the case of Ti based coatings, the oxygen to TIP ratio was fixed at 500:n, where n is a fixed unknown TIP flow and the RF power was varied.

iii) Pressure, oxygen to HMDSO flow rate

In the case of Si based coatings from HMDSO, the oxygen to HMDSO flow ratio was varied, see table 1. For each of these ratios the coating process was performed at two different flow rates and hence the influence of flow rate at a fixed gas ratio was analysed.

	Pure HMDSO	**Oxygen:HMDSO flow ratio**					
		1:1	**2:1**	**5:1**	**10:1**	**15:1**	**20:1**
High flow rate	200 sccm	200 :200	300 :150	500 : 100	500 : 50	480 : 32	500:15
(Pressure)	94 mT	148 mT	244 mT	261 mT	241 mT	218 mT	227 mT
Low flow rate	50 sccm	50 : 50	50 : 25	125 : 25	250 : 25	225 : 15	
(Pressure)	58 mT	78 mT	12 mT	120 mT	124 mT	119 mT	

Table 1. Oxygen to HMDSO flow ratio, flow rate and pressure at 250 W RF

iv) Deposition on floating potential and powered electrode

The CD 300 PECVD system enables the substrate to be placed on both floating potential (FP) and powered electrode (PE), so that films can be grown at floating potential and powered electrode at the same time. It is well known that the ion bombardment will be significantly higher on the powered electrode than the floating electrode because of the negative bias voltage on the powered electrode that attracts high energetic positive ions. This high energy ion bombardment will have an impact on the characteristics of the film. Hence it will be interesting to study the difference in characteristics of films grown on floating potential electrode and on powered electrode. More over, the powered electrode being driven by RF power gets to a higher temperature than the floating potential electrode. This observed difference in temperature will have an effect on the characteristics of the film.

v) Plasma pre-treatment

The adhesion strength of the film to 316L stainless steel depends on the surface finish of the stainless steel. Cleaning the stainless steel substrates with acetone and ethanol was necessary to remove dusts and debris from the stainless steel surface. Studies suggest that plasma pre-treatment ie., plasma cleaning the samples in the chamber just before the deposition process, increases the adhesion strength of PECVD deposited films. It was observed that plasma pre-treatment increased the adhesion strength of SiO_x film significantly. Hence a more systematic way of plasma pre-treatment was necessary to optimise the plasma pre-treatment procedure. Argon and oxygen plasmas were used for plasma pre-treatment. Various aspects of plasma pre-treatment, listed below, were optimised in order to improve the adhesion strength.

a) Effect of pre-treatment time at fixed RF power and pre-treatment gas on the adhesion strength of the film to steel substrate

b) Effect of Argon plasma, Oxygen plasma, Argon & Oxygen mixture plasma on the adhesion strength at a fixed RF power

c) Effect of pre-treatment RF power on the adhesion strength for a fixed pre-treatment plasma

2.4 Characterization techniques

The influence of plasma process parameters on the surface characteristics of the films were investigated by studying their effect on physical and chemical characteristics of the coating. Several characterization techniques were employed to analyse the surface characteristics of the film. The purpose of understanding the variation of the above mentioned properties with process parameters was to deposit films with a range of surface characteristics that can be tailored according to the need. Since both the precursors containing silicon and titanium are organic liquids containing large amounts of hydrocarbons in it, the hydrocarbon, silicon, titanium and oxygen contents in the film can only be tailored through a thorough understanding of the effect of the process parameters on the nature of film being deposited. The hydrocarbon contents in the film can be controlled through a precise control of oxygen content in the plasma. It is important for the wetted surfaces that are exposed to body fluids, such as blood, to inhibit cell adhesion and growth as much as possible to minimise the possibility of clotting. Therefore it is necessary to tailor the surface energy to inhibit the protein adsorption. The surface energy depends on the wettability of the film, which in turn depends on the amount of hydrocarbon contents in the film [147]. The hydrocarbon contents can influence the hardness of the film to a significant extent.

The adhesion of the film to the stainless steel substrate is very crucial. The stent is inserted in to the artery by compressing it and then deployed at the right place by expanding it using a balloon. The adhesion should be high enough so that the film do not peel or crack during expansion. The exposure of even a small area of 316L stainless steel to the blood could lead to blood coagulation that could be fatal; hence the adhesion strength of the film to the implant grade stainless steel and its stability should be high enough. Table 2 lists the techniques and equipments used to characterise the coatings.

Characterisation	Technique	Equipment	Research centres
Film thickness, Refractive index	Spectroscopic Ellipsometry	J.A. Woollam Co., Inc M-2000UI spectroscopic ellipsometer	Nanomaterials processing lab (NPL), Dublin city university
Chemical structure	Fourier transform infrared spectroscopy (FTIR)	Perkin-Elmer Spectrum GX FTIR system	Nanomaterials processing lab (NPL), Dublin city university
Elemental analysis	Energy dispersive analysis by X-ray spectroscopy	EDAX Genesis system, Noran System Six microanalysis system with a 10mm^2 Si(Li) detector	ASTRaL, Lappeenranta university of Technology, Finland Institute for Molecules and Materials, Radbound university nijmegen, Netherlands
Nano hardness	Nano indentation	Berkovitch nano-indenter	National centre for biomedical engineering science (NCBES), National university of Ireland, Galway, Ireland
Wettability	Contact angle analysis	Data Physics OCA 20 video based analyzer.	Surface engineering group, University college dublin, Ireland
Optical bandgap	UV-Vis spectroscopy	Perkin-Elmer Lambda 40 UV-Vis Spectrometer	Nanomaterials processing lab (NPL), Dublin city university
Adhesion strength	Pull off adhesion tester	Quad Group Sebasian Five pull-off tester	Nanomaterials processing lab (NPL), Dublin city university
Roughness	Atomic force microscopy (AFM)	Veecos Dimension D3100 with Nanoscope III electronic control	National centre for sensors research (NCSR), Dublin city university

Conformality, Cell adhesion	Scanning electron microscopy	JOEL JSM-6301F scanning microscope	National centre for plasma science and technology (NCPST), Dublin city university
Film stability	Optical microscopy, Scanning electron microscopy,	Zeiss optical microscope	Nanomaterials processing lab (NPL), Dublin city university
Cell proliferation, cytotoxicity	MTT assay, trypan blue staining		School of Biotechnology, Dublin city university
Protein adsorption	Enzyme Immunosorbent Assay		National institute of cellular biotechnology (NICB), Dublin city university

Table 2 Characterisation techniques, the equipments used and the make

2.5 Enzyme immunosorbent assay (EIA) procedure

Materials required

1) 6 Well plates
2) 25 ml Universal tubes
3) Human fibrinogen (antigen)
4) Anti-fibrinogen antibody from goat (primary antibody)
5) Anti-goat Secondary antibody conjugated with peroxidase
6) 1% Gelatin (blocking solution)
7) 3,3,5,5 Tetramethylbenzidine (TMB) substrate to react with peroxidise enzyme
8) 1N H_2SO_4 to stop TMB and peroxidise reaction
9) Spectrophotometer
10) Table top shaker
11) Pipettes
12) Microbalance
13) Cuvettes

Fibrinogen binding studies method.

1. Uncoated 316L stainless steel, and coated stainless steel samples were placed into the plate wells.
2. 2ml of the fibrinogen @ 100mg/ml was added to the test samples. The uncoated steel was used to make a calibration series 100, 75, 50 25, 12.5 ng/ml. The controls and samples were incubated for 60 minutes at room temperature with gentle agitation.

   The test sample dose was the same as the top calibration standard

   During the sample incubation fibrinogen can:

   a. Remain in solution.
   b. Bind to the plate plastic.
   c. Bind to the 316 steel.
   d. Bind to the coating.
3. At the end of the sample incubation, a blocking solution 10ml consisting of 1% gelatin in Phosphate Buffered Saline (PBS) was added to the fibrinogen coating solution. The blocking solution was incubated for a further 60 minutes, RT, gentle agitation. Note that the four conditions (a-d) above are also true for the gelatin-blocking step.

   The blocking step was used because the molecular size of IgG (150kDa) was less than for Fibrinogen (300kDa). The gelatin blocks non-specific binding of IgG to the steel or coating based on differences in molecular size.
4. After the blocking step the fibrinogen/gelatin/PBS solution was removed from the wells, and the controls and samples were subjected to three five minute washes in PBS incorporating 0.05% Tween 20 (PBST). These washes reduced the amount of non-specifically bound material by a combination of the detergent action and dilution.
5. The metal was transferred to new plate for the next step. At this step, fibrinogen at a & b above i.e. still in solution or bound to the plate were then removed from the equation. Goat anti-fibrinogen antiserum was used. The antiserum was diluted with 1% gelatin in PBST, this diluent minimised non-specific binding. The anti-fibrinogen IgG could theoretically:

   a. Remain in solution.

b. Bind to the plate wells, or
c. Affinity bind to fibrinogen immobilised on either the 316-grade metal or the coating.

The antiserum incubation was performed for 60 minutes at room temperature with gentle shaking. At the end of the antiserum incubation period the solution was removed, and the samples were washed three times, 5 minutes per wash with PBST.

6. The samples were moved to new clean plates, anti-fibrinogen IgG according to 5a & b were now irrelevant. Rabbit anti-goat IgG horseradish peroxidase (HRP) conjugate was prepared in 1% gelatin PBST. This was added to the samples, which were incubated for 30 minutes at room temperature with shaking. At the end of the conjugate incubation period, the samples were washed three times, five minutes per wash with PBST, then a final five-minute wash with PBST.
7. The samples were transferred to sterile 30ml universal tubes, the TMB substrate was added for a fixed period of 10 minutes. Adding an equal volume of 1N acid stopped the reaction.
8. The yellow reaction solution was transferred to plastic cuvettes, and a spectrophotometer was used to measure the absorbance at a wavelength of 450nm.
9. A standard plot was drawn for fibrinogen adsorption of 316 steel substrates with various fibrinogen concentrations. The values for the coated samples were read from this curve. The results were reported in terms of % binding i.e. If a SiO_x coated piece of steel gave the same absorbance as the 25ng/ml calibration standard, it was reported that fibrinogen binding had been reduced and the percentage binding was 25% relative to plain 316L stainless steel substrate.

The peroxidase enzyme present in the secondary antibody would give a coloured reaction after its exposure to tetramethylbenzidine (TMB). The reaction could be stopped by adding 1N sulphuric acid. The purpose of peroxidase conjugation in the secondary antibody was to give a coloured reaction after its reaction with tetramethylbenzidine which is proportional to

the primary antibody bound to fibrinogen. The reason for conjugating the peroxidase enzyme on the secondary antibody rather than directly conjugating on the primary antibody is that the sensitivity will be increased in the former, resulting in signal amplification, since the primary antibody contains several epitopes that can be bound by the labeled secondary antibody. A schematic of the entire fibrinogen adsorption measurement process is given below

Step 1: Place samples in 6 well plate

Step 2: Antigen (Fibrinogen) binding

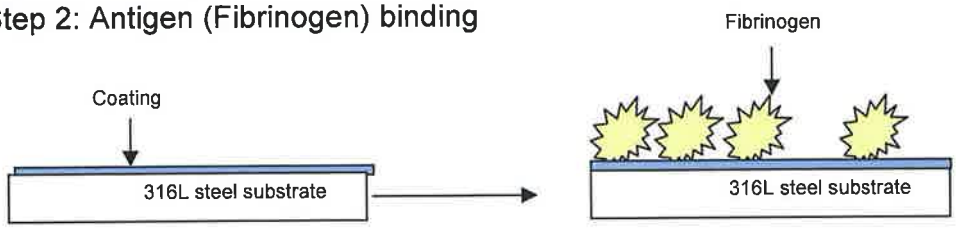

Step 3: Blocking

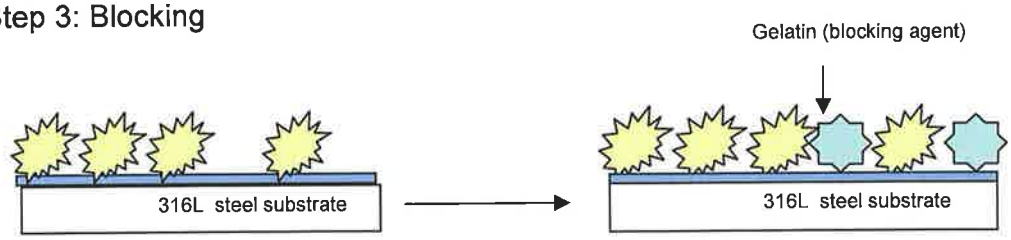

Step 4: Washing with PBS

Step 5: Transfer samples to new plate

Step 6: Anti-fibrinogen anti serum

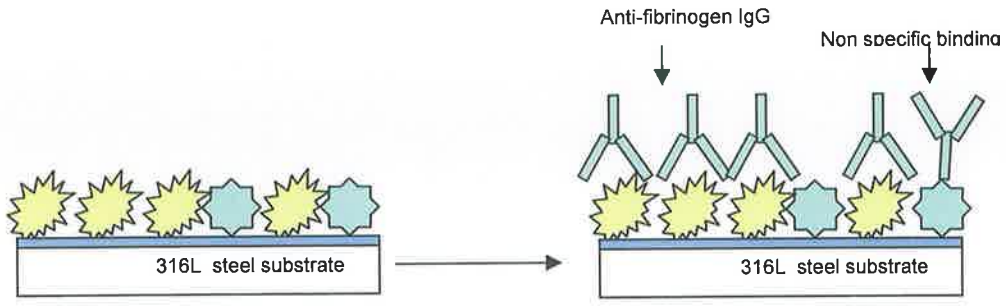

Step 7: Transfer samples to new plate

Step 8: Washing with PBS – Removes non specific binding of primary antibody

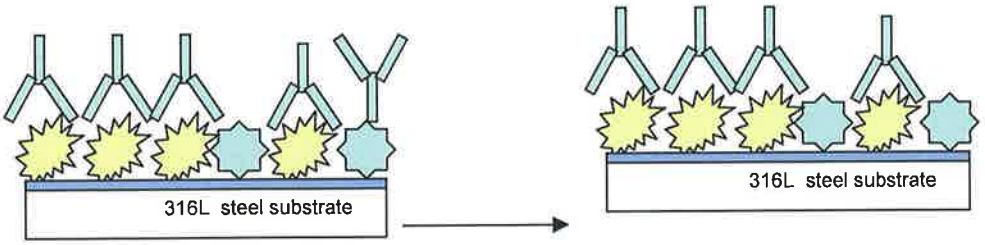

Step 9: Secondary antibody

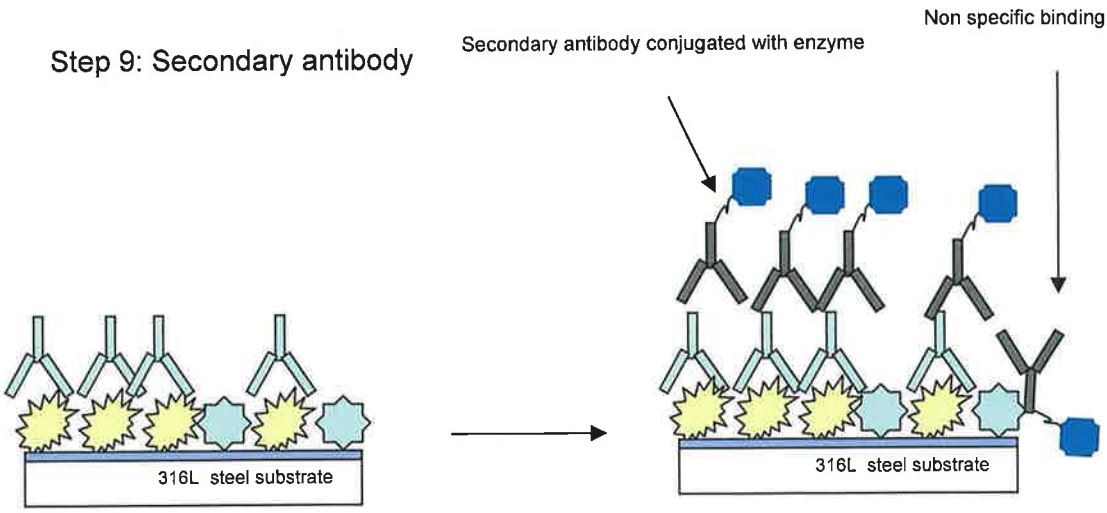

Step 10: Washing with PBS – Removes non specific binding of secondary antibody

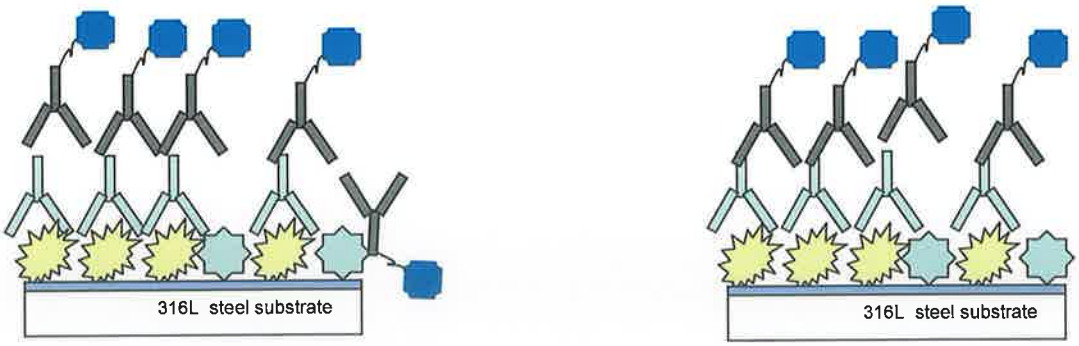

Step 11: Transfer of sample to 25ml universal tube

Step 12: Tetramethyl benzidine (TMB) addition to react with conjugated enzyme

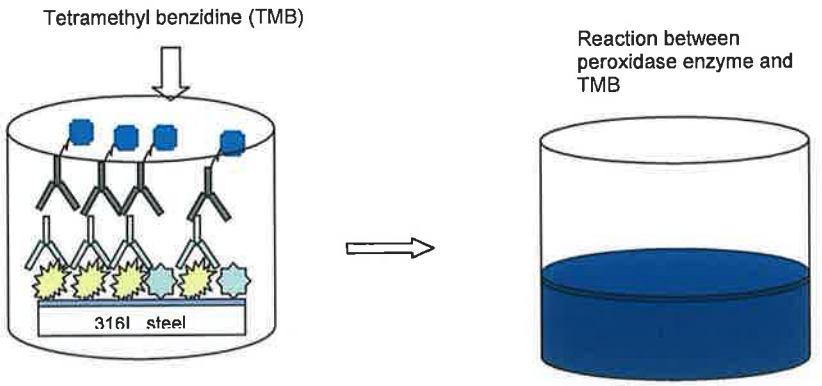

Step 13: H_2SO_4 to stop reaction after 10

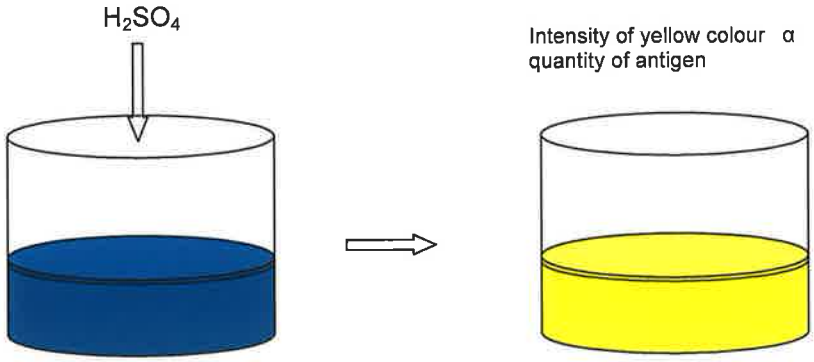

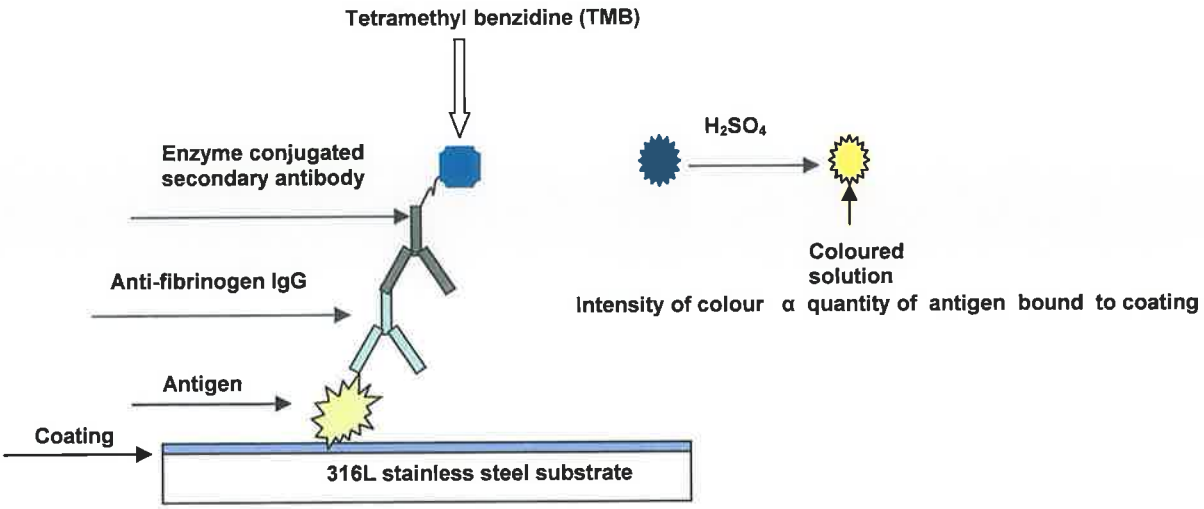

Figure 2 Schematic of overall fibrinogen adsorption procedure

3. SURFACE CHEMICAL AND PHYSICAL CHARACTERIZATION

3.1 Characterization of HMDSO based coatings

The influence of different operating plasma process conditions such as ratios of gas mixtures, different flow rates at fixed ratio and the operating RF power on the film quality had been investigated. The gas flow was varied by introducing different combinations of oxygen to HMDSO flow ratios in the processing chamber ranging from 0:1 to 33:1. The RF power to create the discharge was varied from 50 Watts to a maximum of 450 Watts and the substrate was placed on both floating and powered electrode to study the variation in properties of films deposited on both the electrodes. A detailed analysis of chemical and mechanical characteristics of films grown on floating and powered electrode was carried out. To investigate the influence of flow ratio and flow rates on film properties, the deposition was carried out for a series of oxygen: HMDSO flow ratio conditions and at two different flow rates (low and high) with a fixed RF power of 250 W. To analyse the effect of RF power, the oxygen: HMDSO flow ratio was fixed at 10:1 (250:25) and deposition was carried out at various RF powers from 50 W till 450 W. The operating conditions are tabulated in Table 1.

3.1.1 FTIR studies of films deposited at different oxygen:HMDSO flow ratio, flow rate and RF power

The absorption bands were identified based on the book by Socrates [148]. The characteristic peaks of Si-O-Si appear at 450 cm^{-1}, 800 cm^{-1} and 1070 cm^{-1}. The peak at 450 cm^{-1} corresponds to rocking vibration or symmetric stretching vibration of Si-O-Si and the peak at 800 cm^{-1} corresponds to bending vibration of Si-O-Si and 1070 cm^{-1} peak corresponds to asymmetric stretching vibration of Si-O-Si. The peak at 1278 cm^{-1} corresponds to symmetric deformation vibration of methyl silyl, asymmetric stretching vibration of CH in $Si-CH_3$ occurs at 2960 cm^{-1} and symmetric

stretching vibration of CH in $Si-CH_3$ occurs at 2905 cm^{-1}, $Si-CH_3$ rocking vibration occurs at 840 cm^{-1} [149-151]. Peaks at 930 cm^{-1}, 3380 cm^{-1} and 3650 cm^{-1} corresponds to hydroxyl groups bonded to Si [152,153]. SiC stretching vibration occurs at 668 cm^{-1} and 800 cm^{-1}. The peak at 801 cm^{-1} corresponds to Si-C and $Si-(CH_3)_X$ vibrations.

At low oxygen to HMDSO ratios, the methyl silyl peaks at 845 cm^{-1}, 1278 cm^{-1} and 2965 cm^{-1} [154] in figures 3, 4, 5 & 6 are intense. This confirms the formation of a polymer-like $SiO_xC_yH_z$ film. As the oxygen to HMDSO ratio increases, the intensity of the methyl silyl peaks decreases and it is negligible at oxygen to HMDSO ratio of 10:1. This is because, as the oxygen flow was increased, the methyl group present in HMDSO was oxidized to carbon dioxide and water. At low oxygen flows, the peak corresponding to Si-O-Si appears at 1040 cm^{-1} and as the oxygen flow increases, the peak shifts to higher wave number approaching 1072 cm^{-1} which is characteristic of silica-like films. This is because, at low oxygen to HMDSO flow ratios in polymer-like film, the film density was 1.599 $g.cm^{-3}$ (figure 10) and hence the Si-O-Si bond was not dense enough that resulted in vibration at low energy (low wave number) incident radiation. At high oxygen to HMDSO flow ratio, the film density was 2.309 $g.cm^{-3}$ (figure 10) and hence the Si-O-Si bond in silica-like film was dense with short bond length requiring higher energy (higher wave number) incident radiation for vibration. At high oxygen: HMDSO flow ratios, a silica-like SiO_x film were formed. As the oxygen flow increased, the peak corresponding to Si-OH appeared between 890 cm^{-1} and 910 cm^{-1} in figures 3 & 4, only in films deposited at floating potential. This is because of the formation of SiOH hydroxyl group from the oxidized methyl group. The temperature being low enough, maximum temperature was less than 55°C; the hydroxyl bond formation took place only in floating potential deposited films. The maximum temperature observed on the powered electrode was around 95°C and hence the Si-OH bond formations did not take place in powered electrode.

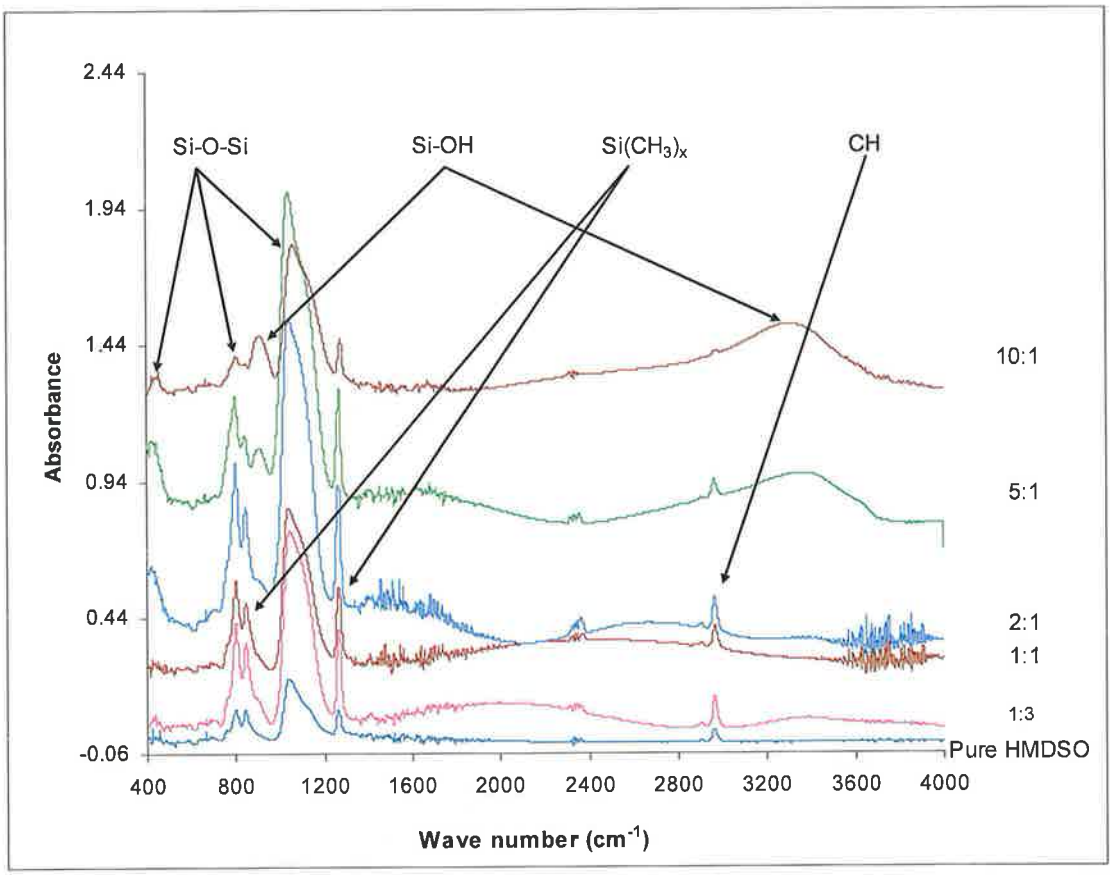

Figure 3 Variation of hydrocarbon content with oxygen to HMDSO flow ratio at high flow rate for films deposited on floating electrode at 250 W RF power

The SiOH peak appeared at lower wave number 890 cm^{-1} for high flow rate films and for low flow rate films, the SiOH peak appeared at 910 cm^{-1}. This shift was due to the formation of a strong SiOH linkage at low pressure resulting in higher energy for vibration.

Unlike the high oxygen to HMDSO flow rate films, the hydrocarbon content for low oxygen to HMDSO flow rate films (fig 4 and fig 6) decreased to a significant extent as the oxygen flow was increased. This is because; at low pressure, more fragmentation of the precursor molecules took place which lead to formation of more ions and radicals. Those fragmented hydrocarbons from precursor molecules got oxidized to water and carbon dioxide, which were driven away from the chamber, and hence the film contained fewer hydrocarbons even for low oxygen to HMDSO

flow ratio. In figures 5 and 6, for 5:1 ratio films, the methyl silyl peaks at 1278 cm^{-1} and 840 cm^{-1} were present in significant quantity for high flow rate films than that for low flow rate films. In floating electrode deposited films (fig 3 and fig 4) the hydroxyl peak (910 cm^{-1}) increased with increase in oxygen, due to the oxidation. Si from $(CH_3)_3$-Si-O-Si-$(CH_3)_3$ formed Si-OH as the oxygen flow increased.

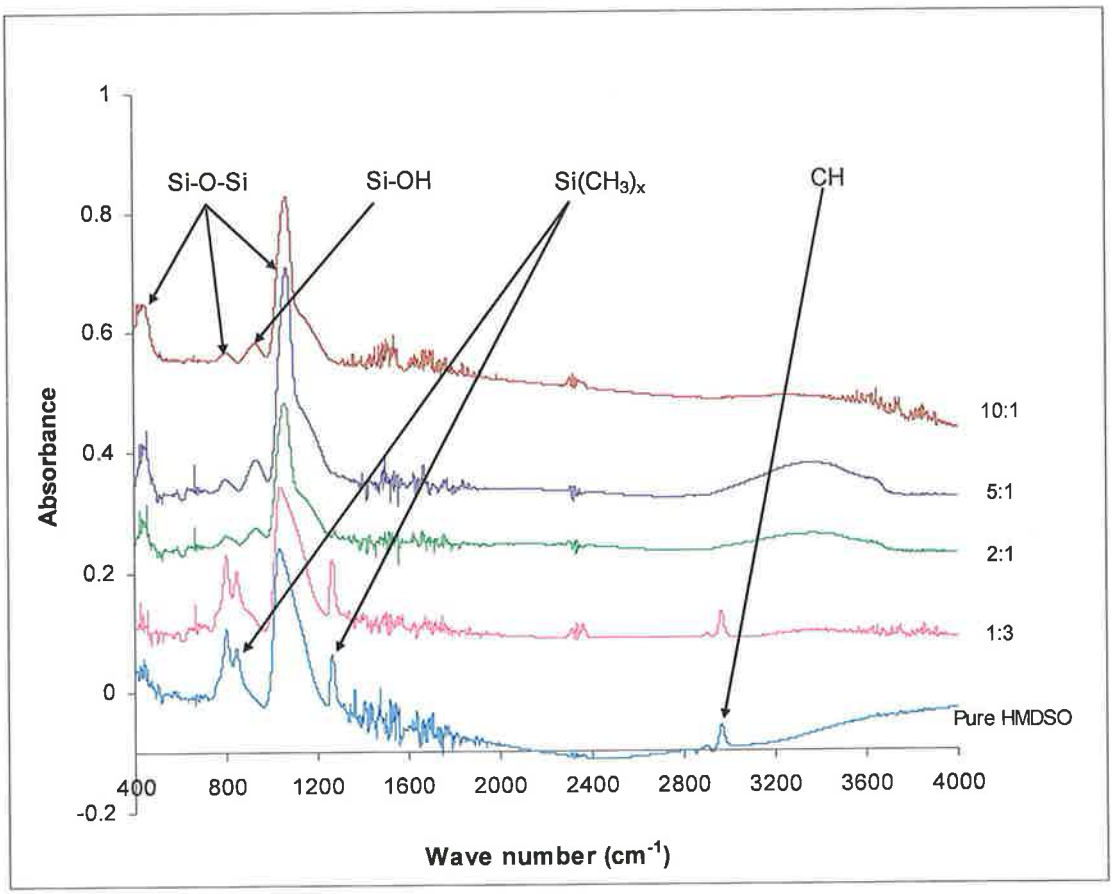

Figure 4 Variation of hydrocarbon content with oxygen to HMDSO flow ratio at low flow rate for films deposited on floating electrode at 250 W RF power

Same changes were observed for films deposited on the powered electrode (fig 5 and fig 6) but the hydroxyl group intensity was much lower.

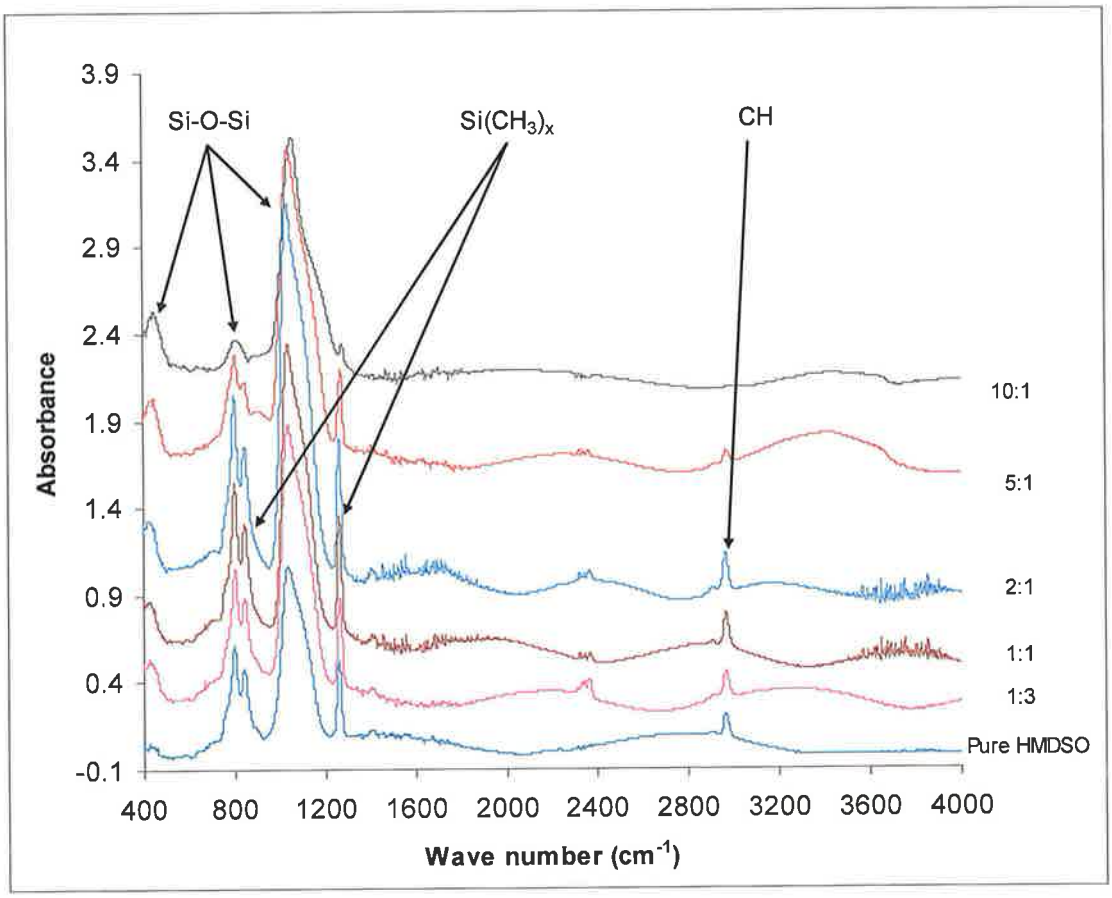

Figure 5 Variation of hydrocarbon content with oxygen to HMDSO flow ratio at high flow rate for films deposited on powered electrode at 250 W RF power

The difference between the floating potential (FP) and powered electrode (PE) deposited films was that the peak corresponding to hydroxyl content in the film disappeared at the powered electrode because of the high temperature and another difference was, the intensity of Si-O-Si peak was higher on the powered electrode than that on the floating electrode deposited film. This increased intensity could be due to the dense Si-O-Si network caused by the energetic ion bombardment. The density of powered electrode film was always higher than that of floating electrode deposited films as shown in Table 3.

RF power (Watts)	FP Density (g/cm^3)	PE Density (g/cm^3)
50 W	1.305	1.487
250 W		1.960
500 W	2.11	2.499

Table 3 Film density calculations for films deposited at fixed 10:1 oxygen to HMDSO flow ratio at varying RF powers

The film density on silicon wafer was calculated by dividing the mass of the coating with its volume. The film mass was calculated by measuring the mass of the silicon wafer before and after deposition and taking its difference. The film volume was calculated by multiplying the surface area of the substrate with the film thickness.

1) 50 W FP

Substrate area (cm^2)	Film thickness (nm)	Volume (area X film thickness) 10^{-4} (cm^3)	Mass of sample (mg)		Net mass of coating (mg)
			Before deposition	After deposition	
1.333	1150	1.333 X 1.150	152.8	153	0.2

Density = Mass/ Area X Thickness

$= 0.2 \text{ X } 10^{-3} / 1.333 \text{ X } 1.15 \text{ X } 10^{-4} \text{ g/cm}^3$

$= 0.2 \text{ X } 10^{1} / 1.5329$

$= 1.305 \text{ g/cm}^3$

2) 50 W PE

Substrate area (cm^2)	Film thickness (nm)	Volume (area X film thickness) 10^{-4} (cm^3)	Mass of sample (mg)		Net mass of coating (mg)
			Before deposition	After deposition	
1.755	1533	1.755 X 1.533	203.9	204.3	0.4

Density = Mass/Area X Thickness

$= 0.4 \text{ X } 10^{-3} / 1.755 \text{ X } 1.533 \text{ X } 10^{-4} \text{ g/cm}^3$

$= 1.487 \text{ g/cm}^3$

3) 250 W - PE

Substrate area (cm^2)	Film thickness (nm)	Volume (area X film thickness) 10^{-4} (cm^3)	Mass of sample (mg)		Net mass of coating (mg)
			Before deposition	After deposition	
1.546	1650	1.546X 1.650	182.6	182.1	0.5

Density = Mass/Area X Thickness

$= 0.5 \text{ X } 10^{-3} / 1.546 \text{ X } 1.650 \text{ X } 10^{-4}$

$= 1.960 \text{ g /cm}^3$

4) 500 W – FP

Substrate area (cm^2)	Film thickness (nm)	Volume (area X film thickness) 10^{-4} (cm^3)	Mass of sample (mg)		Net mass of coating (mg)
			Before deposition	After deposition	
1.529	930	1.529X 0.930	175.6	175.9	0.3

Density = Mass/Area X Thickness

$= 0.3 \text{ X } 10^{-3} / 1.529 \text{ X } .930 \text{ X } 10^{-4}$

$= 2.11 \text{ g /cm}^3$

5) 500 W – PE

Substrate area (cm^2)	Film thickness (nm)	Volume (area X film thickness) 10^{-4} (cm^3)	Mass of sample (mg)		Net mass of coating (mg)
			Before deposition	After deposition	
1.530	1831	1.530X 1.831	181.6	182.5	0.7

Density = Mass/Area X Thickness

$= 0.7 \text{ X } 10^{-3} / 1.530 \text{ X } 1.831 \text{ X } 10^{-4}$

$= 2.499 \text{ g /cm}^3$

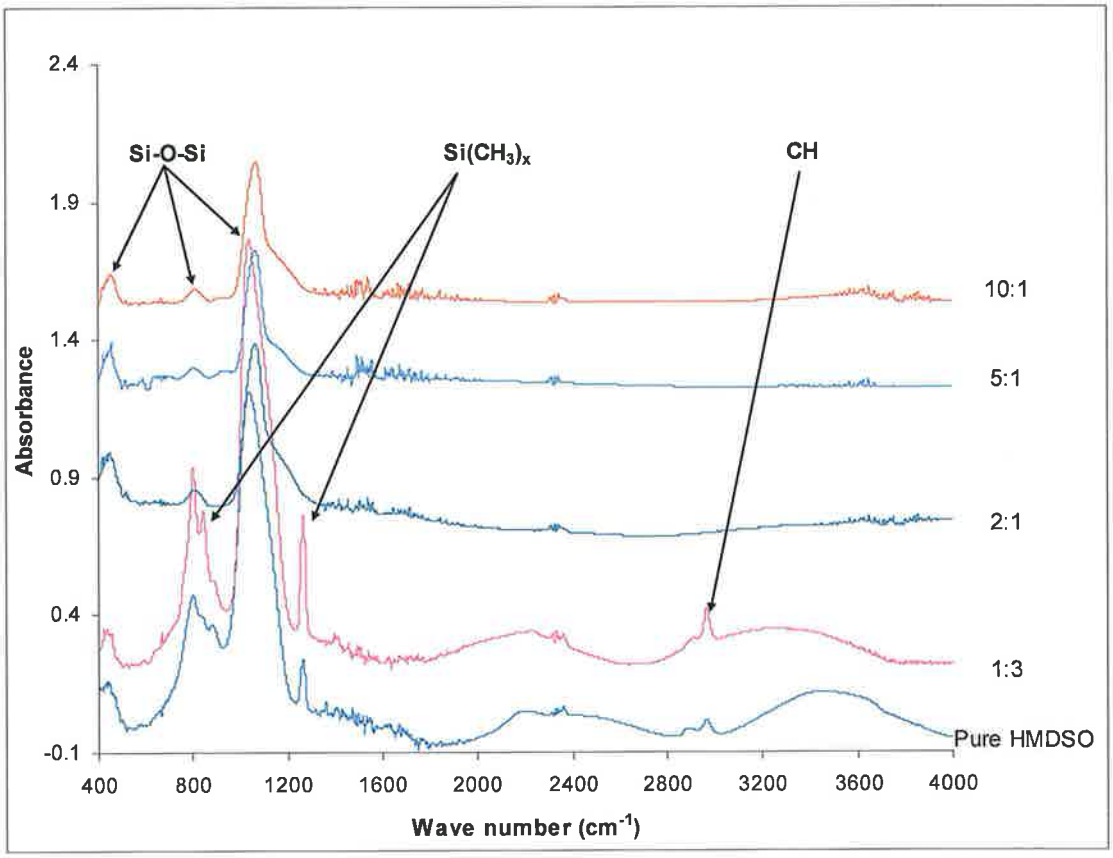

Figure 6 Variation of hydrocarbon content with oxygen to HMDSO flow ratio at low flow rate for films deposited on powered electrode at 250 W RF power

As the RF power increased, there was a significant decrease of hydrocarbon content (fig 7 and fig 8). The peak at 1278 cm^{-1} corresponding to methyl group decreased in intensity as the RF power increased and it disappeared for the films deposited on the powered electrode. In the case of floating electrode deposited films, there was a considerable amount of hydrocarbon content present in the films but much lower than that present at lower RF powers. Hence, the temperature on the substrate holder also played a role in deciding the quality of films, which was very clear from the contact angle analysis to be discussed in the later part of this section.

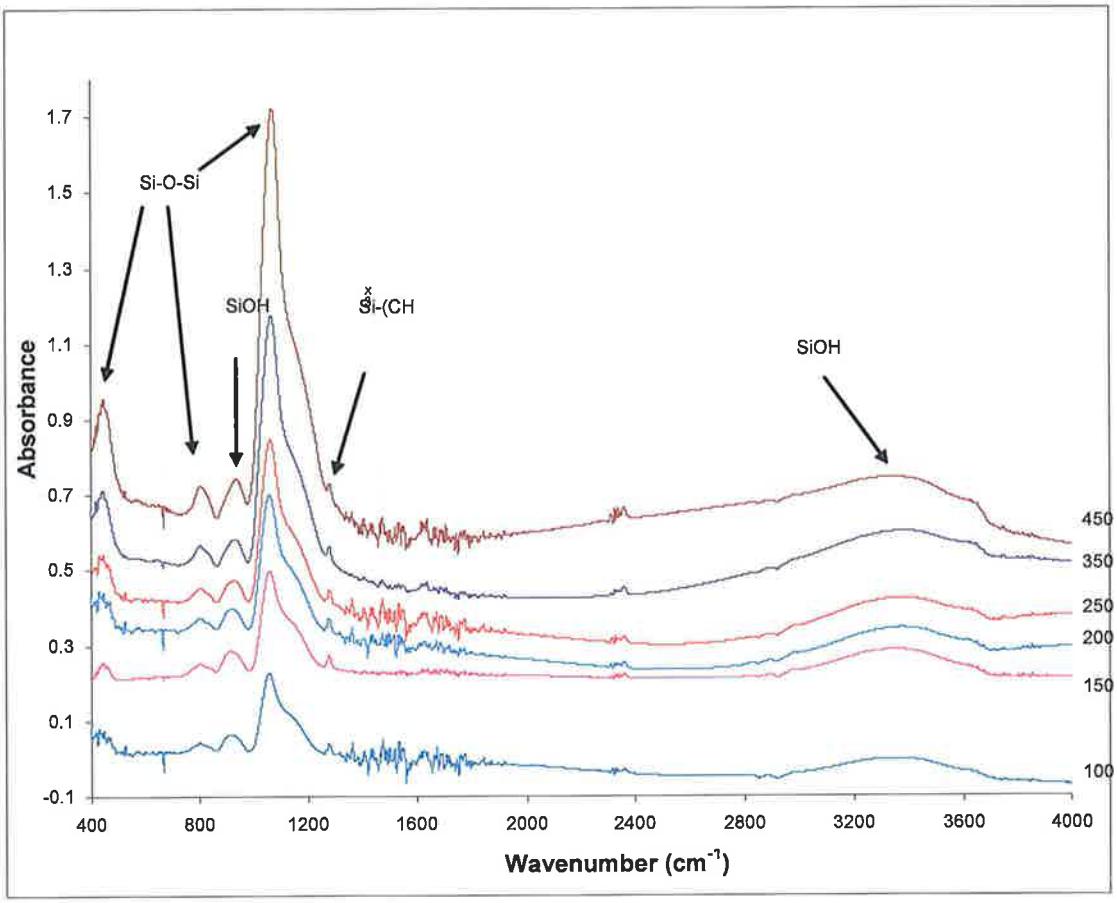

Figure 7 Variation of hydrocarbon content with RF power for fixed oxygen to HMDSO flow ratio (10:1) at low flow rate for films deposited on floating potential

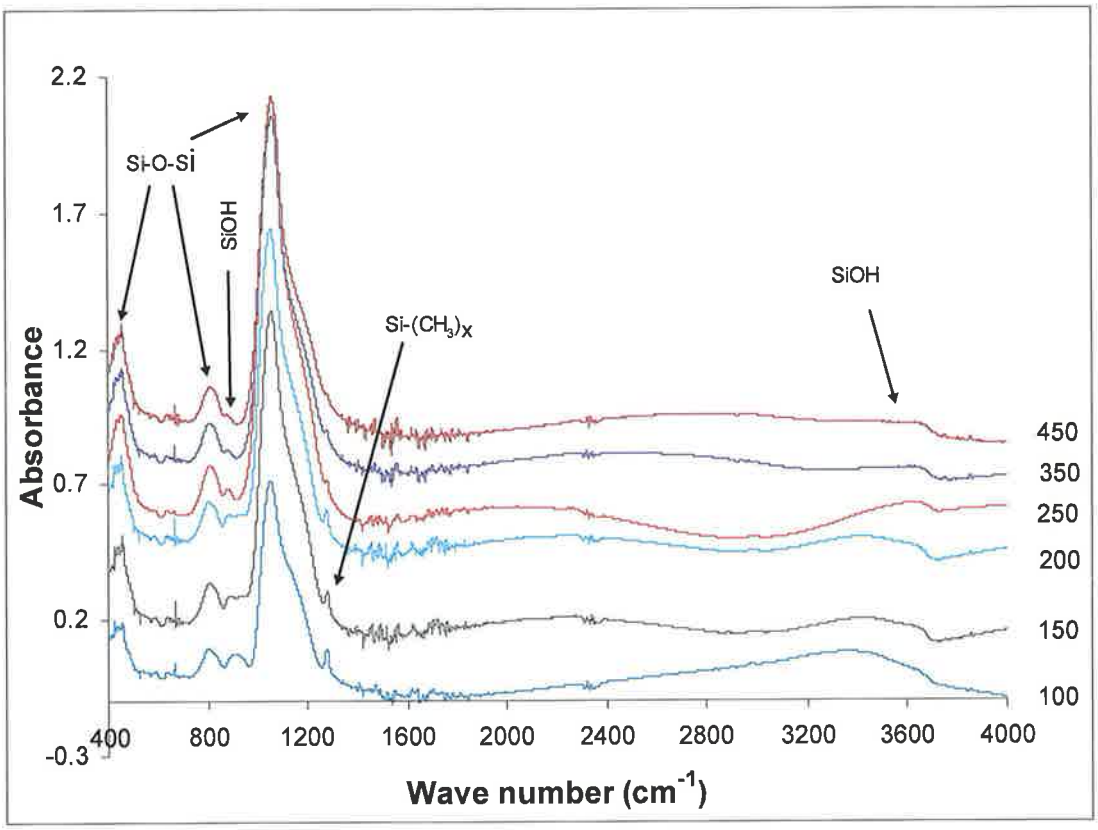

Figure 8 Variation of hydrocarbon content with RF power for fixed oxygen to HMDSO flow ratio (10:1) at low flow rate for films deposited on powered electrode

The peak at 930 cm^{-1} corresponds to hydroxyl group bonded to Si. This peak also decreased in intensity with increase in RF power for the films deposited on powered electrode where as for the floating electrode deposited films; there was no decrease in intensity with power. This is because, as the RF power increased, the temperature on the powered electrode became very high, which dissociated the SiOH bonding and hence the hydroxyl group did not appear at high powers in the powered electrode and for the floating potential electrode, there was not much increase in temperature with power. So the hydroxyl group in the films deposited on the floating electrode was retained.

3.1.2 Variation of deposition rate with oxygen:HMDSO flow ratio in floating and powered electrode deposited films

The deposition rate of the films grown on floating and powered electrode was calculated by measuring the film thickness using spectroscopic ellipsometry and dividing it by deposition time. Figure 9 shows the deposition rate on floating and on powered electrode, as a function of the oxygen to HMDSO flow ratio for the films deposited at high flow rate/pressure. The RF power in the experiment was fixed at 250 Watts. The experimental data showed an initial rise in the deposition rate in both floating and powered electrode deposited films followed by a decrease with the higher oxygen flow. Then the deposition rate stabilized at higher oxygen: HMDSO flow ratios.

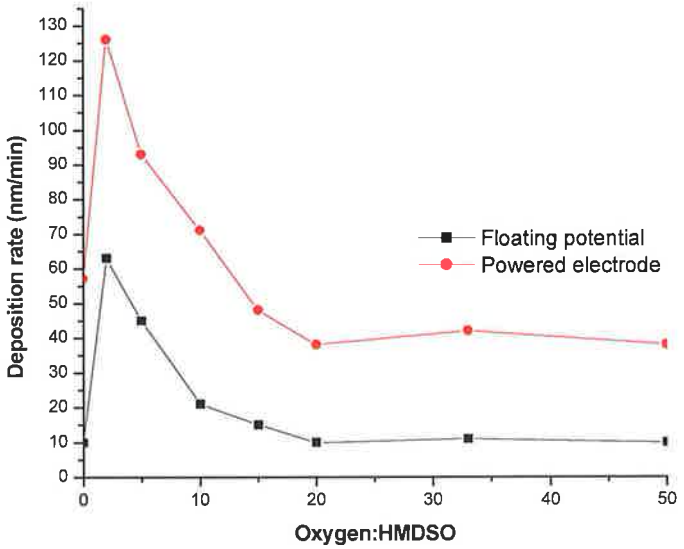

Figure 9 Variation of deposition rate with oxygen: HMDSO flow ratio at 250 W RF power

The flow rates corresponding to various flow ratios are tabulated in Table 1. The reason for lower deposition rate at 0:1 (oxygen: HMDSO) flow ratio was that the deposition rate was limited by the unavailability of oxygen other than that present in the HMDSO precursor itself. As additional oxygen flow was introduced in the chamber the deposition rate increased due to the availability of oxygen to react with hydrocarbons in the precursor. With higher oxygen to HMDSO flows ratios the hydrocarbons present in the precursor begun to oxidize more into water and carbon

dioxide and were pumped out of the chamber and hence the amount of hydrocarbons contributing to film formation decreased as the oxygen flow was increased. The FTIR spectra in figures 3 and 5, show that at low oxygen: HMDSO flow ratio the hydrocarbon peaks were present in considerable amount, forming $SiO_xC_yH_z$ film, and as the ratio was increased, the intensity of hydrocarbon peaks decreased and it was insignificant at high oxygen: HMDSO flow ratio of 10:1, forming SiO_x film. Thus the high deposition rate at low flow ratio was due to the contribution of hydrocarbons for film formation and increase in oxygen:HMDSO flow ratio increased the oxidation and decreased the hydrocarbon contribution towards film formation resulting in SiO_x film formation, which in turn resulted in decreased deposition rate at high flow oxygen:HMDSO flow ratio. Also the densification of film at higher oxygen: HMDSO flow ratio contributed for decreased deposition rate. The decrease in deposition rate with increase in oxygen flow is in agreement with G. Borvon et al [155].

The hydrocarbon rich low oxygen: HMDSO ratio (1:1) deposited $SiO_xC_yH_z$ films had a high refractive index of 1.842 in figure 10. The experimental studies of C. Vallee et al [156], Stephanie Roualdes et al [157], and C. Vallee et al [158] on the refractive index measurements of silicon based oxide coatings suggested that the carbon contents in $SiO_xC_yH_z$ films contributed for higher refractive index.

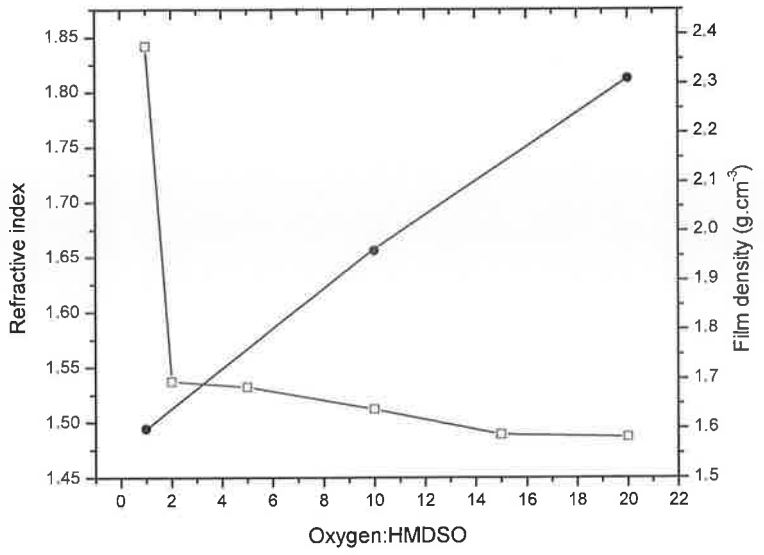

Figure 10 Variation of refractive index (□) and film density (■) with R (oxygen:HMDSO flow ratio) at 250 W RF power

It is evident from figure 6 in the FTIR measurements that low oxygen: HMDSO ratio films had higher hydrocarbon content and as the oxygen flow was increased, the hydrocarbon intensity decreased. The refractive index decreased with increase in oxygen: HMDSO ratio, figure 10. The refractive index change correlated well with the observed hydrocarbon content variation in FTIR spectra. Since the refractive index of fused silica was 1.46, a refractive index value of 1.487 for oxygen: HMDSO ratio of 20:1 indicated the formation of sub-stoichiometric SiO_x film. At oxygen: HMDSO ratio of 20:1, the hydrocarbon contents were negligible hence the higher refractive index was due to the formation of a Si rich sub-stoichiometric SiO_x film. The film density calculations also correlated well with the refractive index measurements. The density of low oxygen: HMDSO ratio films (1:1) were 1.599 $g.cm^{-3}$ and as the oxygen flow increased the density increased to 2.309 $g.cm^{-3}$. This was due of the formation of a dense SiO_x network. The film density calculations are in agreement with E. Bapin et al [159].

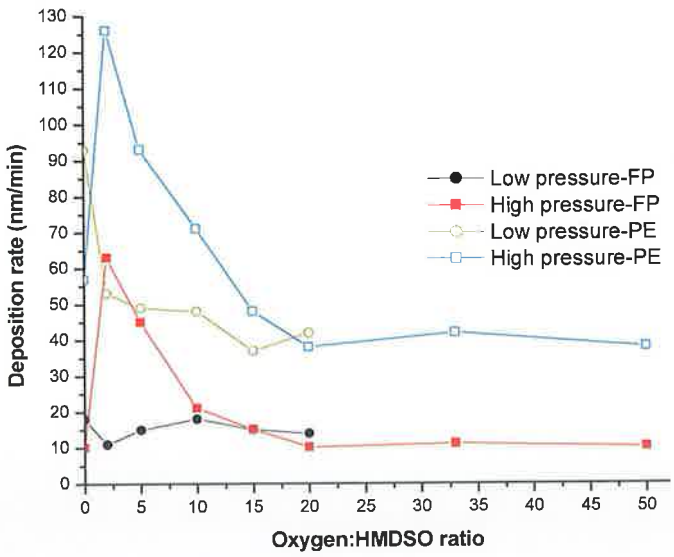

Figure 11 Variation of deposition rate with oxygen:HMDSO flow ratio with low and high flow rates deposited at 250 W RF power

The deposition rate varied in the same way with various oxygen:HMDSO flow ratios for both low and high flow rates, in figure 11. At low oxygen: HMDSO flow ratio, the deposition rate of films deposited with high flow rate was much higher than that

deposited with low flow rate. High deposition rate with high flow rate films was because of more film forming flux present in the plasma. As the oxygen flow was increased, the deposition rate of both low and high flow rate films was nearly the same. At higher oxygen: HMDSO flow ratio, most of the hydrocarbons present in the plasma was oxidized and only Si-O-Si contributed for film formation resulting in more or less the same deposition rate above a certain flow ratio.

The experimental data in figure 12 showed an increase in deposition rate on floating potential deposited films with increase in RF power at fixed oxygen: HMDSO flow ratio of 10:1. The increase in RF power caused higher fragmentation of the precursor molecules resulting in increased plasma density and hence we observed an increase in the deposition rate. This is in good agreement with E.Bapin et al [160]. However in the powered electrode, the deposition rate decreased at higher RF powers (above 200 Watts). This was due to the film densification, as shown in figure 13, on the powered electrode caused by increased energetic ion bombardment with increase in RF power. Nano hardness measurement confirmed the formation of a dense layer at higher RF powers. In figure 14, the film hardness showed a linear increase for powered electrode deposited films whereas this remained almost constant for the floating electrode deposited films.

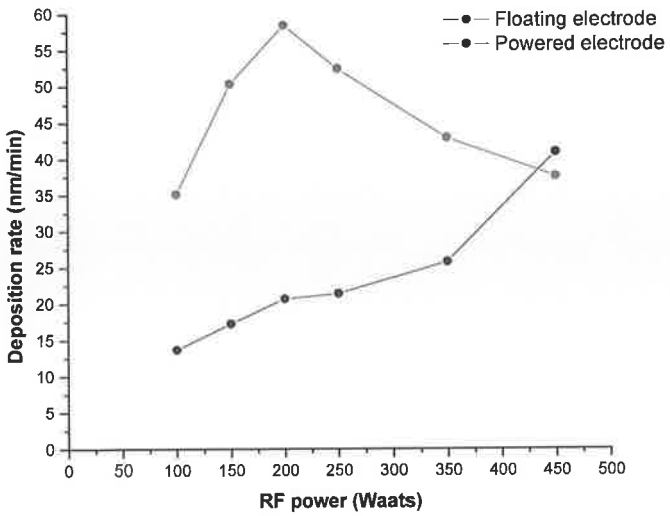

Figure 12 Variation of deposition rate with RF power for 10:1 oxygen:HMDSO flow ratio films

The bias voltage varied from -2 V at 50 W to -30V for 450 W, since there was no significant rise in bias voltage with increase in RF power the possibility for sputtering of the deposited films was very low. On comparing figures 11 and 12 we observed that the deposition rates at the floating electrode to be lower than at the powered electrode. This was because, the plasma density at the floating electrode which was situated 10 cm away from the source was lower.

The refractive index was measured at varying RF powers for a fixed oxygen: HMDSO ratio of 10:1. Studies by S. Spiga et al [161], Yizhou Song et al [162] and Yasumi Yamada et al [163] suggests that the silicon rich - SiO_x films possess a higher refractive index than the fused silica. In figure 13, as the RF power increased, the refractive index increased, this was because of a dense layer that was formed by a silicon rich sub-stoichiometric SiO_x film.

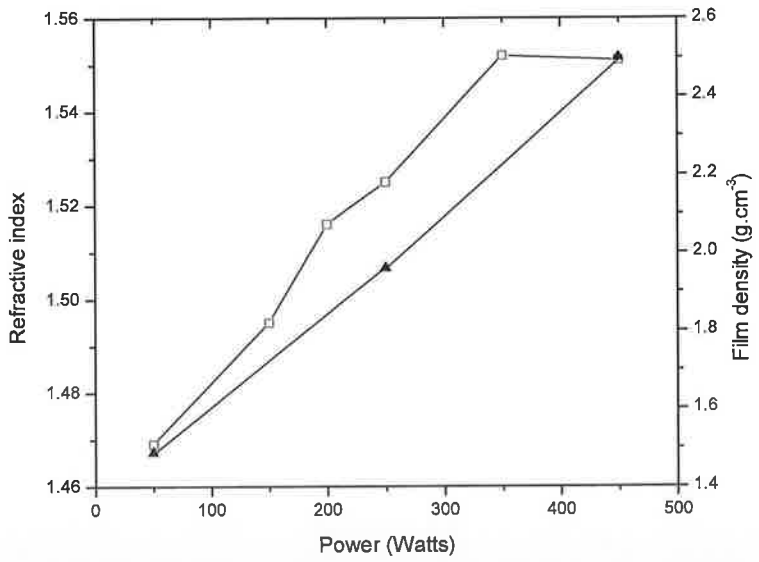

Figure 13 Variation of refractive index (□) and film density (◀) with RF power for films deposited on powered electrode at 10:1 oxygen to HMDSO flow ratio

It was evident from the film density measurements that the density increased with increase in RF power and hence a dense layer was formed at higher RF power. The light oxygen and carbon atoms were being replaced by heavy Si atoms. The higher refractive index in this case was not because of carbon incorporation in the film rather it was because of its silicon rich nature. This was evident from FTIR and contact angle investigations. The carbon peak intensity decreased to a significant extent with rise in RF power and the water contact angle decreased with increase in RF power denoting the decrease of hydrocarbon content with increase in RF power.

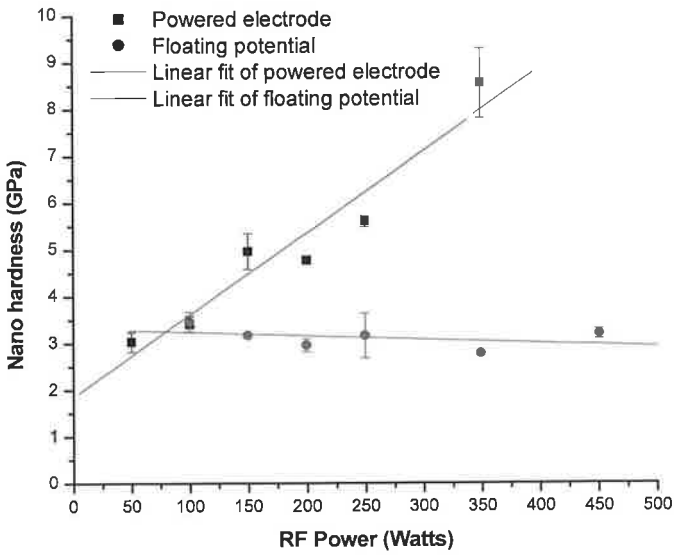

Figure 14 nano hardness data of 10:1 oxygen to HMDSO ratio deposited film, at various RF power, on floating and powered electrode

Fig 14 showed the variation of hardness with RF power for films deposited on floating electrode and on powered electrode. The hardness for the films deposited on the floating potential electrode was independent of RF power. The linear increase of hardness with increase in RF power was attributed to the increased fragmentation of precursor molecules with increase in RF power which resulted in formation of more ions and radicals in the plasma. Increased ions in the plasma lead to increased energetic ion bombardment on the powered electrode resulting in densification of the film, which in turn lead to increased hardness.

3.1.3 Contact angle analysis

The wettability of the film was determined by the contact angle the water made with the surface with which it was in contact. It was measured by drawing a tangent at the point of contact and measuring the angle between the tangent and the surface. The contact angle would be high if the cohesive force existing within the liquid drop is higher than the adhesive force between the liquid and the surface. If the adhesive force between the liquid and the surface overcomes the cohesive force between the liquid molecules then the contact angle would be less. If the water contact angle is high (approx more than 70^{o} or 80^{o}) then the surface is hydrophobic, if it is less then the surface is hydrophilic.

The water contact angle was measured by using Sessile drop technique and by Wilhelmy plate method. The contact angle was measured for films deposited with varying oxygen to HMDSO flow ratios at fixed RF power (250 W) and for varying RF power for fixed oxygen to HMDSO ratio (10:1).

The film wettability was measured by water contact angle analysis using a video based OCA 20 Data Physics contact angle measurement system. The pictures taken from sessile drop analyzer in figure 15 shows the variation of contact angle with change in oxygen to HMDSO ratio. It was clearly seen that the contact angle was high for pure HMDSO films and water spreaded out and formed low contact angle at high oxygen to HMDSO ratio.

The HMDSO deposited films could be used to produce a hydrophobic surface with a water contact angle above 100^{o} [164]. The film hydrophobicity depends on the oxygen concentration in the plasma and the post-plasma treatment [165,166]. The hydrophobic nature of polymer-like $SiO_xC_yH_z$ films, deposited from pure HMDSO was due to the presence of methyl groups and hydrocarbons in the film [167]. The hydrophobicity arouse from the fact that the water molecules were not able to form a hydrogen bond with the non polar hydrocarbons present in large quantity. FTIR measurements in figures 3 to 6 confirmed the presence of more hydrocarbons in the film. The cohesive force within the water molecules was higher than the adhesive

force between the water and the film surface. The water contact angle depended on the polarity of the surface. By increasing the polarity, it was possible to increase the hydrophilicity. By reducing the hydrocarbons in the film and by increasing the oxygen content it was possible to create polarity in the surface. The oxygen:HMDSO ratio was increased and the water contact angle measured. The water contact angle was found to decrease as the oxygen flow was increased. FTIR spectra in figures 3 to 6 showed that the hydrocarbon content decreased as the oxygen: HMDSO ratio was increased. As a result, a polar Si-O-Si network was formed. This allowed the formation of hydrogen bond with water resulting in lower water contact angle. The adhesive force between the surface and water molecule overcame the cohesive force between the water molecules and the water drop spreaded.

The water contact angle was measured for various oxygen:HMDSO flow ratios at two different precursor flow rates, figure 15. The maximum and minimum water contact angle of 115°, 74° was achieved with high flow rate films and 105.5°, 65° with low flow rate films respectively. The hydrophobicity of polymer-like $SiO_xC_yH_z$ films was close to the values obtained by F. Benitez et al [168], R. Mahlberg et al [169] and J. Behnisch et al [170].

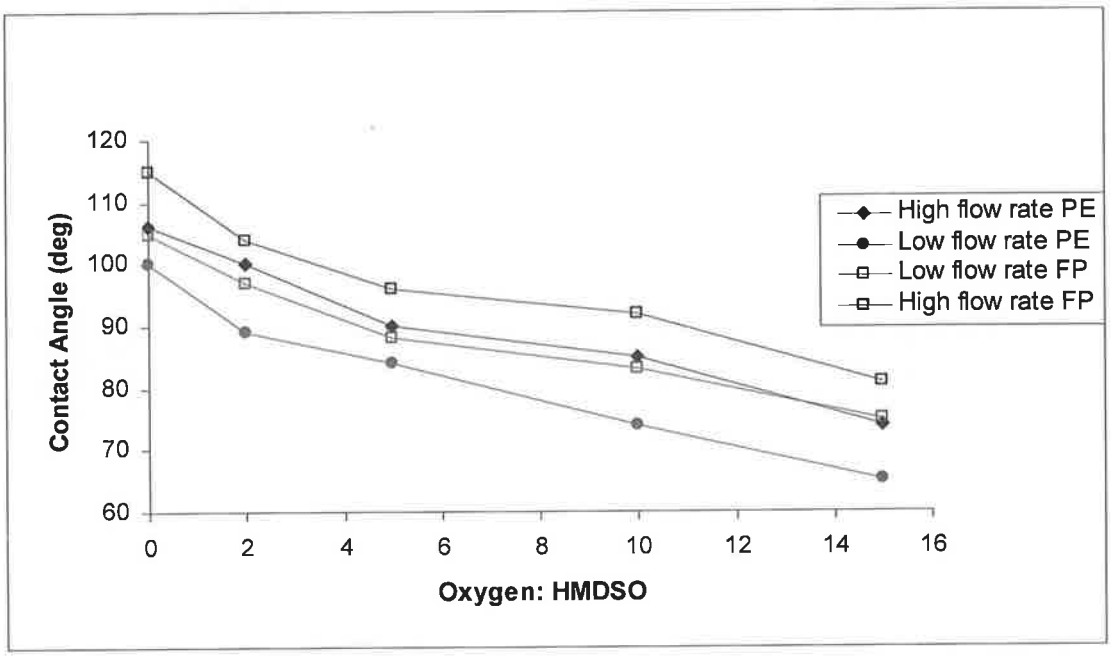

(a)

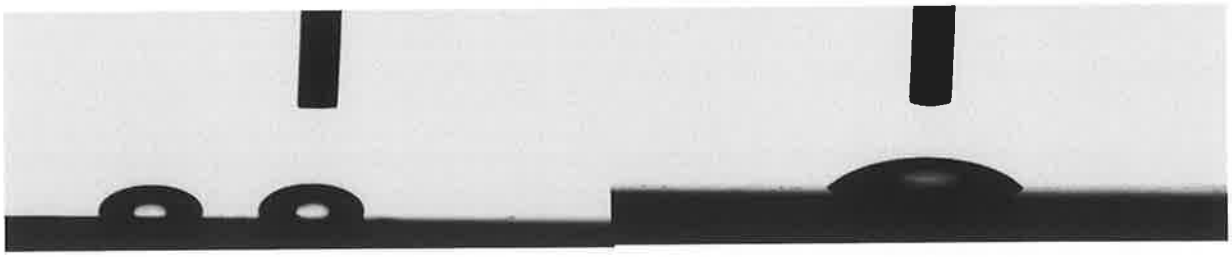

(b)

Polymer-like $SiO_xC_yH_z$ - 106 deg **Silica-like (SiO_x) - 65 deg**

Figure 15 (a) Variation of water contact angle with oxygen:HMDSO flow ratio for low and high flow rates for films deposited at floating potential and powered electrode, at 250 W and (b) Image of water contact angle of $SiO_xC_yH_z$ and SiO_x films

There were two major observations and conclusions to be drawn from fig 15.

They were

1) The floating electrode deposited films always exhibited a slightly higher water contact angle than the powered electrode deposited films. This behaviour was explained from the FTIR results. The hydrocarbon content of floating electrode deposited films was slightly higher than the powered electrode deposited films resulting in a slightly hydrophobic surface. The intensity of Si-O-Si peak was always higher in powered electrode deposited films and favoured the formation of hydrogen bond with water resulting in lower water contact angle in powered electrode deposited films.

2) For all oxygen: HMDSO flow ratios, films deposited at low flow rate had much lower water contact angle than the high flow rate films. This behaviour was also explained from the FTIR observations. Table 1 shows the pressure values at different flow rates, it was clear that the operating pressure at low flow rate was much lower than that at high flow rate. At lower pressure, the fragmentation of precursor molecule was more and hence the hydrocarbons were easily oxidized and were pumped out of the chamber. The resulting film will had lower hydrocarbon content in them than that deposited at high flow rate. This accounted for the observed higher wettability of low flow rate deposited films. It was clear from figure 5 and 6 that the peak at 1278 cm^{-1}, that corresponds to hydrocarbon contents, appeared at high flow rate 10:1 film, where as it was missing in the low flow rate film.

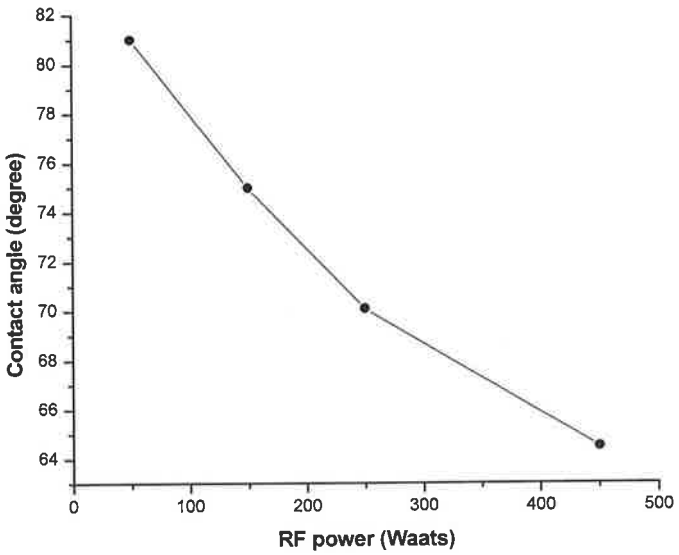

Figure 16 Variation of water contact angle with RF power for fixed oxygen:HMDSO flow ratio (10:1) films deposited on powered electrode

To study the influence of RF power on the film properties, a fixed oxygen:HMDSO flow ratio film (10:1) was deposited at various RF powers from 50 W to 450 W. Figure 16 shows the variation of contact angle with RF power for 10:1 oxygen:HMDSO ratio film. For silica-like films, the increase in RF power lowers the contact angle ie., the film becomes more hydrophilic with increase in RF power. This is due to the decrease of hydrocarbon content in the film with increase in RF power. As the RF power increased, the fragmentation of precursors increased resulting in formation of a dense Si-O-Si network with less hydrocarbon contents. FTIR spectroscopic study showed that the hydrocarbon contents in the film decreased with increase in RF power, figure 7. The film density calculations in figure 13 showed that the film density increased with increase in RF power. Nano indentation tests in figure 14 showed that the film nano hardness increased with increase in RF power indicating a dense network being formed.

The lowest contact angle that could be achieved for 10:1 oxygen:HMDSO ratio film at a maximum RF power of 450 W was 65°, Figure 16. We observed that the high hydrophilicity attained by higher dissolution of oxygen in the plasma was transient (Fig. 17). The contact angle values changed with time only for high oxygen:HMDSO ratio films. The contact angle did not change for oxygen:HMDSO ratio of 1:1, 2:1, 5:1 and 10:1, but for 15:1, there was a drastic change in contact angle with time.

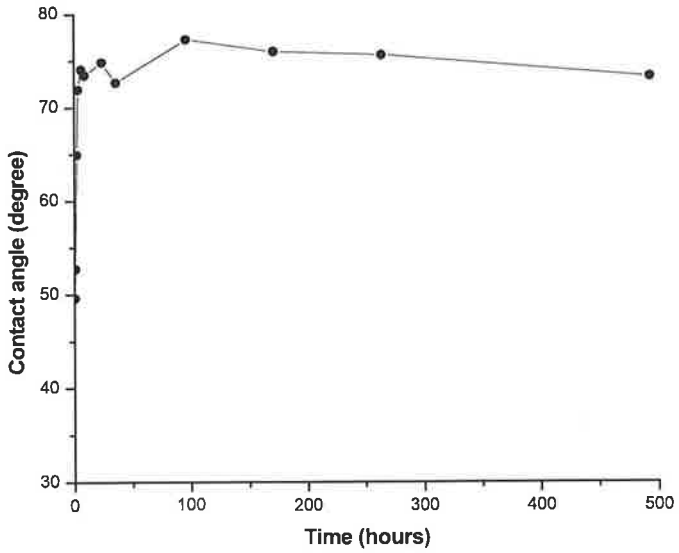

Figure 17 Variation of water contact angle with time for 15:1 oxygen to HMDSO flow ratio film deposited at 250 W RF power

Fig. 17 shows the temporal effect of 15:1 oxygen: HMDSO ratio films. When measured immediately after deposition, the contact angle was found to be approximately 50° which is hydrophilic but it increased with time and attained saturation with in hours.

To further lower the water contact angle, the films were deposited at an oxygen:HMDSO ratio of 33:1. The water contact angle was obtained around 60°. The contact angle was found to be stable over a period of time, figure 18. The contact angle measurement was carried out after a day and hence the variation of contact angle within the first few hours of deposition, like the figure 17, is not shown in figure 18. A further increase of oxygen:HMDSO ratio did not seem to provide a lower stable water contact angle. The floating potential deposited films exhibited a slightly higher water contact angle than the powered electrode deposited films.

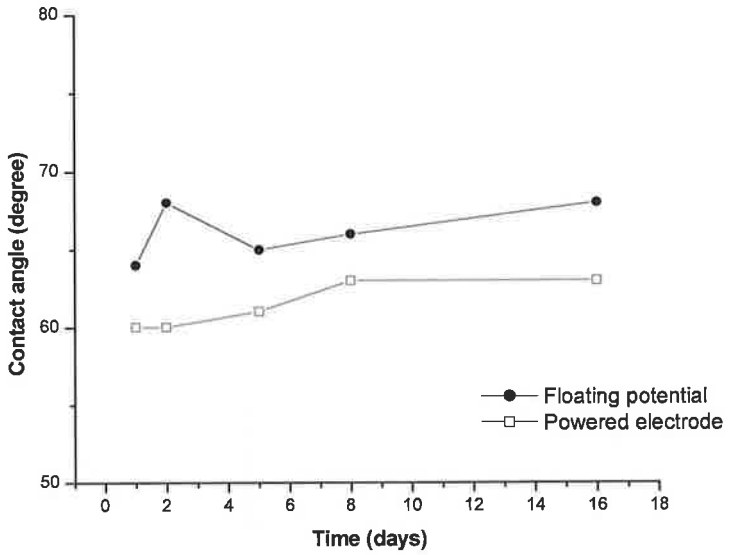

Figure 18 Variation of water contact angle with time for 33:1 oxygen:HMDSO flow ratio films deposited at 250 W RF power

Surface Energy:

The Surface energy of the film was calculated from the contact angle values of water, diiodomethane and ethylene glycol with the surface and then using Owens and Wendt to calculate the surface energy from the contact angle [171].

Flow ratio Oxygen : HMDSO	Pure HMDSO	5 : 1	10 : 1
Contact angle (deg)	105.5	93.0	75.1
Surface Energy (mN/m)	20.31 mN/m Disp : 19.71 Polar : 0.60	24.61 mN/m Disp : 22.44 Polar : 2.18	31.37 mN/m Disp : 20.20 Polar : 11.16

Table 4. Surface energy values for varying oxygen to HMDSO flow ratio

Hydrophobic surfaces had lower surface energy and as the hydrophobicity decreased, the surface energy increased. Polar component of the surface energy measurement was much less (0.60 mN/m) for pure HMDSO deposited $SiO_xC_yH_z$ films than for 10:1 (oxygen: HMDSO) films, where the polar component was comparatively high (11.16 mN/m) and hence the contact angle of water was less for 10:1 ratio films. Since the surface energy increased with decrease in water contact angle, the contact angle measurements were taken as a qualitative measure of surface energy.

3.1.4 Nano hardness measurement

The film hardness was measured by using a CSM Instruments nano indentation tester with a Berkovich indenter. Loads of 3 mN and 5 mN were used. The indentation depth was less than 20% of the film thickness. The hardness of the sample material was calculated using the method of Oliver and Pharr [172]. The measurements were calibrated using a bulk copper material as standard. The load and displacement were recorded continuously throughout the process to produce a load-displacement curve from which the nano-mechanical properties such as hardness, Young's modulus, plastic & elastic energy of the sample material could be calculated.

The oxygen to HMDSO ratio was varied at fixed RF power (250 W) and the hardness values were measured at low and high oxygen: HMDSO flow ratio and at low and high flow rates. Table 5 tabulates the hardness values for low (1:1) and high (10:1) oxygen: HMDSO flow ratios at two different flow rates. At low oxygen: HMDSO flow ratio, the film hardness was very low around 1.6 GPa, which was more like a polymer-like surface. At an oxygen:HMDSO flow ratio of 10:1, the film hardness was much higher for powered electrode deposited films, 5.5 GPa for low flow rate films and it approached a silica-like surface hardness of 7.2 GPa for an oxygen:HMDSO flow ratio of 20:1. The hard silica-like surface formation was because of reduced carbon and hydrogen content [173]. Since the oxygen flow was high, the hydrocarbon ions present in the plasma were oxidized and the Si-O-Si bonds form a network that lead to increased hardness. It was clear that at low flow ratio, in the case of polymer-like $SiO_xC_yH_z$ films the nanohardness values of floating

potential deposited films and powered electrode deposited films did not show any difference.

Oxygen:HMDSO	Low flow rate		High flow rate	
	FP	PE	FP	PE
1:1	1.6	1.6	1.5	1.6
10:1	3.0	5.5	2.8	4.3

Table 5 Nano hardness measurement of polymer-like $SiO_xC_yH_z$ and silica-like films deposited on floating (FP) and powered electrode (PE) at a fixed RF power of 250 W

The hardness values of films deposited on the powered electrode at low oxygen to HMDSO flow rate was found to be higher than that of the high oxygen: HMDSO flow rate. For 10:1 oxygen: HMDSO ratio at low oxygen: HMDSO flow rate, the powered electrode deposited film had higher hardness value than that deposited at high oxygen: HMDSO flow rate. This was because the pressure at low flow rate was about 80 mTorr lower than that at high flow rate. The energy of the ions that bombarded the electrode was higher at lower pressure; hence the resulting film was more hard and dense.

In order to find the effect of RF power on the film hardness, the oxygen:HMDSO ratio was fixed at 10:1 (250:25) and the RF power was increased from 50 W till 450 W.

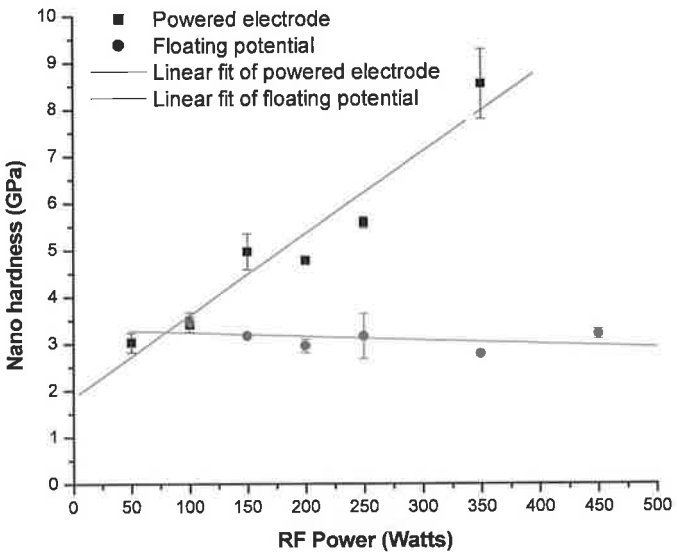

Figure 19 Variation of nano hardness RF power for an Oxygen to HMDSO flow ratio of 10:1, at low flow rate for films deposited on both floating and on powered electrode.

Figure 19 shows the variation of hardness with RF power for films deposited on floating electrode and on powered electrode. The hardness for the films deposited on the floating potential electrode was independent of RF power, figure 19. The linear increase of hardness with increase in RF power was attributed to the increased fragmentation of precursor molecules with increase in RF power which resulted in formation of more ions and radicals in the plasma. Increased density of ions in the plasma lead to increased energetic ion bombardment on the powered electrode resulting in densification of the film which in turn lead to increased hardness. Refractive index and film density increased with increase in RF power, figure 13 justified the formation of a dense layer on powered electrode deposited films.

3.1.5 Bandgap measurements

A photon with certain energy, when absorbed, can excite an electron from a lower to a higher energy state. The rapid rise in absorption called fundamental absorption is due to the excitation of an electron from the valence band to the conduction band. The energy gap can be determined from the fundamental absorption.

Absorption is expressed in terms of a coefficient α(hν) which is defined as the relative rate of decrease in light intensity along its propagation path:

$$\alpha = 1/d \ln (Io/I)$$

Where d is the film thickness and Io and I are intensities of the initial and transmitted beams, respectively.

The absorption edge of an UV-Visible spectrum corresponds to the bandgap of the semiconductor and can be evaluated by calculating the absorption coefficient α from the transmittance spectra. The absorption coefficient α near the absorption edge was determined from the optical transmission measurements at various wavelengths using the above relation.

The optical bandgap can be calculated by using the Tauc relationship [174]

$$\alpha h\nu = A (h\nu - E_g)^m$$

where m is 2 for amorphous semiconductors with indirect optical transitions [175,176,177]

which gives

$$(\alpha h\nu)^{\frac{1}{2}} = \sqrt{A}(h\nu - Eg)$$

By plotting a graph between hν and $(\alpha h\nu)^{1/2}$ and extrapolating the curve to zero the energy band gap can be calculated. When the curve is extrapolated to zero the X intercept which is the energy gives the optical bandgap of the film.

so when extrapolated to zero, we have $(\alpha h\nu)^{\frac{1}{2}} = 0$ and hence $h\nu = E_g$

If the actual absorption is αt, where t is thickness we get

$$(\alpha h\nu)^{\frac{1}{2}} = \sqrt{\frac{B}{t}}(h\nu - Eg)$$

which still gives $h\nu = E_g$ *when* $(\alpha h\nu)^{\frac{1}{2}} = 0$

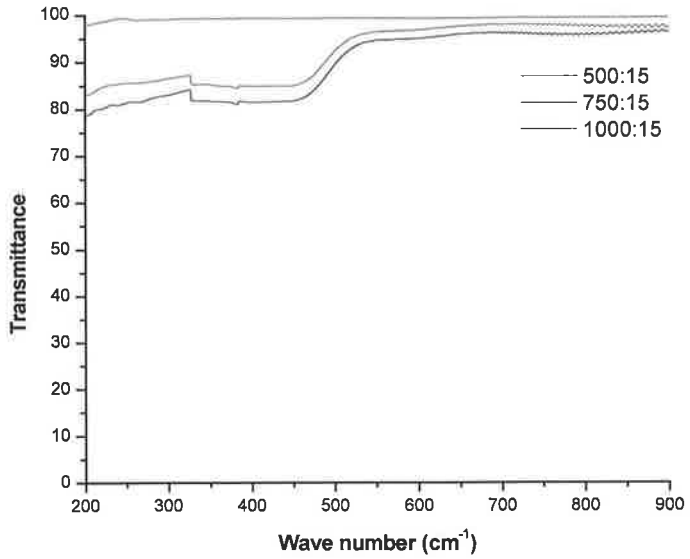

Figure 20 UV-Visible transmittance spectra of SiO_x films deposited at various oxygen:HMDSO flow ratio at 250 W RF power

Since the fundamental light absorption appeared in deep UV wavelength rang, it was not possible to determine the refractive index of SiO_x coatings based on the Tauc plot using the normal UV-Vis spectrometer. As per the literature, the energy bandgap of SiO_x films was around 9 eV [178]. Hence 9 eV was considered as the bandgap value of our SiO_x films. The figure above shows the transmittance spectrum of SiO_x films deposited at various oxygen:HMDSO flow ratio

3.1.6 Energy dispersive analysis by X-ray spectroscopy (EDS) studies

The EDS spectrum (figure 21) showed the presence of both Si and O confirming the formation of SiO_x coating. The peak corresponding to carbon should appear around 0.25 keV. The absence of carbon peak confirmed that the silica-like SiO_x film was free of carbon.

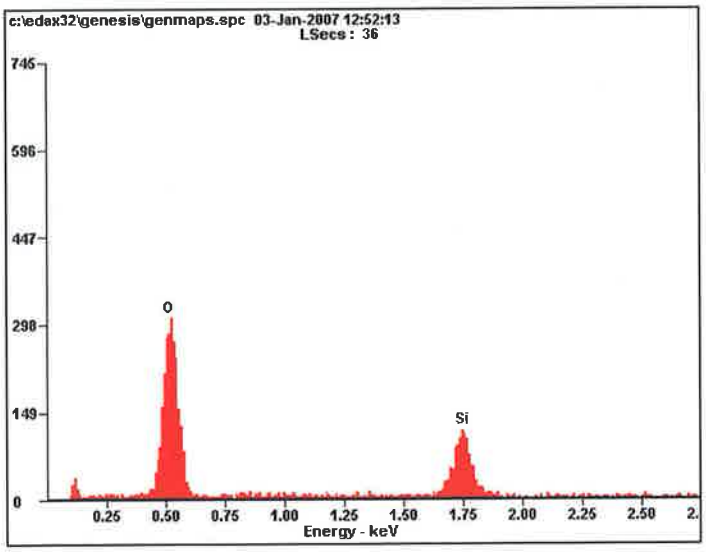

Figure 21 EDS spectrum of SiO_x coating 33:1 oxygen:HMDSO flow ratio deposited on 316L stainless steel at 250 W RF power

3.2 Characterization of TiO_x coatings

The titanium oxide coatings were deposited using a mixture of the organic precursor TIP and oxygen. The TIP is a widely used organic precursor for TiO_2 film deposition [179,180]. TIP flow that was kept constant throughout the process was controlled by using a needle valve and the oxygen flow was varied in order to tune the composition of the film. The process was optimized to get a TiO_x film by varying the oxygen flow at a fixed RF power of 250 Watts and by varying the RF power at a fixed oxygen flow. The film thickness was measured by using spectroscopic ellipsometry and the nature of chemical bonds present in the film was analysed by Fourier transform infrared spectroscopy (FTIR). The water contact angle was measured by contact angle analyzer and stability of the contact angle with time was also observed by measuring the water contact angle at different time intervals. The optical energy bandgap was calculated by using Tauc plot from the UV-Vis transmission spectra.

The influence of precursor flow ratios and RF power on the energy bandgap was studied.

3.2.1 FTIR studies of films deposited at different oxygen flows and RF power

The FTIR spectrum of TiO_x films showed the formation of a broad Ti-O-Ti peak around 430cm^{-1}, which was characteristic of Ti-O-Ti vibration [181,182], figure 22 & 23. The peak around 650 cm^{-1} corresponds to Ti-O-Ti vibration [183,184]. The broad peak centered around 3270 cm^{-1} and 1640 cm^{-1} were due to the hydroxyl and Ti-OH groups [185]. The peaks corresponding to Ti-H vibration and CH vibration appeared around 1600 cm^{-1}. Several peaks at 1358, 1528 and 1583 cm^{-1} corresponds to organic solvents from TIP [186].

Broad band in the 900 -500 cm^{-1} intervals may be assigned to the Ti-O bond [187]. The low absorption intensity due to the Ti-O bonds in most spectra may be related to the amorphous nature of the films and to further distortions on their structure due to the incorporation of carbon and excess oxygen. There was no significant difference observed in the FTIR spectra with increase in oxygen flow except for the film deposited at floating potential with 250 sccm oxygen. The film deposited at 250 sccm of oxygen at floating potential had higher hydrocarbon contents than all other films. The peak at 640 cm^{-1} corresponds to Ti-O-Ti vibration. The presence of high intensity hydrocarbon peaks will increase the hydrophobicity of the film.

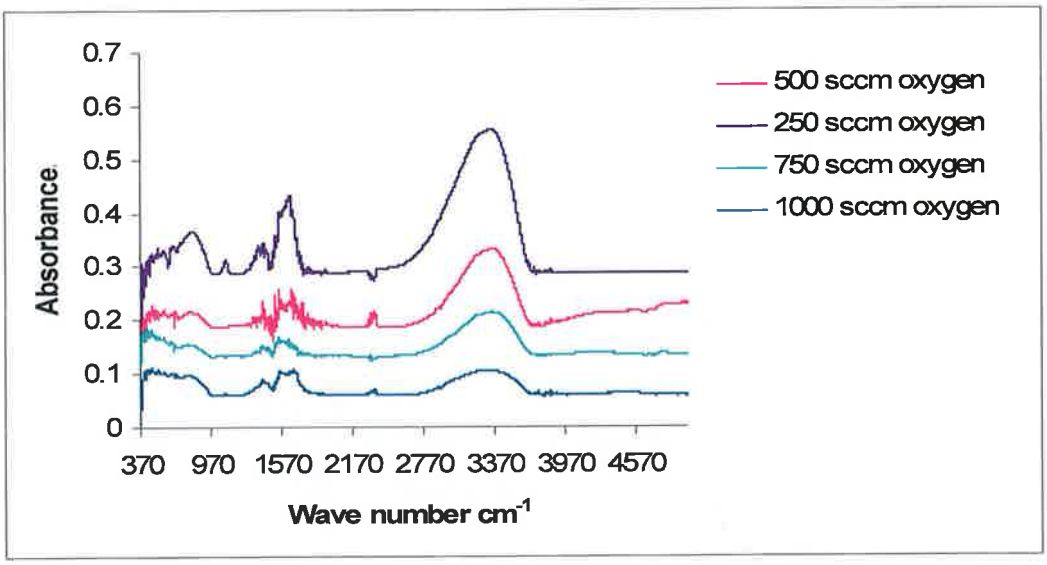

Figure 22 FTIR spectrum of TiOx films deposited at floating potential with varying oxygen flows at 250 W RF power

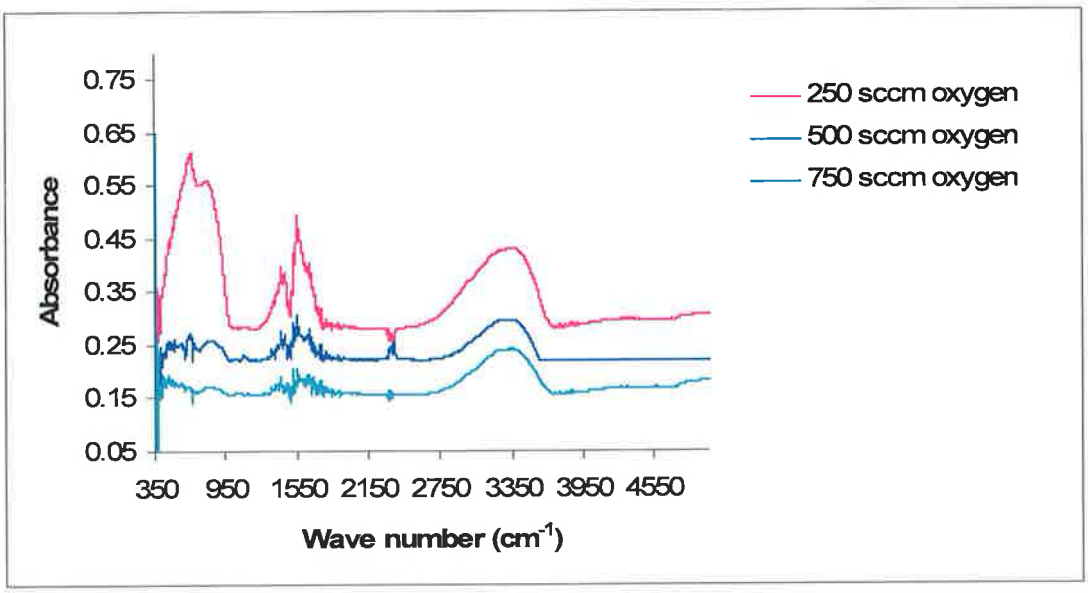

Figure 23 FTIR spectrum of TiOx films deposited on powered electrode with varying oxygen flows at 250 W RF power

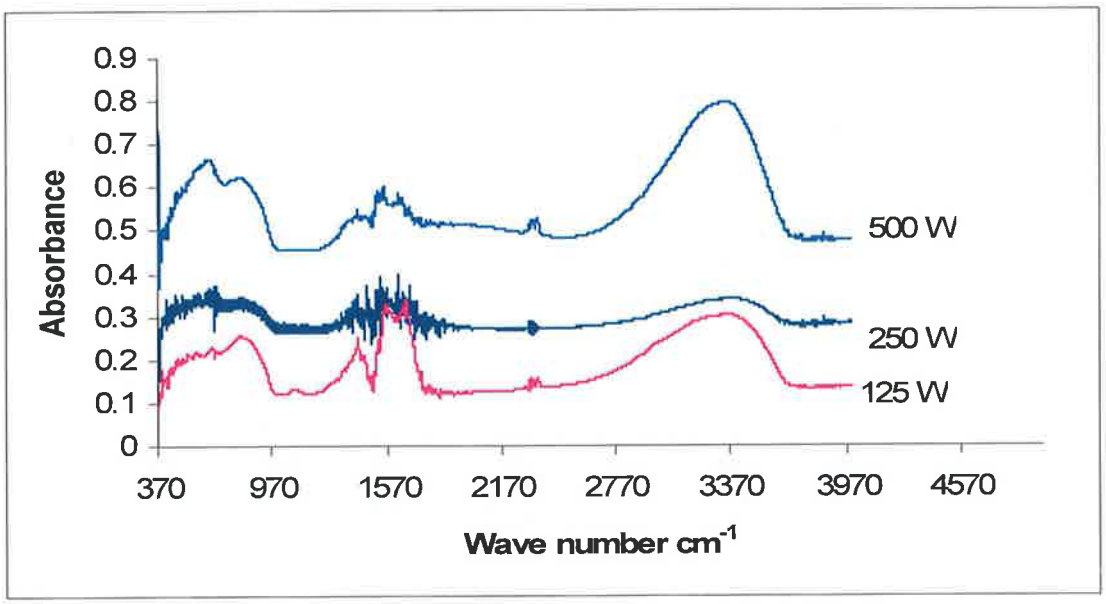

Figure 24 FTIR spectrum of TiOx films deposited at varying RF power, for fixed oxygen flow of 500 sccm on powered electrode

The TiO_x films with an oxygen flow of 500 sccm were deposited at three different RF powers to study the influence of RF power on the film properties. The broad peak between 400 and 550 cm^{-1} corresponded to Ti-O-Ti vibration. The broad peak centered around 3300 cm^{-1} and 1640 cm^{-1} corresponded to hydroxyl groups. It was observed that at low RF power (125 Watts) the hydrocarbon content, 1580 cm^{-1} were present in significant amount along with a Ti-O-Ti and OH stretching vibration. As the RF power increased, the hydrocarbon contents decreased.

3.2.2 Variation of deposition rate with varying oxygen flows on floating and powered electrode

The deposition rate was calculated by measuring the film thickness using spectroscopic ellipsometry and then dividing the film thickness by deposition time. It was observed that the deposition rate decreased with increase in oxygen flow. This was because, at low oxygen flow the contribution of hydrocarbon content to film formation was more and hence the deposition rate was high. As the oxygen flow was increased, the hydrocarbons in the precursor were oxidized and were pumped out of the chamber resulting in decreased deposition rate. At high oxygen flow, the film

was more TiO_x like. There was no significant variation in the deposition rate between the films deposited at floating potential and on the powered electrode.

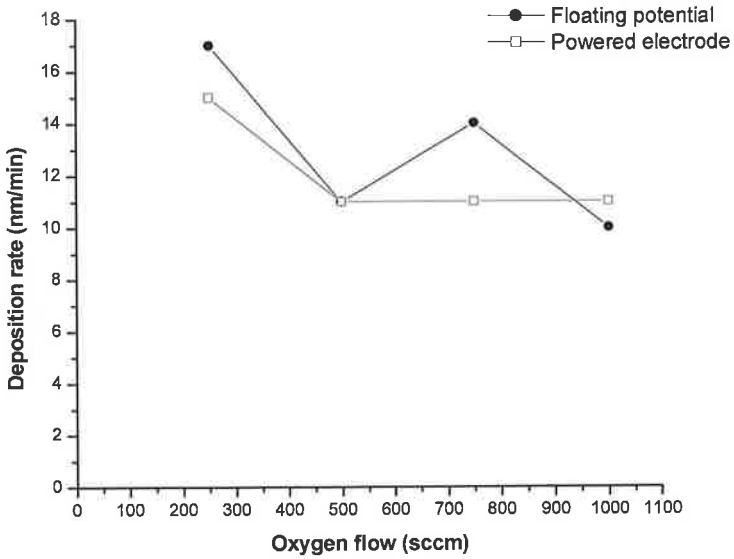

Figure 25 Variation of deposition rate with oxygen:TIP flow ratio for films deposited at floating potential and on powered electrode at 250 W RF power

3.2.3 Variation of water contact angle with flow ratios and RF power

Figure 26 showed the variation of water contact angle with various oxygen flows deposited at a fixed RF power. The water contact angle for the films deposited at 250 sccm oxygen and at floating potential was very high indicating the presence of a hydrophobic layer. FTIR spectra in figure 22 showed the presence of intense hydrocarbon peaks for the film deposited at floating potential at 250 sccm oxygen flows. That contributed for the observed higher water contact angle. As the flow ratio was increased the contact angle decreased and it do not decrease with further increase in flow ratio. There was no significant change observed in the FTIR spectrum with increase in oxygen flow. The films deposited at floating potential and on the powered electrode did not show any significant difference in the water contact angle except for the films deposited at an oxygen flow of 250 sccm.

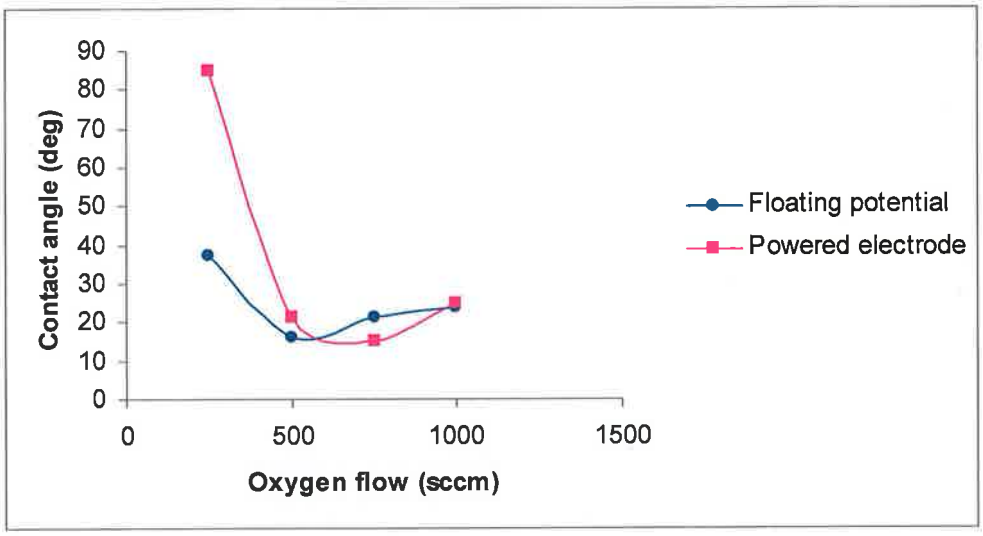

Figure 26 Water contact angle analysis of films deposited at different oxygen flows and at 250 W RF power

The RF power influenced the water contact angle to a significant extent for films deposited at a fixed oxygen flow of 500 sccm, figure 27. At low RF power, 125 W, the contact angle was high around 30° and 50° for films deposited on powered electrode and at floating potential. The increase in RF power decreased the contact angle to around 20° for both the films and a further rise in RF power increased the contact angle to around 50°. A minimum contact angle of 20° could be attained with an optimum oxygen flow of 500 sccm at a fixed TIP flow and a fixed RF power of 250 W.

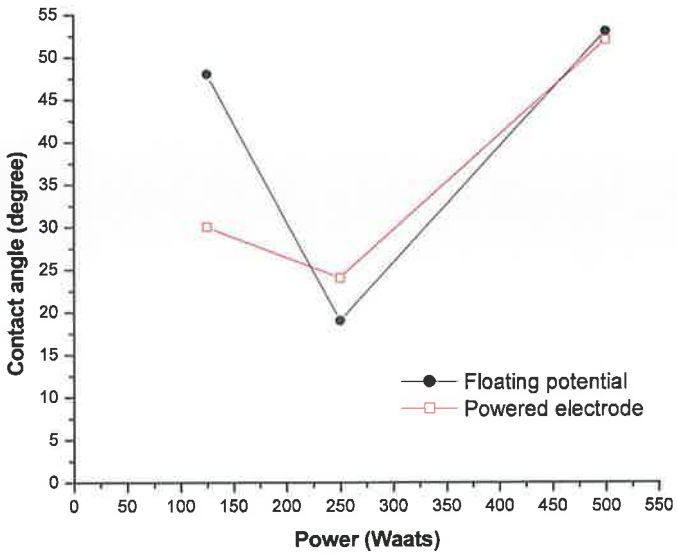

Figure 27 Variation of water contact angle with RF power for films deposited at 500 sccm oxygen

Unlike Si based coatings, a further rise in RF power to 500 W increased the contact angle. The FTIR spectra did not show any significant difference between the films deposited at various RF powers, fig 24. Hence the reason for the rise in water contact angle at 500 W is still not clear.

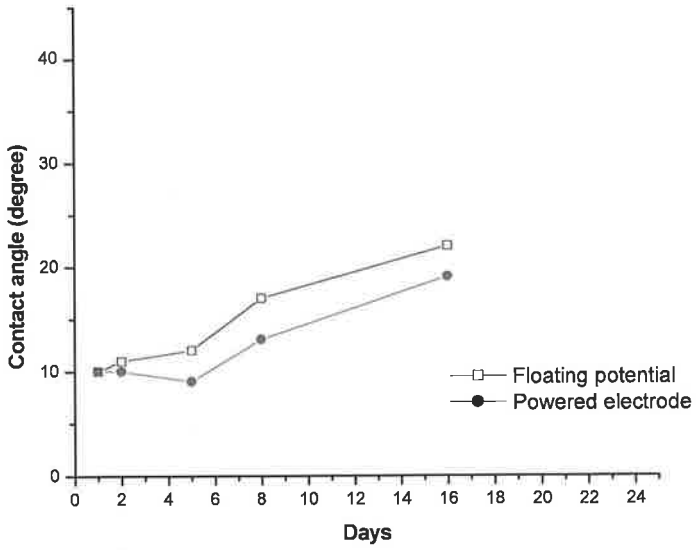

Figure 28 Variation of contact angle with time for TiO_x film deposited at 250W with an oxygen flow of 500 sccm on powered electrode and at floating potential

The contact angle measured immediately after deposition showed the presence of a very hydrophilic surface with contact angle less than 10^o. Over a period of time the contact angle increased gradually but still it remained hydrophilic with a contact angle of 20^o even after 2 weeks time. Both the floating potential and powered electrode deposited films behaved in the same way, with the difference between the two being very less.

3.2.4 Bandgap measurement of films deposited at different oxygen:TIP flow ratios and RF power

The sharp decrease in transparency of the films in the UV region was caused by the fundamental light absorption in the semiconductor. Figure 29 shows the UV-Vis transmittance spectra of TiO_x films deposited at 500 sccm oxygen flow at 250 W RF power. The fundamental light absorption corresponds to the bandgap of the film.

By plotting a graph between hν and $(\alpha h\nu)^{1/2}$ and extrapolating the curve to zero the energy band gap can be calculated. The reason for plotting the graph between hν and $(\alpha h\nu)^{1/2}$ is given in section 3.1.5 When the curve is extrapolated to zero the X intercept which is the energy gives the optical bandgap of the film.

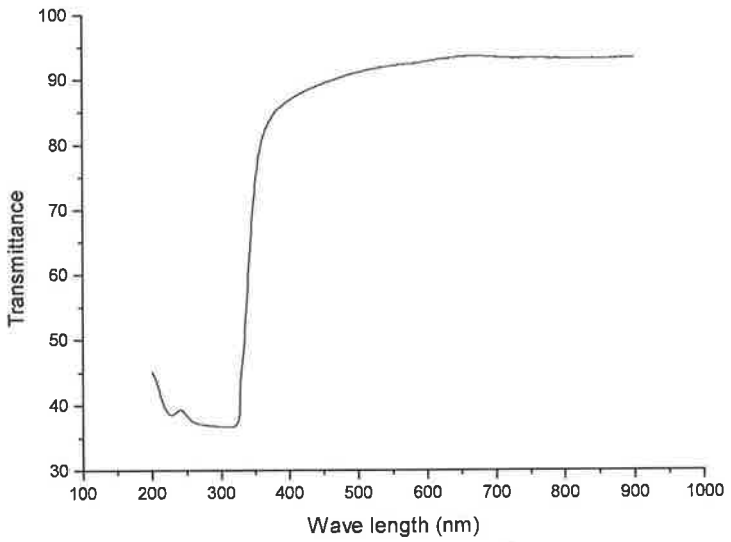

Figure 29 UV-Vis spectra of TiO_x films deposited at 500 sccm oxygen flow at fixed RF power 250 W.

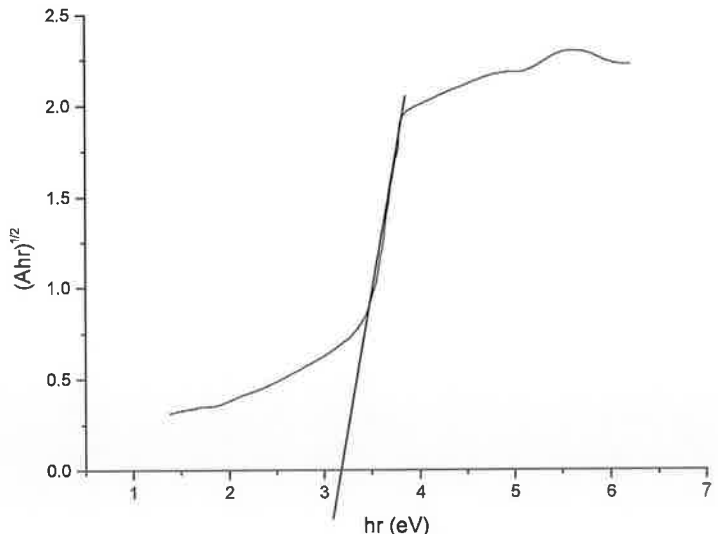

Figure 30 The graph between hν and $(\alpha h\nu)^{1/2}$ (Tauc plot) of TiOx film deposited at 250 W for 500 sccm oxygen flow

It was evident from the figure 30 that when extrapolated to zero the X intercept gives a value of 3.18 eV. Thus the optical bandgap of TiO_x film deposited at an oxygen flow of 500 sccm and fixed TIP and RF 250 W calculated by using Tauc plot was estimated to be 3.18 eV

TiO_x film deposited at an oxygen flow of 500 sccm had its fundamental light absorption at a much higher wavelength than when compared to other oxygen flows. The optical bandgap values of TiO_x films deposited at various oxygen flows and a fixed RF and TIP flow were shown in figure 31.

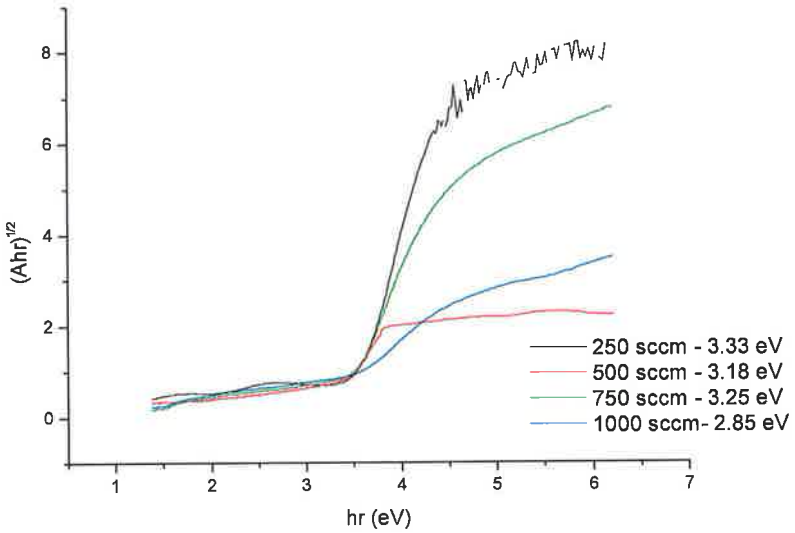

Figure 31 The graph between hν and $(\alpha h\nu)^{1/2}$ (Tauc plot) of TiO_x film deposited at 250 W for varying oxygen:TIP flow ratio

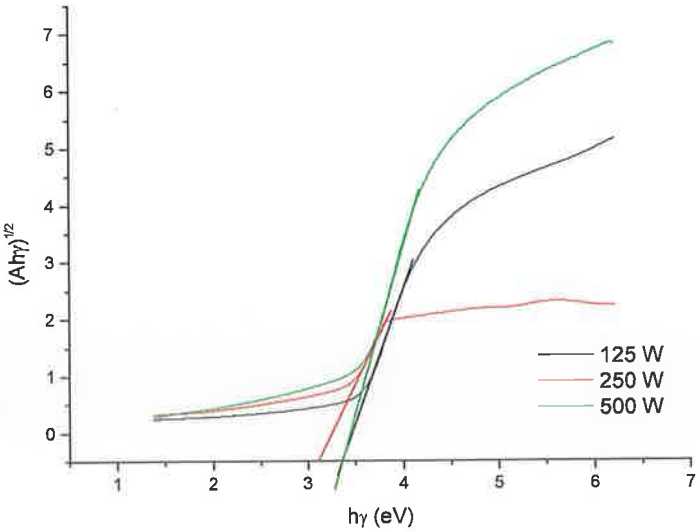

Figure 32 The graph between hν and $(\alpha h\nu)^{1/2}$ (Tauc plot) of TiO_x film deposited at varying RF power and fixed oxygen:TIP flow ratio of 500:n

The films deposited at an RF power of 500 W seem to have its absorption edge at higher wavelength than that deposited at 125 W and 250W, figure 32. The bandgap

values are 3.33 eV, 3.18 eV and 3.38 eV for 125 W, 250 W and 500 W respectively. The energygap was lower for 250W deposited films than that for 125 and 500 W deposited films. The energy gap of 3.18eV for 250W deposited films was in close agreement with the bandgap measurements calculated by G.A. Battiston et al [188] and G.K. Boschloo et al., [189]. How ever the bandgap values of TiO_x films deposited at 125 W and 500 W were also in agreement with the works done by Feng Zhang et al [190]. The contact angle data showed that the water contact angle for 250W deposited films was lower than that for 125 W and 500 W deposited films. Hence an RF power of 250 W lead to the formation of TiO_x film with better hydrophilicity and bandgap values that were in good agreement with the literature.

3.2.5 Energy dispersive analysis by X-ray (EDS) studies

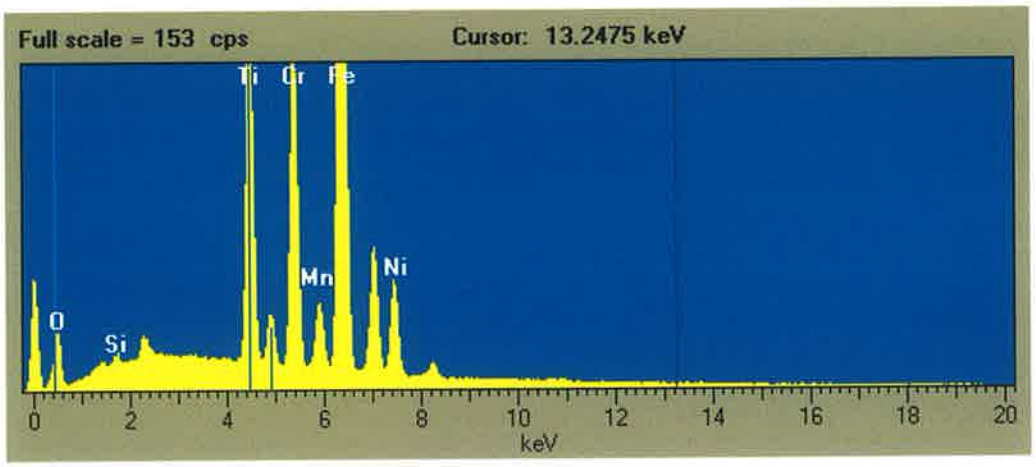

Figure 33 EDS spectrum of TiO_x films deposited at 250W RF power with oxygen:TIP flow ratio of 500:n

Elementt	Spect Type	element %	Atomic %
O K	ED	11.07	29.71
Si K	ED	0.40	0.62
Ti K	ED	12.69	11.37
Cr K	ED	13.65	11.27
Mn K	ED	01.07	00.84
Fe K	ED	51.89	39.88

Ni K	ED	07.72	05.64
Mo L	ED	01.51	00.68
Total		100.00	100.00

The TiO_x films deposited on 316L stainless steel with an oxygen flow of 500 sccm at 250W was analysed by energy dispersive analysis by X-ray (EDS) for the composition studies. The EDS spectrum in figure 33 confirmed the presence of titanium (Ti) and oxygen (O) from the film along with chromium (Cr), iron (Fe), manganese (Mn) and nickel (Ni) which came from the 316L steel substrate. The atomic percentage of Ti was 11.37% and O was 29.71 %. The excess oxygen might have come from the steel substrate.

3.3 Characterization of Si-Ti mixed oxide coatings

The silicon and titanium mixed oxide coatings were deposited by using the organic precursors HMDSO) and TIP containing silicon and titanium respectively along with the oxygen gas. For depositing either Si or Ti based oxide coatings any of the two precursors alone was used. But in the case of mixed oxide coatings both the precursors had to be used at the same time which resulted in hydrocarbon rich plasma. Hence the HMDSO and TIP flow had to be kept minimum, while maintaining a high oxygen flow to deposit an oxide film with less hydrocarbon incorporation in it. The high oxygen flow oxidized the hydrocarbons in the plasma reducing the possibility of formation of hydrocarbon rich films. The objective of this coating was to deposit a Si-Ti mixed oxide film with minimum water contact angle and maximum energy bandgap. The films were first characterized by Ellipsometry, FTIR and then the water contact angle was measured. The optical energy bandgap was determined by using a Tauc plot from the UV-Vis absorbance spectra. In all the mixed oxide depositions the HMDSO flow was fixed at 15 sccm, TIP flow was kept constant through a needle valve and the oxygen flow was controlled through a mass flow controller.

3.3.1 FTIR studies of films deposited at different oxygen:HMDSO:TIP flow ratios and RF power

The FTIR spectroscopic investigation of all the coatings showed the presence of three characteristic peaks of Si-O-Si centered around 450 cm^{-1}, 800 cm^{-1} and 1070 cm^{-1} [191] as shown in figure 34. The band at 450 cm^{-1} corresponded to both Si-O and Ti-O vibrations [192,193]. A wide band lying between 3000 cm^{-1} and 3650 cm^{-1} corresponded to the stretching vibrations of hydroxyl groups. The methyl silyl peaks which appeared at 1278 cm^{-1} in the case of $SiO_xC_yH_z$ films did not appear for the mixed oxide coatings indicating the oxidation of hydrocarbons in the plasma leaving behind a SiO-TiO mixed coating.

The films deposited on both powered electrode and at floating potential have the Si-O-Ti characteristic peak centered between 910 cm^{-1} and 940 cm^{-1} [194,195,196]. The maximum temperature during deposition on the floating potential electrode, with maximum RF power, was less than 55° and that for the powered electrode was around 95°. The peak centered between 910 cm^{-1} and 940 cm^{-1} corresponded to both Si-O-Ti and OH bonded to Si and Ti i.e. SiOH and TiOH. In the case of HMDSO based coatings the films deposited on the powered electrode did not show the presence of SiOH bond formation due to the observed higher temperature, figure 4 and figure 5. Hence it was clear in figure 33 that the peak at around 910 cm^{-1} was due to the formation of Si-O-Ti bond that may or may not contain overlapping SiOH and TiOH bonds.

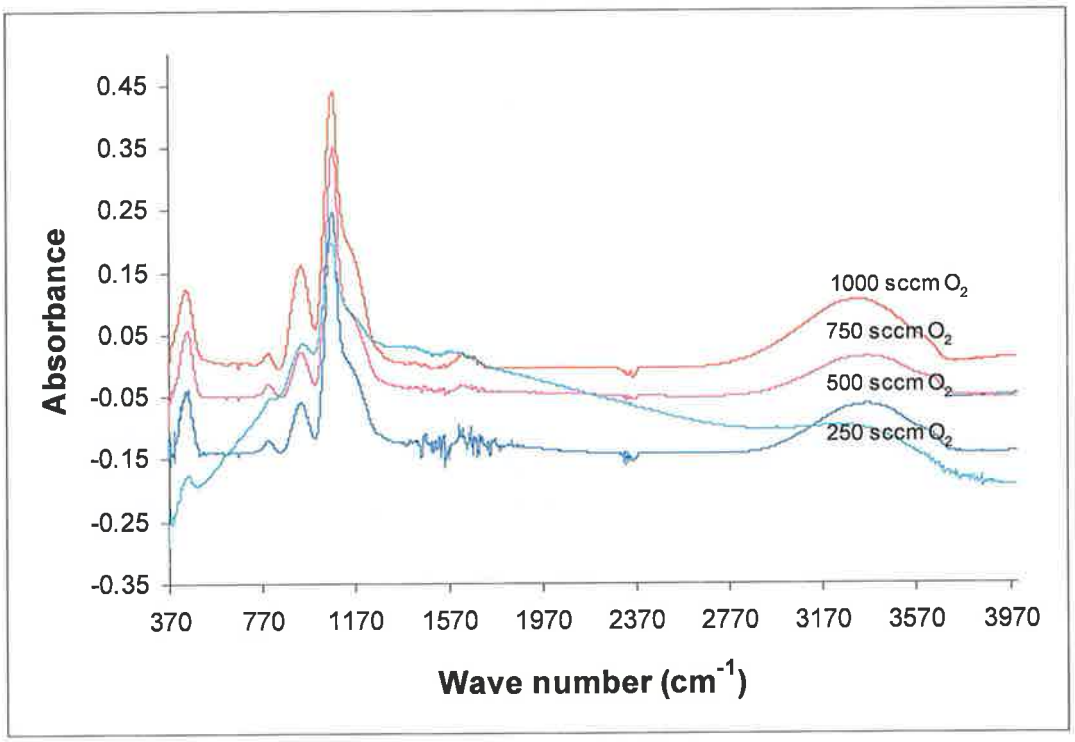

Figure 34 FTIR spectra of mixed oxide coatings deposited at various oxygen flows at fixed HMDSO (15 sccm) and TIP flow rate (n) deposited at 250 W RF power at floating potential

The peak around 910 cm^{-1}, in figure 36, 125 W, corresponded to hydroxyls bonded to Si and Ti and the peak at 935 cm^{-1} , 500 W, corresponded to Si-O-Ti vibrations [197]. In figure 34, at 125 W, the peak around 910 cm^{-1} corresponded to the hydroxyl group that may or may not be overlapped with Si-O-Ti. At 250W the broad band around 923 cm^{-1} confirmed the presence of both hydroxyl groups and Si-O-Ti linkage. At 500 W, it was clear that the hydroxyl group was missing and the only dominating peak next to Si-O-Si was Si-O-Ti centered around 935 cm^{-1}. A wide band lying between 3000 cm^{-1} and 3650 cm^{-1} correspond to the stretching vibrations of hydroxyl groups.

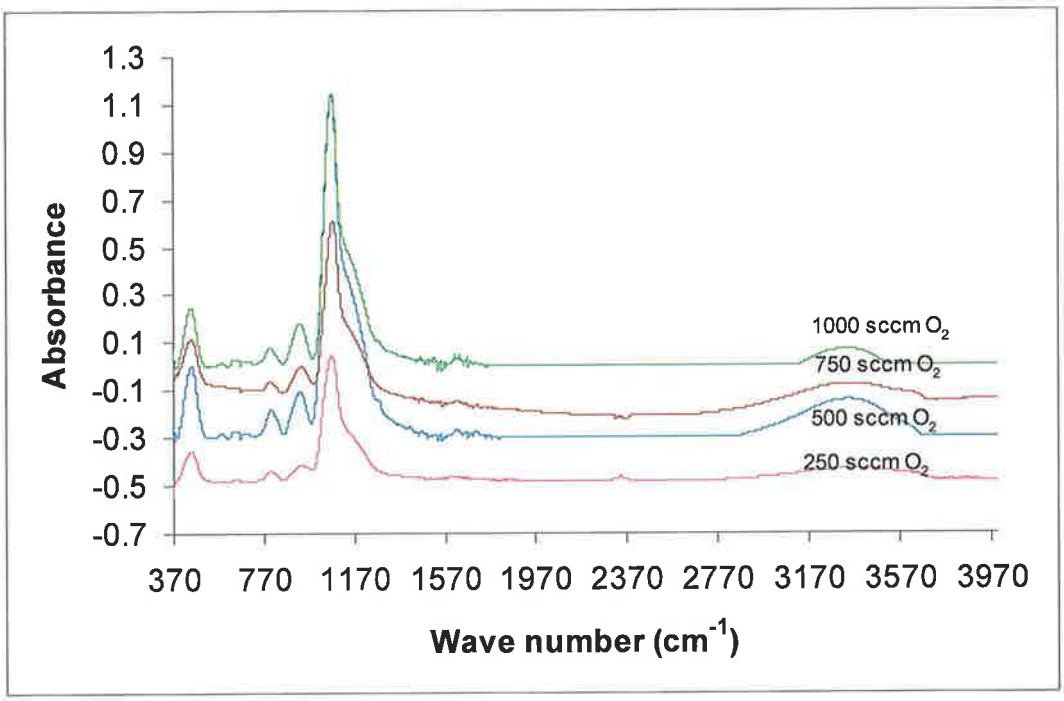

Figure 35 FTIR spectra of mixed oxide coatings deposited at various oxygen flows at fixed HMDSO (15) and TIP (n) flow rates deposited on powered electrode at 250 W RF power

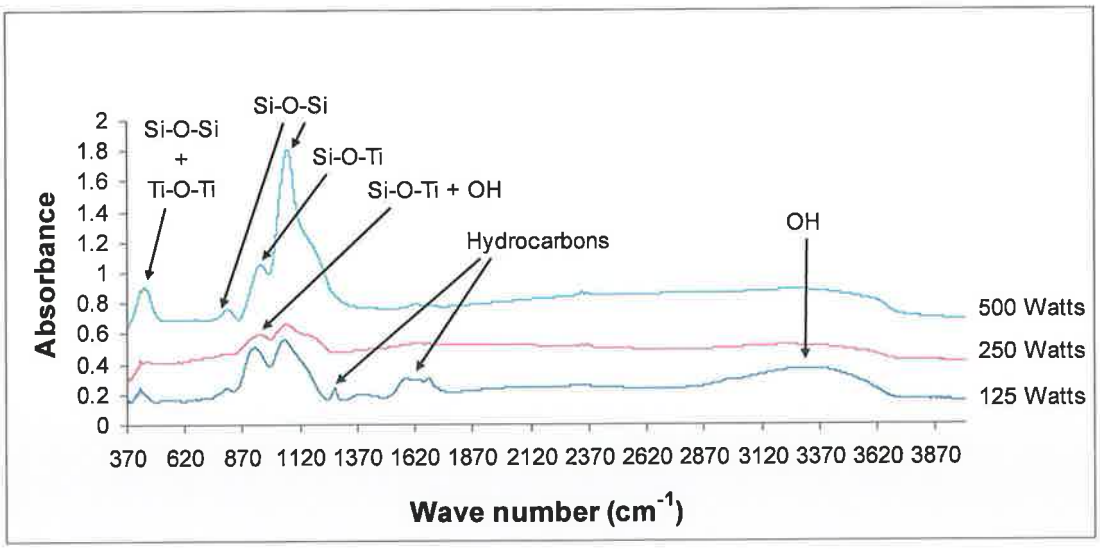

Figure 36, FTIR spectroscopic investigation of mixed oxide coatings deposited at various RF powers for 500 :15:n oxygen:HMDSO:TIP flow ratio

3.3.2 Variation of deposition rate with Oxygen:HMDSO:TIP flow ratios on floating and powered electrode

The deposition rate was calculated by measuring the film thickness using spectroscopic ellipsometry and then dividing it by deposition time. Since the oxygen flow was kept high the deposition rate did not vary with oxygen:HMDSO:TIP flow ratio i.e., the precursor flow ratios did not influence the deposition rate, in figure 37. This behaviour was similar to HMDSO based coatings deposited at high oxygen:HMDSO flow ratio as shown in figure 11. As the oxygen flow was increased the hydrocarbons in the precursor got oxidized resulting in very low contribution of hydrocarbons to film formation. Above an oxygen:HMSO:TIP flow ratio of 500:15:TIP the hydrocarbon contribution to film formation was nearly the same. Hence the deposition rate did not vary with flow ratios in the case of mixed oxide coatings.

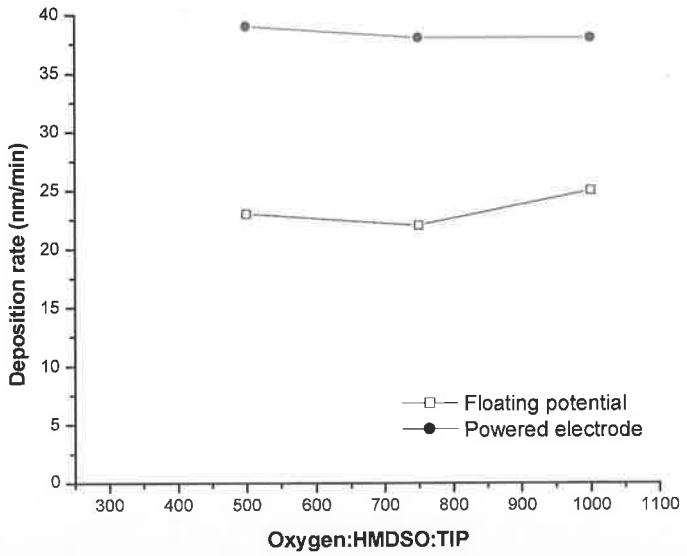

Figure 37 Variation of deposition rate with increase in oxygen flows at fixed HMDSO (15 sccm) and TIP flow for films deposited at floating potential and on powered electrode at 250 W

The deposition rate of floating potential deposited films was lower than that of the powered electrode deposited films. This was due to greater ion flux to the powered electrode. This behaviour was again similar to HMDSO based coatings where the deposition rate of powered electrode deposited films were always higher than that of floating potential deposited films. The deposition rate in the case of mixed oxide

deposition was considerably higher than that of TiO_x deposition rate but quite close to the SiO_x deposition rate.

3.3.3 Variation of water contact angle with flow ratios and RF power

The water contact angle depends on the polarity of the surface. By increasing the polarity, it was possible to increase the hydrophilicity [198]. The difference in electronegativity between the Si (1.9 on Pauling's scale) and O (3.44 on Pauling's scale) atoms makes the SiO_2 molecule polar, which helped hydrogen bonding with the hydroxyl groups of water. The wettability of silica-like film could be further increased by increasing the polarisation, which would create the possibility for formation of more hydrogen bonds between the water and the film. This was done by incorporating the more electronegative titanium (1.54 on Pauling's scale) in the film. The water contact angle of silicon-titanium mixed oxide coatings varied from around 80^o up to 40^o depending on the hydrocarbon content, hydroxyl groups and polar component in the film. The film with least hydrocarbon and most hydroxyl groups had a lower water contact angle

Figure 38 showed the variation of water contact angle with oxygen:HMDSO:TIP flow ratio deposited at a fixed RF power of 250 W. The water contact angle stayed around 40 deg for all the precursor flow ratios and for both floating potential and powered electrode deposited films. There was no significant change observed in the FTIR spectrum with increase in oxygen:HMDSO:TIP flow ratio, figure 34, 35. Hence the contact angle data correlated well with the observed FTIR spectra. The films deposited at floating potential and on powered electrode did not show any significant difference in the water contact angle. This behaviour was similar to that of TiO_x films deposited from oxygen and TIP but the contact angle of TiO_x film was around 20 deg and that of SiO-TiO was around 40 deg.

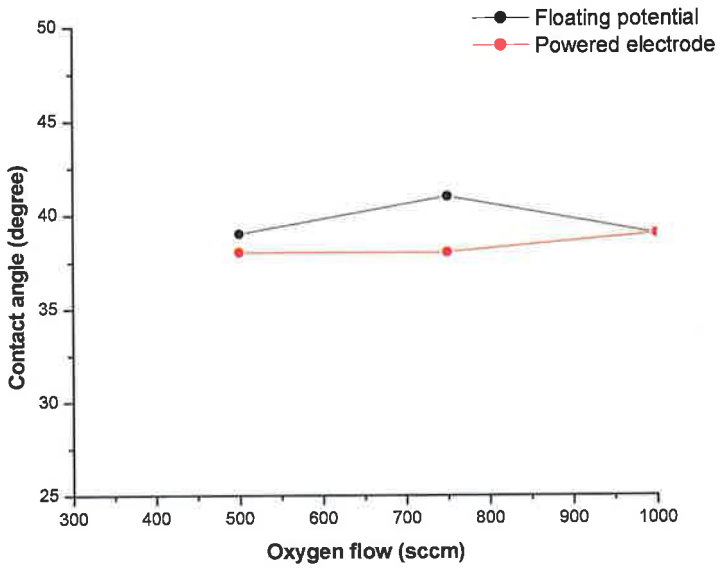

Figure 38 Variation of water contact angle with various oxygen flow at fixed HMDSO (15 sccm) and TIP (n) flow rate deposited at 250 W RF power

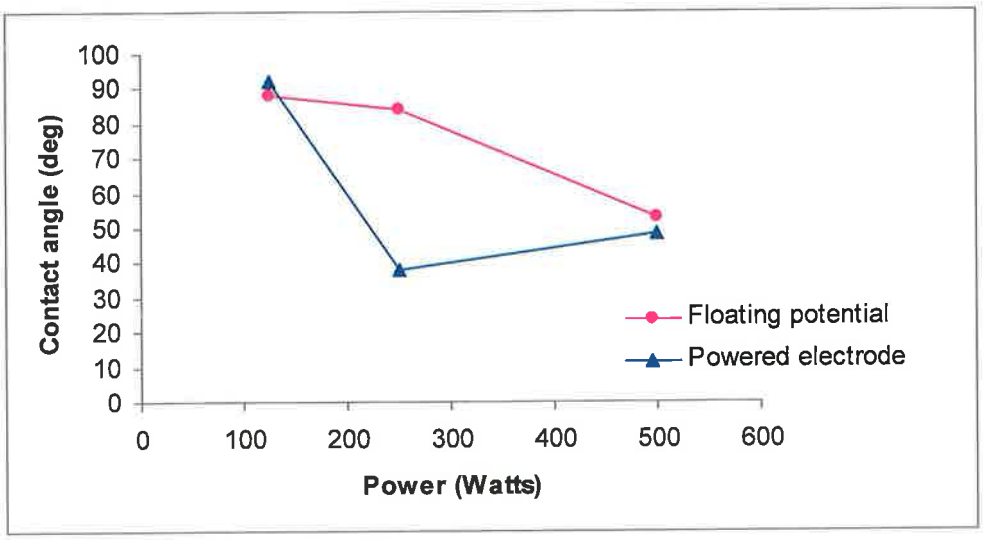

Figure 39 Variation of contact angle with RF power for films deposited with a flow ratio of 500:15:n (oxygen:HMDSO:TIP)

The effect of RF power on the film properties was studied, figure 39. As the RF power was increased from 125 W to 500 W, the water contact angle of the mixed coating initially decreased significantly and then increased slightly, as shown in figure 39. The observed change in contact angle with increase in RF power was explained by FTIR studies in figure 36. At low RF power, 125 W, the peak around

910 cm^{-1} correspond to OH and Si-O-Ti linkages, figure 36. Although the Si-O-Ti peak was supposed to decrease the water contact angle, the bands due to hydrocarbon linkages centered around 1268 cm^{-1}, 1345 cm^{-1}, 1569 cm^{-1} , and 1670 cm^{-1} made the film hydrophobic. As the RF power was increased, the fragmentation of precursor increased. This resulted in decreased hydrocarbon content. At 250 W, the hydrocarbon contents in the film were much less, whereas the peak around 923 cm^{-1} was broadened, indicating the presence of both hydroxyl groups and Si-O-Ti linkages which contributed to the observed hydrophilicity. Studies have suggested that hydroxygenated TiO_x films were more hydrophilic than TiO_2 films [199]. At much higher RF power, 500 W, the peak around 935 cm^{-1} was narrow indicating the presence of Si-O-Ti band. The loss of hydroxyl group bonded to Si or Ti could have come from the fact that the temperature of the substrate holder was much higher than that on the lower RF powers. This resulted in a slight increase in water contact angle but still much lower than that for the SiO_x film.

3.3.4 Bandgap measurement of films deposited at different oxygen:HMDSO:TIP flow ratios and RF power

The sharp decrease in transparency of the films in UV region was caused by the fundamental light absorption in the semiconductor.

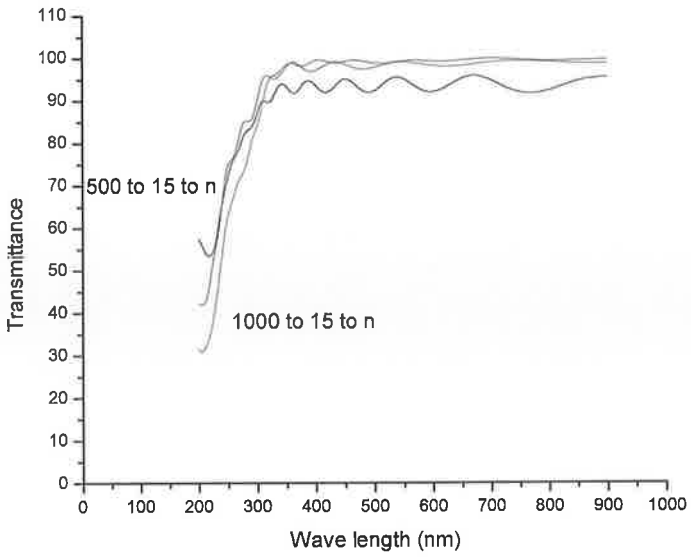

Figure 40 UV-Vis spectra of mixed oxide coatings deposited at different oxygen:HMDSO:TIP flow ratios and at fixed RF power of 250 W.

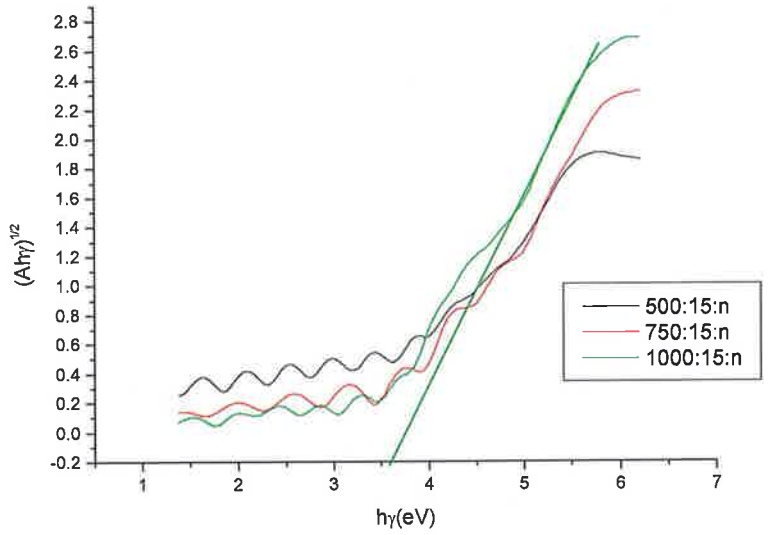

Figure 41 The graph between hν and $(\alpha h\nu)^{1/2}$ of mixed oxide coatings deposited at 250 W for 500:15:n oxygen:HMDSO:TIP flow ratio

The bandgap of the films deposited with three different oxygen flows 500 sccm, 750 sccm and 1000 sccm with fixed HMDSO (15 sccm) and fixed TIP flow (n) was calculated by using Tauc plot as explained in section 3.1.5. There was no significant variation observed in the optical bandgap values of the films with various oxygen:HMDSO:TIP flow ratios.

The bandgap values calculated from the above graphs are listed below.

1. 500 oxygen: 15 HMDSO:n TIP- 250W TE - 3.80 eV
2. 750 oxygen: 15 HMDSO:n TIP- 250W TE - 3.76 eV
3. 1000 oxygen:15 HMDSO:n TIP- 250W TE - 3.67 eV

The FTIR measurements and the contact angle analysis did not show any significant difference for the films deposited at various oxygen:HMDSO:TIP flow ratios.

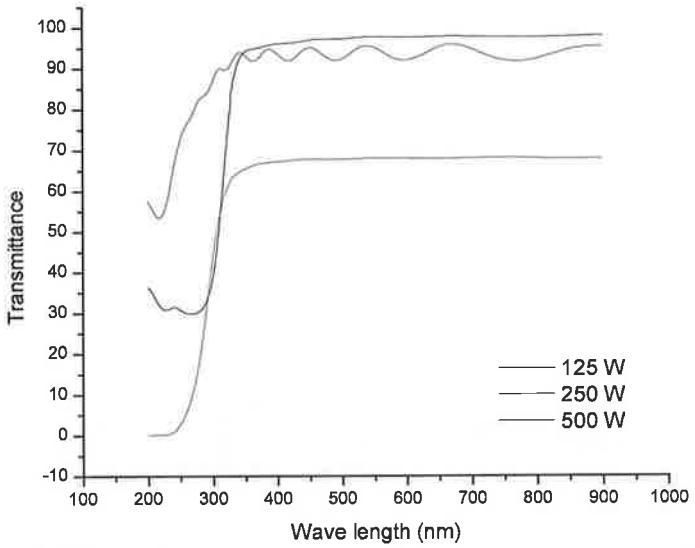

Figure 42 UV-Vis absorbance spectra of 500:15:n , oxygen:HMDSO:TIP flow ratio films deposited at various RF powers.

The films deposited at an RF power of 250 Watts had the optical absorbance edge at a higher wavelength region than that deposited at 125 and 500 Watts, figure 42. A bandgap of 3.80 eV for the films deposited at 250 W was close to that of the film deposited at 500 W with a bandgap of 3.76 eV. A low deposition power of 125 W gave a bandgap of 3.45 eV. A higher bandgap observed at 250 and 500 W was due to the formation of hydrocarbon less Si-Ti mixed oxide coatings which was confirmed in the FTIR and contact angle analysis. G. Lassaletta et al., obtained a bandgap value of 4.1 eV for the Si-O-Ti interface [200] and Xingtao Gao et al., also observed an increase in bandgap of TiO_2 film with Si incorporation [201]. 3.80 eV for 250 W deposited SiO-TiO film was close to the value obtained by G. Lassaletta et al.,

3.3.5 Energy dispersive analysis by X-ray (EDS) studies

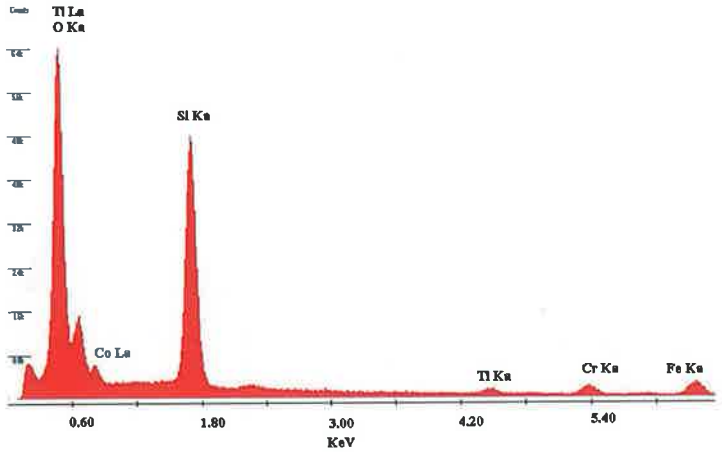

Figure 43 EDS spectrum of SiO-TiO oxide coatings deposited on 316L stainless steel at 250 W RF power with 500:15:n, oxygen:HMDSO:TIP flow ratio

Figure 43 showed the presence of Ti, Si and O along with the peaks corresponding to Co, Cr and Fe that were from the stainless steel substrate. In figure 43, the Ti La peak overlaps with O Ka peak and hence the peak at 0.5 keV corresponded to Ti + O [202]. A small peak at 4.5 keV was also observed for Ti Ka and Si Ka peak was observed at 1.74 keV [203].

3.4 Summary

Polymer-like ($SiO_xC_yH_z$) films, silica-like (SiO_x), titanium oxide (TiO_x) and silicon-titanium mixed oxide (SiO-TiO) coatings had been deposited. It was observed that by controlling the plasma process parameters including oxygen:HMDSO flow ratio, flow rate and RF power the surface chemical and mechanical characteristics could be tailored.

- High oxygen:HMDSO flow ratio resulted in a hard silica-like SiO_x coating and low flow ratio resulted in a soft polymer-like $SiO_xC_yH_z$ coating.
- The decrease in refractive index and increase in film density with increase in oxygen:HMDSO flow ratio correlated well with the observed surface chemical and mechanical characteristics.

- The increase in wettability with increase in flow ratio was due to the formation of polar SiO_x coating that was evident from FTIR and refractive index measurements.

- The increase in film density and nano hardness with increase in flow ratio was due to the decrease in hydrocarbon and increase in Si-O bonding in the film.

- The increase in film density and nano hardness with increase in RF power confirmed the formation of a dense layer at high RF powers.

- The increased refractive index at higher RF powers was because of the formation of a silicon rich sub-stoichiometric SiO_x film.

- Wettability and nano hardness could be increased by increasing the RF power.

- The films grown on powered electrode exhibited comparatively higher wettability than the floating electrode deposited films. But the trend was the same for both floating and powered electrode deposited films

- The nano hardness results showed that the floating electrode deposited films did not vary much in their mechanical characteristics with increase in RF power.

A hydrophobic surface with a contact angle of 105° and a stable intermediate contact angle of 60° was obtained with $SiO_xC_yH_z$ and SiO_x coatings respectively. The TiO_x and SiO-TiO coatings had been optimised to get a contact angle of 24° and 38° respectively. The bandgap values were about 9 eV for SiO_x, 3.17 eV for TiO_x and 3.8 eV for SiO-TiO.

4. ADHESION STRENGTH ANALYSIS

4.1 Influence of pre-treatment time and RF power on adhesion strength of $SiO_xC_yH_z$, SiO_x, TiO_x and SiO-TiO coatings on 316L stainless steel

The adhesion strength of the films with the oxygen/HMDSO flow ratio varying from 2:1 to 10:1 at low and high flow rates was tested. It was observed that the polymer-like, low gas flow ratio deposited films had very poor adhesion to the 316L stainless steel. The silica-like film had better adhesion to the steel than the polymer-like film. Figure 44 shows that the adhesion strength was higher for the silica-like films deposited at lower flow rate than that for the films deposited at higher flow rate. Though the standard deviation of low flow rate 10:1 films is significantly higher than all other films, the p values with respect to high flow rate 10:1, high flow rate 2:1 and low flow rate 2:1 were 0.0077, 0.0034 and 0.0043 respectively for a two tailed distribution with unequal variance, which is lower than 0.05 and hence the calculated mean is statistically reliable. It has been reported that the HMDSO film adhesion to polymers and metals can be improved by oxygen plasma pre-treatment of the substrate [204,205]. Hence plasma pre-treatment was done and the adhesion strength measured. In order to study the effect of the plasma pre-treatment time and pre-treatment RF power on the film adhesion, the low flow rate 10:1 gas flow ratio film alone was taken for consideration.

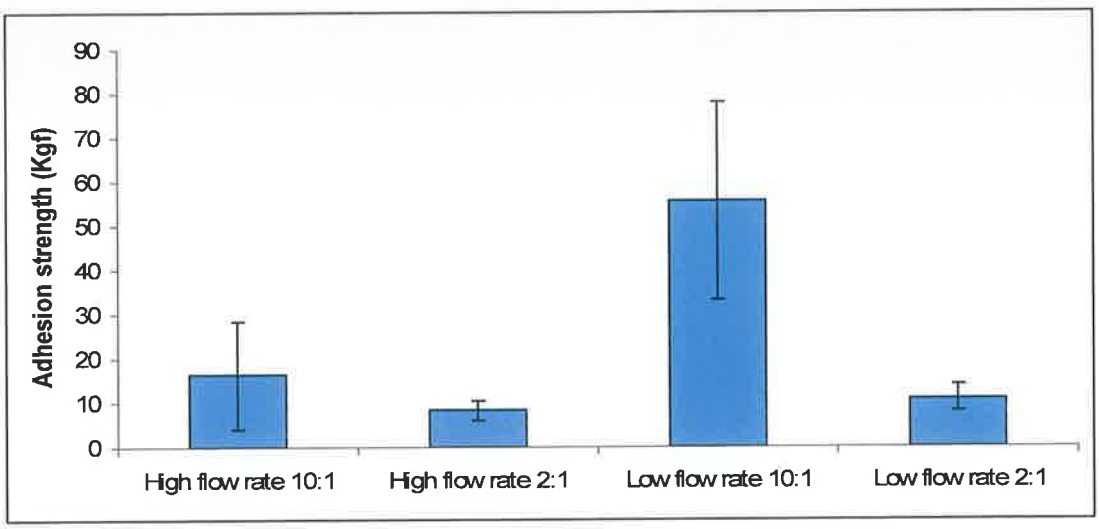

Figure 44 Adhesion strength of various oxygen:HMDSO flow ratio film deposited at 250 W RF power

The effect of plasma pre-treatment on adhesion strength of the silica-like film was studied by using argon, oxygen, Argon + oxygen mixture plasma at various pre-treatment times and pre-treatment RF power.

4.1.1 Effect of pre-treatment RF power on adhesion strength of silica-like SiO_x film

Figure 45 shows the variation of adhesion strength with the pre-treatment RF power for a fixed oxygen/HMDSO ratio of 10:1 deposited at a fixed RF power of 250W. It was observed that the argon+oxygen mixture plasma provides better adhesion over a range of pre-treatment RF powers. Bertrand et al., reported that the argon, nitrogen and ammonia plasma pre-treatment removed the adsorbed hydrocarbon contaminants present on the stainless steel surface and increased the adhesion strength of silica films to stainless steel [206]. The native oxide along with the hydrocarbon contamination can decrease the adhesion strength of the films to stainless steel surface [207,208]. With an increase of pre-treatment RF power, the oxygen plasma decreased the film adhesion. The probable reason for decreased adhesion strength with increase in pre-treatment RF power in oxygen plasma could be that the surface contaminants were modified rather than cleaned by the plasma at higher RF powers that produce highly reactive species. The highest adhesive strength was obtained for the argon+oxygen mixture plasma at a pre-treatment RF power of 250W. The negative bias voltage observed during plasma pre-treatment is shown in Table 6. It was observed that for all the three pre-treatment plasmas the induced bias voltage increased significantly with increase in RF power. The bias voltage was highest for pure oxygen plasma and lowest for the argon+oxygen mixture though the difference between the mixture and pure argon plasma was small. Based on the adhesion strength data of argon, oxygen and argon+oxygen plasma pre-treatments, it was expected that the combined chemical and mechanical effects of oxygen and argon species accounts for enhanced adhesion.

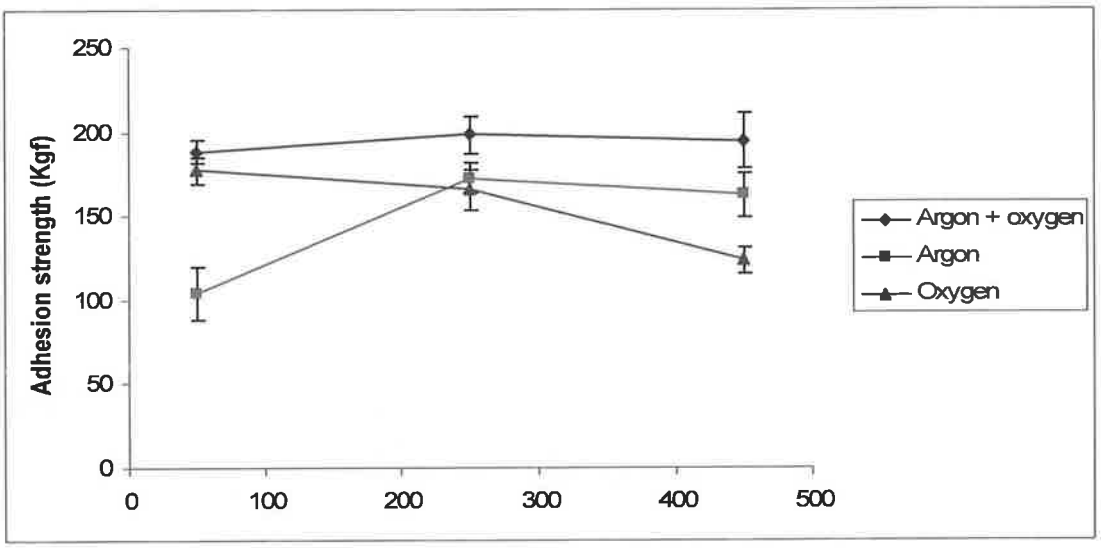

Figure 45 Variation of adhesion strength of SiO_x films with varying pre-treatment RF power

RF Power (Watts)	Negative Bias Voltage (-V)		
	Argon plasma	Oxygen plasma	Argon + Oxygen plasma
50 W	7 V	7 V	3 V
250 W	130 - 170 V	180 - 200 V	140 V
450 W	262 V	313 V	250 V

Table 6 Induced bias voltage measurements of pre-treatment plasmas for SiO_x

4.1.2 Effect of pre-treatment time on adhesion strength of silica-like film

The adhesion strength of the silica-like film (oxygen/HMDSO of 10:1) deposited at a fixed RF power of 250W was analyzed at four different pre-treatment times i.e., 30 seconds, 3 minutes, 5 minutes and 11 minutes as shown in figure 46. It was observed that the adhesion strength increased initially with pre-treatment time and then decreased. In figure 46 in the case of argon plasma, the longer pre-treatment time brought down the adhesion strength to a value similar to that of the untreated stainless steel. The probable reason for the observed decrease in adhesion strength with higher pre-treatment time in argon plasma could be, the mechanical effect

caused by argon plasma at longer duration. A pre-treatment time of 3 minutes provided highest adhesion strength.

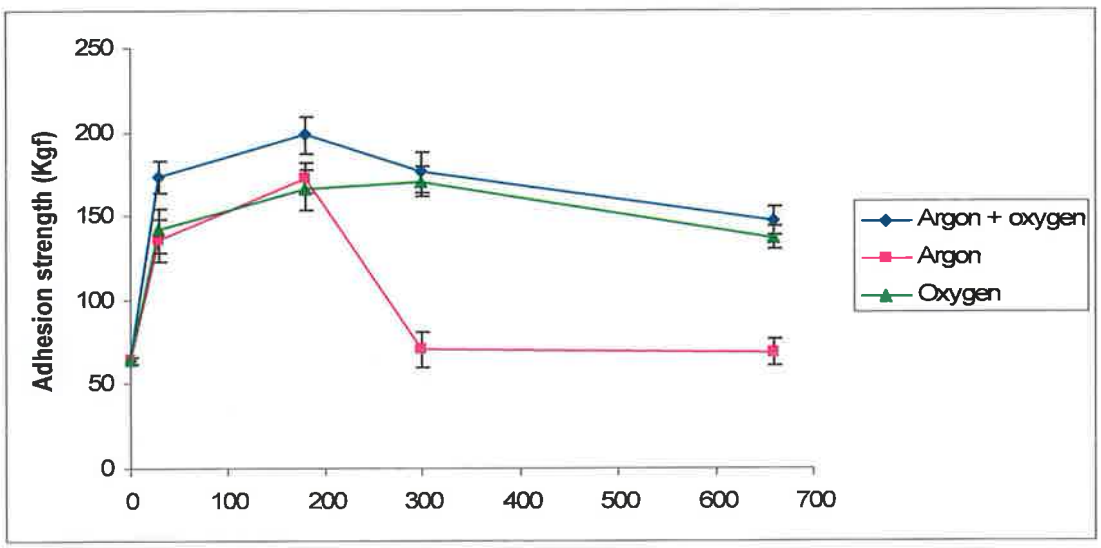

Figure 46 Variation of adhesion strength of SiO_x films with pre-treatment time and with different pre-treatment plasmas

4.1.3 Effect of pre-treatment time on adhesion strength of TiO_2-like films

The adhesion strength of the titanium oxide films, deposited at a fixed RF power of 250W, was analyzed at five different pre-treatment times i.e., 30 seconds, 3 minutes, 5 minutes, 11 minutes and 20 minutes as shown in figure 47.

The adhesion strength increased initially with increase in pre-treatment time from 30 seconds to 3 minutes and then decreased slightly. Though the trend was somewhat similar to SiO_x film behaviour the decrease in adhesion strength with increase in pre-treatment time is very low.

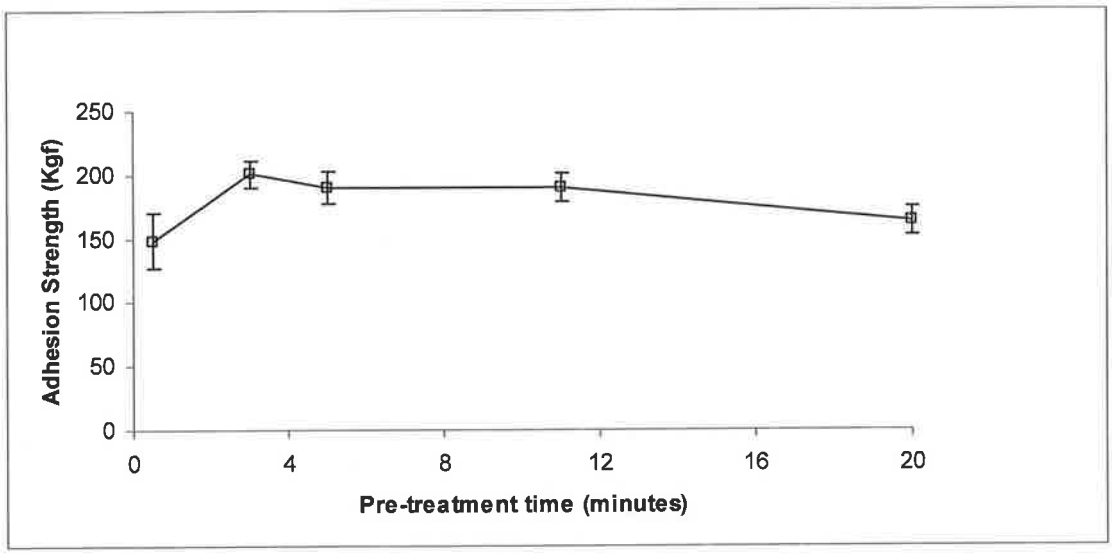

Figure 47 Variation of adhesion strength of TiO_x films with pre-treatment time at fixed pre-treatment RF power (125 W)

4.1.4 Effect of pre-treatment time on adhesion strength of SiO-TiO films

The adhesion strength of the mixed oxide films, deposited at a fixed RF power of 250W, was analyzed at five different pre-treatment times i.e., 30 seconds, 3 minutes, 5 minutes, 11 minutes and 20 minutes as shown in figure 48.

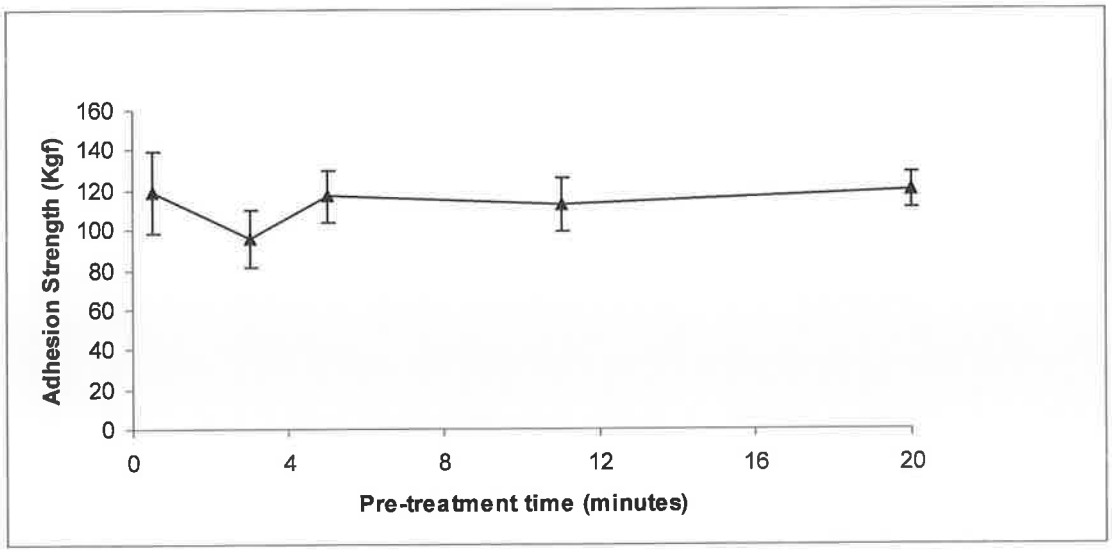

Figure 48 Variation of adhesion strength of SiO-TiO mixed oxide coating with pre-treatment time at fixed RF power (125 W)

Again the adhesion strength was much lower than that of SiO_x and TiO_x films. The reason for the observed lower adhesion strength with mixed oxide coating was not completely understood. As the hydrocarbon contents were more in HMDSO and titanium isopropoxide mixture, we speculated that a thin hydrocarbon layer could have formed in the steel substrates before it was broken down by the plasma resulting in lower adhesion strength than SiO_x and TiO_x films. It was observed that the pre-treatment time did not have any impact on the adhesion strength.

4.1.5 Effect of pre-treatment time on adhesion strength of SiO_2-like, TiO_2-like and SiO-TiO mixed oxide coatings

The effect of plasma pre-treatment time on the adhesion strength, of SiO_x, TiO_x and the mixed coating, to 316L stainless steel was studied by varying the pre-treatment time from 30 seconds to 20 minutes. The plasma pre-treatment was carried out with an argon flow of 50 sccm, oxygen flow of 50 sccm and a fixed RF power of 250 W. The negative induced bias voltage varied from about 100 V to 140 V.

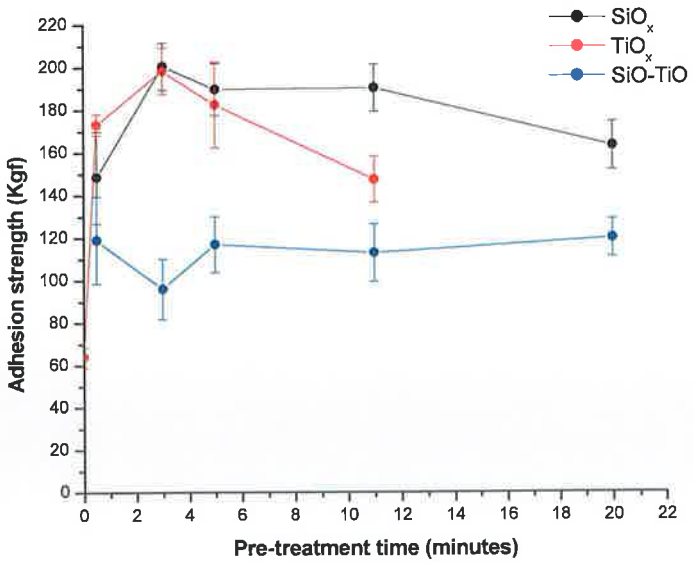

Figure 49 Variation of adhesion strength of SiO_x, TiO_x and SiO-TiO mixed oxide coatings deposited at various pre-treatment time

Figure 49 shows the consolidated graph of the variation of adhesion strength of all the coatings with pre-treatment time. The adhesion strength of the mixed coating was

very less compared to SiO_x and TiO_x films, figure 49. The decreased adhesion strength for the mix coating could be due to the presence of more hydrocarbons in the precursor (HMDSO $C_6H_{18}Si_2O$ and Titanium isopropoxide $C_{12}H_{28}O_4Ti$), which might get bonded to the steel substrates immediately when they were let into the chamber.

4.2 Stability in biological media and pH

The $SiO_xC_yH_z$, SiO_x, TiO_x and SiO_x-TiO_x films deposited without pre-treatment were immersed in dulbacoe's modified eagle media (DMEM) and to test the stability in incubation. But all the films flake off immediately after exposure to the medium. The plasma pre-treated samples were then tested for their stability in autoclave and in biological media.

4.2.1 Autoclave treatment and immersion in biological media of polymer-like and silica-like films

The film adhesion depends on numerous factors such as substrate roughness, contamination on the substrate surface, stress in the film and the chemical bonding between the substrate and the layer that was in immediate contact with the substrate [209 - 211]. When the plasma pre-treated films were placed in DMEM media and incubated at 37^0C in 5% CO_2 for 48 hours, the polymer like SiOxCyHz films flaked off from the substrate edges as shown in Fig 50 (a) and (b).

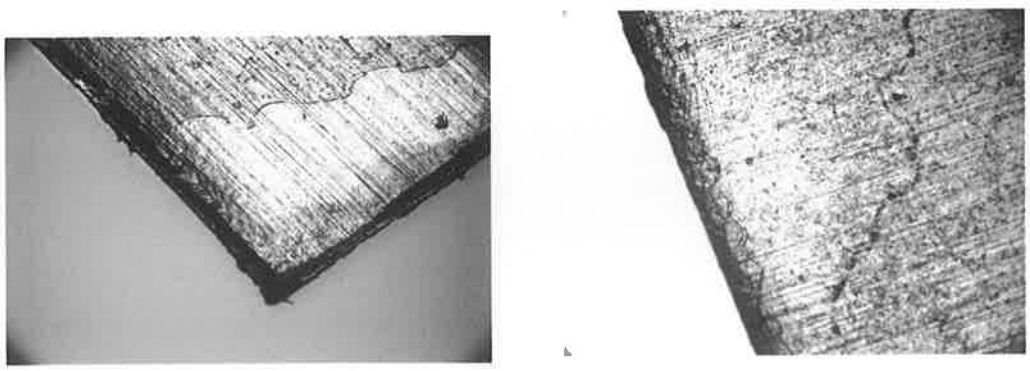

Figure 50 Flaking of plasma pretreated $SiO_xC_yH_z$ films after exposure to biological media

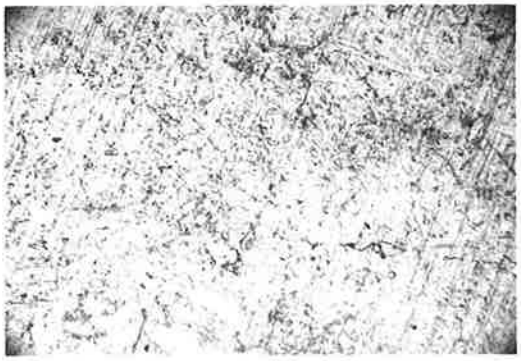

Figure 51 Cracking of plasma pre-treated silica-like $SiO_xC_yH_z$ films after autoclave and exposure to biological media

It was also noted that the 10:1 ratio film tended to crack despite its good adhesion to the steel Fig 51. This could be due to the internal stresses developed in the hard silica-like film, which has a thickness greater than 2 microns [212,213]. The adhesion strength of both polymer-like and silica-like films has to be improved further to enhance its stability in biological media.

4.2.2 Layering of films to improve the stability in biological media

Layered film deposition is a technique by which the adhesion strength can be improved to enhance the performance of the coating. Film with higher adhesion strength to 316L stainless steel can be used as an adhesion layer and then the plasma parameters can be changed to tune the surface characteristics.

Following a sequence of layered deposition, where films of varying property were deposited sequentially, no peeling was observed when the samples were exposed to the same biological media (Fig 52 (a) and (b)). The 10:1 ratio film that had better adhesion in comparison to all other films was deposited as a base layer. Then the oxygen/HMDSO ratio was varied to get a preferred surface. To deposit a pure HMDSO film, the 10:1 ratio film was deposited first and then the oxygen/HMDSO ratio was changed to 5:1 and then to 2:1 and at the end the pure HMDSO film was deposited. The layering prevented a drastic change in the hardness content in the layer and stopped the film from peeling.

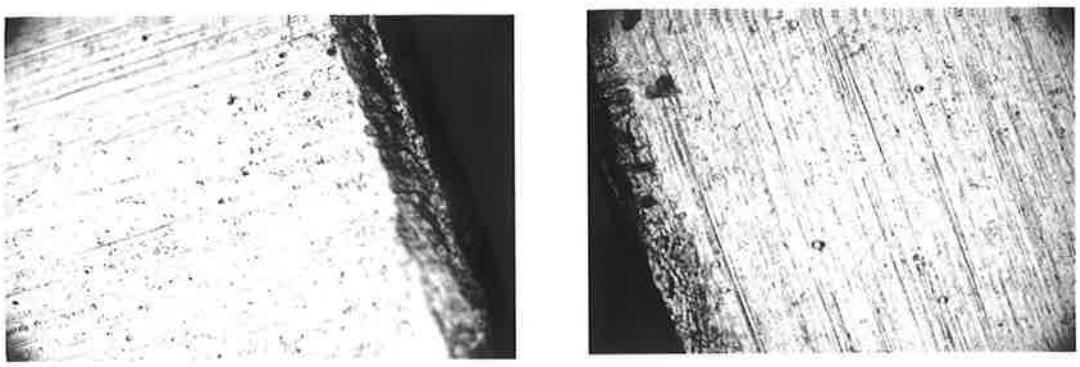

Figure 52 (a) Stability of plasma pre-treated, layered polymer-like film, (b) plasma pre-treated layered silica-like film, after exposure to biological media

In the case of silica-like films, studies suggest that the elastic behaviour of the polymer like film can be used to relieve the stress effect [214,215]. Therefore, a polymer-like film was sandwiched between the two hard silica-like films. The 10:1 ratio film was deposited at the bottom, then a polymer like film was deposited and then the silica like film was deposited on top. The layering relieved the high intrinsic stress developed in the thicker films. The cracks that appeared in the non-layered silica like film did not appear in the layered silica like film figure 52 (b).

4.2.3 Stability of polymer-like, silica-like, TiO_2-like and SiO-TiO mixed oxide coatings in acidic, basic and physiological pH

The stability of the film in acidic, basic and physiological pH was tested by altering the pH of the solution using different standard pH buffers and also with extreme temperature conditions (steam sterilization method).

Cell culture media DMEM /F-12 Ham (1:1) mixture (Sigma product code D8900) with 10% serum and three different pH values (7.3, 4.0 and 9.0) of the media were adjusted using standard buffer solutions of pH 7.0, 4.0 & 10.0, (Merck KgaA, Germany). The 316L stainless steel samples coated with SiOCH, SiO_x, TiO_x and silicon-titanium mixed oxide were immersed in the three different pH solutions with acidic (pH 4), basic (pH 9) and physiological (pH 7) pH at 37+/- 1^0C for 24 hrs and observed by optical microscopy. The samples were subjected to steam sterilization in an autoclave employing saturated steam under a pressure of approximately 15 psi to achieve a chamber temperature of at least 121°C (250°F) for 30 minutes.

To determine the stability of the coatings, on 316L stainless steel, in different pH solutions, the coated steel samples were immersed in a solution with the acidic (pH 4), basic (pH 9) and physiological (pH 7) pH at 37 +/- 1^0 C for 24 hours. In the case of mixed oxide coatings, the films deposited without pre-treatment flaked off immediately after immersing in the solution. The films deposited with plasma pre-treatment enhanced the adhesion strength of the film to the medical grade stainless steel. However, when the samples were immersed in the buffer solutions, the coating tended to peel at some parts of the surface. To overcome that, a layered coating was used. Since SiO_x film had a much higher adhesive strength than the mix, a thin SiO_x layer was deposited first after pre-treatment and then the mixed coating was deposited on top. This enhanced the stability of the film in the biological conditions to a significant extent and no peeling was observed, as shown in optical microscopic image figure 54 and scanning electron microscopic image figure 55.

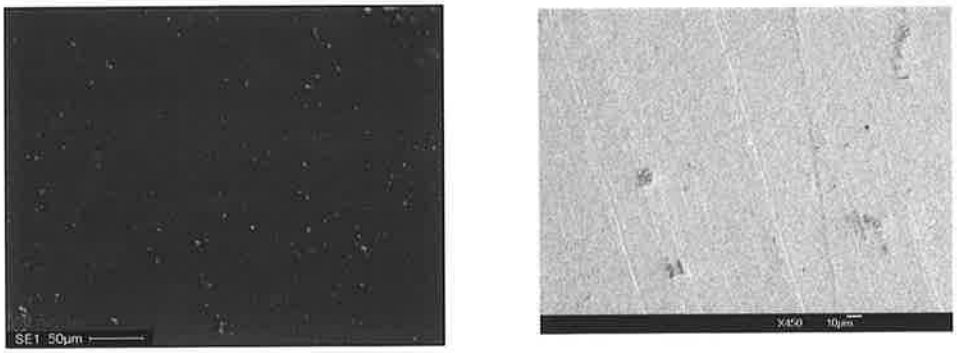

Figure 53 SEM images of SiO_x and TiO_x coatings after immersion in biological medium

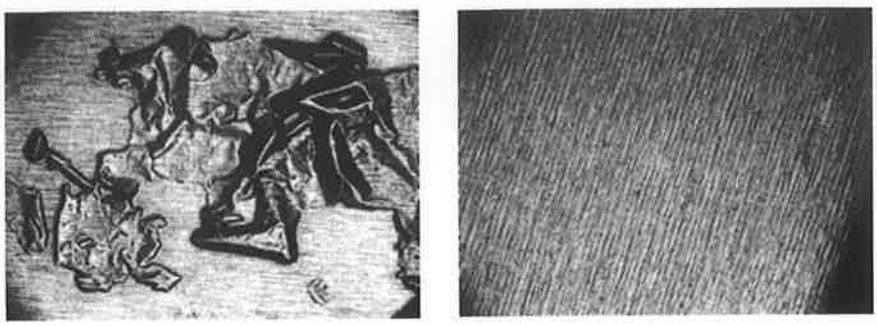

Figure 54 Optical microscopic studies of mixed oxide coated steel samples after exposing to biological media (a) without layering (b) with layering

Figure 55 SEM image of mixed oxide coating after immersion in biological medium, deposited (a, b) without adhesion layer and (c) with SiO_x adhesion layer

The oxide coatings on 316L stainless steel substrates were also subjected to steam sterilization for 30 minutes at 121° C and 15 psi pressure. The films were observed through optical microscope before and after the steam sterilization and found to be stable without any flaking.

The TiO_x films were tested with EDS after immersing the coated 316L stainless steel sample in a physiological (pH 7) pH at 37 +/- 10 C for 24 hours.

Element	Line	Weight %	Atom %
Oxygen	K	43.82	69.25
Phosphorus	K	3.82	3.12
Titanium	K	52.36	27.64
Total		100.00	100.00

The composition looks like TiO_x where x>2.

If we assume 3.12 atoms of phosphorus to bind 12.48 atoms of oxygen, then we have 56.77 atoms to bind to 27.64 titanium atoms. The extra oxygen may be in the form of OH in the sample.

4.3 Surface roughness

The surface roughness was measured using atomic force microscopy (AFM). The surface roughness of untreated 316L stainless steel was around 3.8 nm and the roughness of SiOCH, SiO_x, SiOTiO and TiO_x were 5.6 nm, 6.1 nm , 6.6 nm and 7.8 nm respectively.

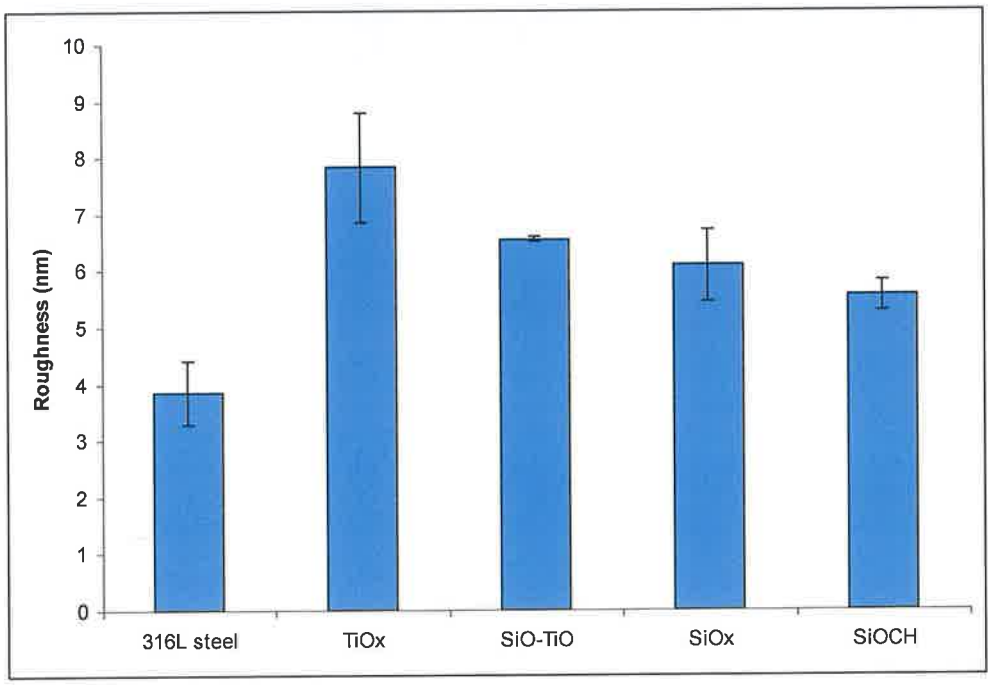

Figure 56 AFM measurements of surface roughness of plain and coated 316L stainless steel

The influence of surface roughness on the protein adsorption is discussed in chapter 5.

4.4 Uniformity of coating on three dimensional steel substrates

4.4.1 Silica-like coating on copper wires

Deposition of biocompatible coatings on biomedical devices requires complete uniform coverage of complex three dimensional substrates. With plasma enhanced chemical vapor deposition it is possible to deposit on complex three dimensional substrates. Having stable plasma in the chamber, depositing on three dimensional substrates was not a difficult task. In order to test the conformality of the coating on a

complex shape metallic substrate, a copper wire was wound like a spring, SiO_x coatings were then deposited on the spring and the deposited copper spring was observed through a scanning electron microscope (SEM).

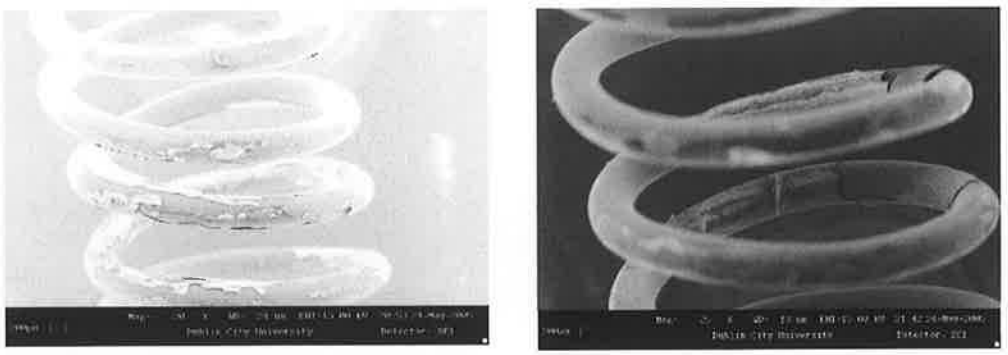

Figure 57 Deposition on copper wire - conformal coating with very poor adhesion

The SEM micrographs in figure 57 show that the film flaked off from the copper wire as a result of poor adhesion. But the coating was observed through out the spring indicating a complete coverage on three dimensional copper wire.

4.4.2 Silica-like coating on 316L steel springs

Stents in general have slotted tube geometries, such as the Palmaz stents or coil geometries such as Gianturco-Roubin Flex stent. The stent geometries were broadly classified as coil, helical spiral, woven, individual rings, or sequential rings. 316L stainless steel stents are most widely used.

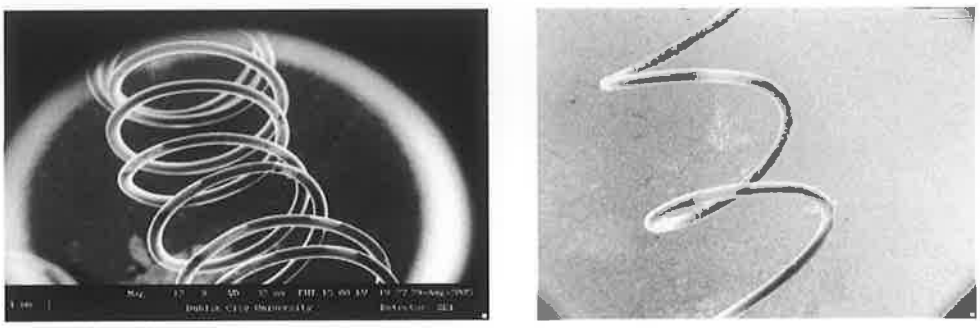

Figure 58 316L Stainless steel spring covered with kapton strips in between showing coated and uncoated areas

SiO_x coatings were deposited on 316L stainless steel springs. Part of the spring was covered with kapton tape and the coated spring was observed in scanning electron microscope. The coated and uncoated part of the spring could be clearly distinguished, figure 58.

The coated springs were then cut and their cross sectional view was observed in scanning electron microscope, shown in figure 59. The spring was coated uniformly throughout. The cross sectional image taken at various locations in the same spring suggest that the coating has been covered uniformly on the complex three dimensional metallic substrate.

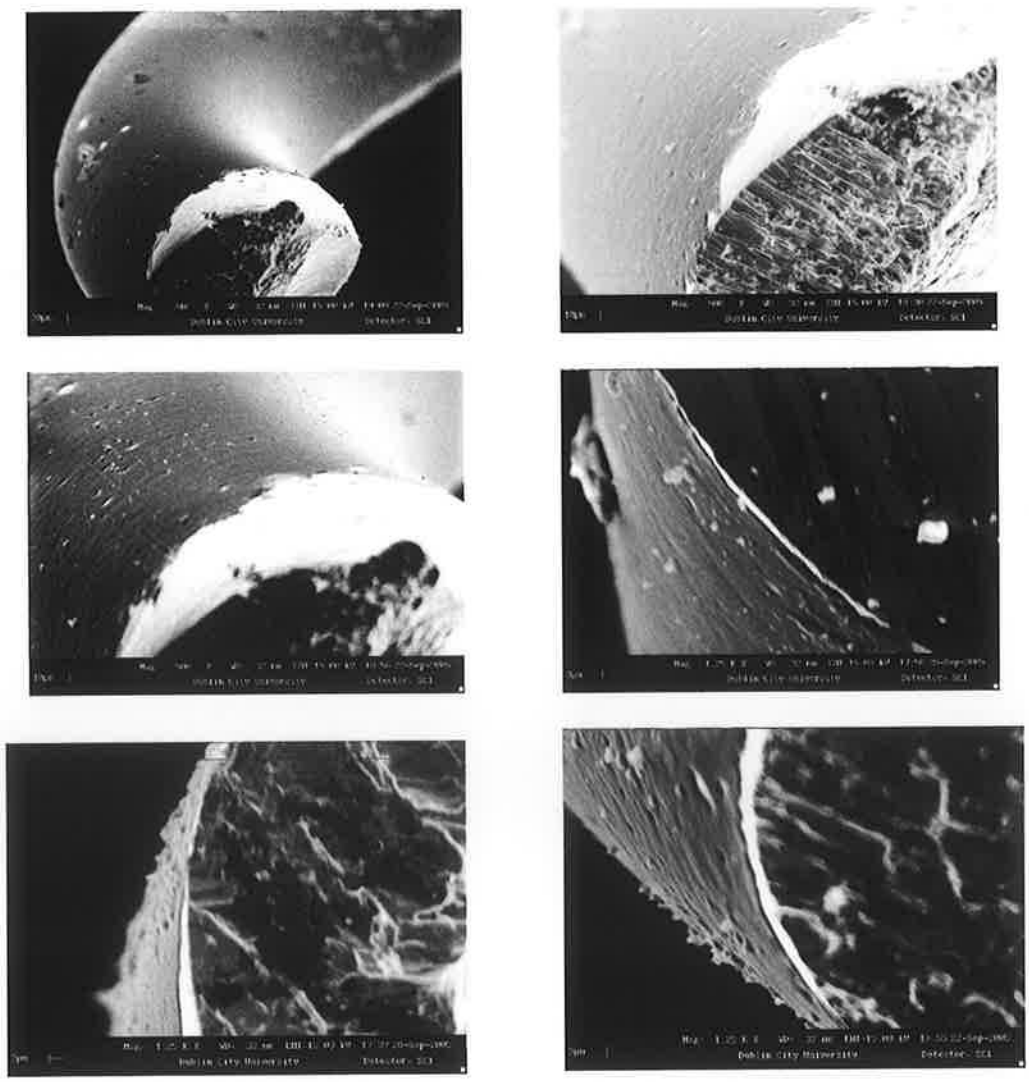

Figure 59 Cross section images at different locations in the coated spring

4.4 Summary

Silicon dioxide (SiO_x), titanium oxide (TiO_x), $SiO_xC_yH_z$ and silicon-titanium mixed oxide (SiO-TiO) coatings have been deposited on 316L stainless steel substrates. The adhesion of $SiO_xC_yH_z$ to 316L stainless steel was found to be very poor. However, SiO_x coatings exhibited a better adhesion than $SiO_xC_yH_z$. When the SiO_x coatings were exposed to biological medium, the coating peeled off from the substrate. To improve the adhesion strength of the film to 316L stainless steel, plasma pre-treatment procedure was followed.

- Argon, oxygen and argon+oxygen mixture plasma were taken as pre-treatment gases and the plasma pre-treatment was carried out at various pre-treatment time and pre-treatment RF power for SiO_x coatings.

- The optimum pre-treatment time for enhanced adhesion of SiO_x on 316L stainless steel was found to be 3 minutes for argon + oxygen mixture pre-treatment plasma at the applied RF power of 250W.

- To deposit a $SiO_xC_yH_z$ coating on steel, SiO_x coating was used as an adhesion layer.

- Layered deposition was performed to prevent the formation of cracks that could possible arise due to the increased stress in the powered electrode deposited films.

- A pre-treatment RF power of 125W and a pre-treatment time of 3 minutes were found to be optimum for TiO_x and SiO-TiO coatings.

- When the films were exposed to biological medium, the mixed oxide coating peeled even after plasma pre-treatment and hence SiO_x coating was used as an adhesion layer.

- After exposure to biological media, the films were tested with SEM and EDS and the films were found to be stable without cracking and peeling.

- The elemental analysis using EDS after incubation in physiological pH solution showed that the coating was stable in biological medium. The film was also found to be stable under steam sterilization.

- The conformality of the coating observed by depositing SiO_x coating on 316L stainless spring showed that the coatings had covered uniformly on complex three dimensional substrates.

5. BIOCOMPATIBILITY STUDIES

5.1 Cytotoxicity and cell proliferation studies of HMDSO based films

This work also studied the bio-response of the films deposited on 316L stainless steel. Rat aortic smooth muscle (RASM) cells donated by the Vascular Health Research Group in Dublin City University, were cultured in standard 75cm^2 cell culture flasks in a medium composed of: Dulbecco's modified Eagle's medium (DMEM) supplemented with 10% Fetal Calf Serum (FCS), 2% L-glutamine and appropriate antibiotics (Penicillin 100 units/ml and Streptomycin 100ug/ml). The cells were grown @ 37°C in a humidified atmosphere with 5% $C0_2$ [216] .The metal samples were seeded in 24 well culture plates at a density of 10,000cells/ml [217]. Each batch of samples was plated in triplicate for both MTT assay and cell proliferation and viability determination, with appropriate controls. Assays were conducted on Day 2, 4 & 6. Post-incubation in culture all samples were removed and the adherent cells fixed with gluteraldehyde for SEM analysis.

5.2 Cytotoxicity studies of various oxygen:HMDSO ratio films

MTT assay is a standard colourimetric assay (an assay which measures changes in colour) for measuring cellular proliferation (cell growth). The amount of yellow MTT (3-(4,5-Dimethylthiazol-2-yl)-2,5-diphenyltetrazolium bromide) reduced to purple formazan was measured spectrophotometrically by a spectrometer. This reduction takes place only when mitochondrial reductase enzymes are active, and thus conversion is directly related to the number of viable cells. The production of purple formazan in cells treated with an agent was measured relative to the production in control cells.

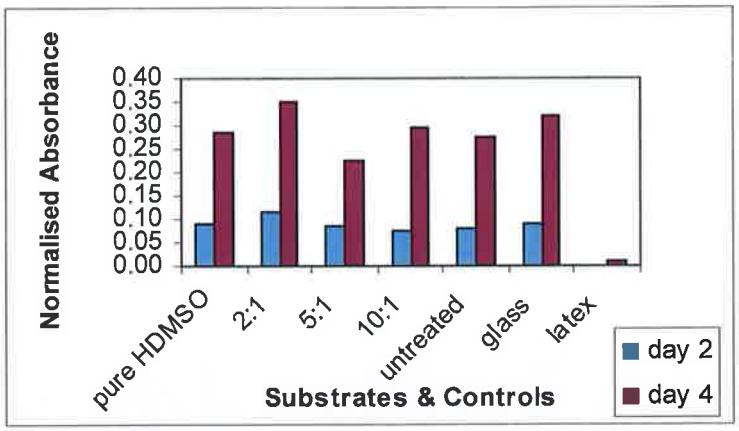

Figure 60 MTT assay of various oxygen:HMDSO ratio film

The films did not adversely effect the growth of the cells, and the RASM cells did not die off in culture in the presence of the coated stainless steel. The growth of the cells with coated substrates was comparable to those seeded with no substrates.

The results of the Cytotoxicity tests are shown in figure 60. A commercial kit purchased from Roche was used to perform an MTT assay on the cells in culture post incubation with the coated substrates. The cells were incubated with the yellow MTT solution for 4 hours. After this incubation period, purple formazan salt crystals were formed. These salt crystals were insoluble in aqueous solution, but might be solubilised by adding the solubilisation solution and incubating the plates overnight in humidified atmosphere. The resultant product was spectrophotometrically quantified using an ELISA plate reader. An increase in the number of living cells resulted in an increase in the total metabolic activity in the sample. This increase directly correlated to the amount of purple formazan crystals formed, as monitored by the absorbance [218].

5.3 Cell proliferation and viability studies

Cell proliferation & viability was assessed by Trypan blue staining and counting with haemocytometer. Trypan blue is a vital stain that colours dead tissues or cells blue. It is a diazo dye. Live cells or tissues with intact cell membranes will not be coloured.

Since cells are very selective in the compounds that pass through the membrane, in a viable cell trypan blue is not absorbed, however, it traverses the membrane in a dead cell. Hence, dead cells are shown as a distinctive blue colour under a microscope. The reactivity of trypan blue is based on the fact that the chromopore is negatively charged and does not interact with the cell unless the membrane is damaged. Therefore, all the cells which exclude the dye are viable.

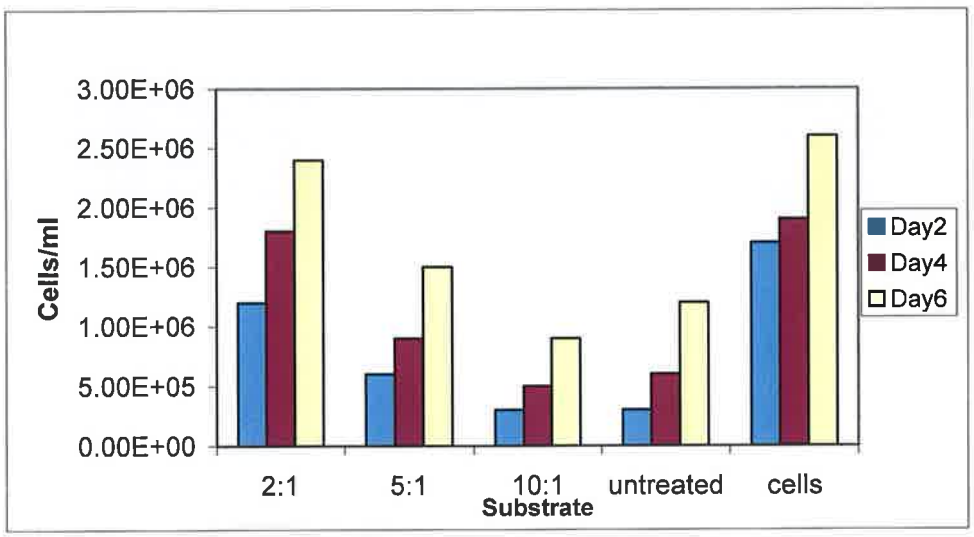

Figure 61 Cell proliferation and viability studies of various oxygen:HMDSO ratio films

Figure 61 shows initial results of the cell proliferation & viability tests, which were determined by Trypan blue staining and counting with a Neubauer haemocytometer. The lowest ratio of oxygen to HDMSO (2:1) showed the greatest proliferation, almost comparable to the proliferation and growth of cells seeded in absence of any substrate. Cell proliferation in higher oxygen to HMDSO flow ratio was similar to 316L stainless steel. The cell viability tests were based on the ability of dead cells to take up Trypan blue dye, where as live healthy cells remained white. Percentage viability was calculated to be >90% in all cases except for the negative control, latex, which is known to be highly toxic to cells.

Based on the data in both figs. 60 & 61, it was clear that the film coated substrates did not adversely effect the growth of the cells, and that the RASM cells did not die off in culture in the presence of these foreign materials. In fact the growth of the cells with coated substrates was comparable to those seeded with no substrates at all.

5.4 Cell adhesion studies of various oxygen:HMDSO ratio films

The cell adhesion on plain 316L stainless steel, polymer like $SiO_xC_yH_z$ and silica like SiO_x coatings on 316L stainless steel was carried out by fixing the cells post-incubation in culture with glutaraldehyde and treating with osmium tetroxide. The adhesion of fixed cells was assessed with scanning electron microscopy.

10:1 (Oxygen:HMDSO)

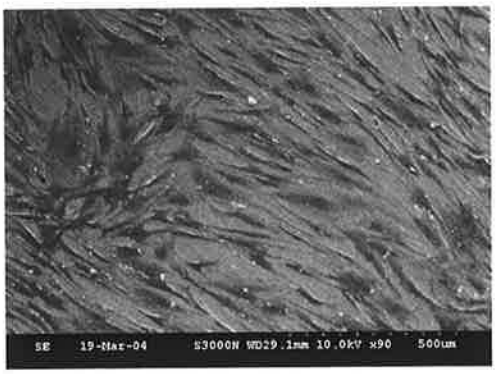

5:1 (Oxygen:HMDSO)

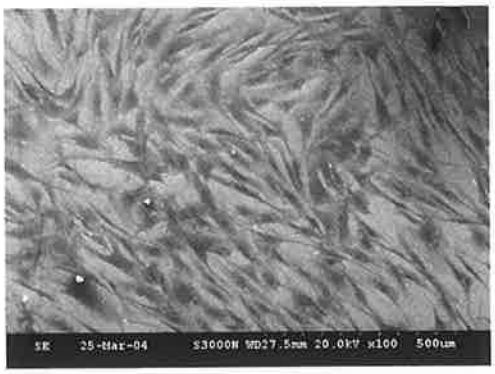

2:1 (Oxygen:HMDSO)

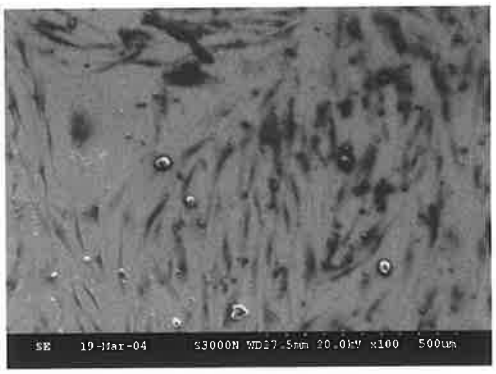

Untreated stainless steel

Figure 62 SEM images of cell adhesion studies of HMDSO based coatings on 316L stainless steel

The SEM pictures in figure 62 clearly demonstrated that the polymer like $SiO_xC_yH_z$ films with low oxygen:HMDSO flow ratio favoured higher cell proliferation and silica like films deposited at high oxygen:HMDSO flow ratio had lower cell proliferation than the low oxygen:HMDSO flow ratio films.

5.5 Protein adsorption studies

The complex protein solutions can be analysed using several techniques like electron spectroscopy for chemical analysis (ESCA), Matrix-assisted laser desorption/ionization time-of-flight mass spectrometry (MALDI-TOFMS), time-of-flight secondary ion mass spectrometry (ToF-SIMS), radio active labelling, enzyme immunosorbent assays (EIA), Total internal reflection fluorescence (TIRF) spectroscopy, ellipsometry, X-Ray photoelectron spectroscopy, surface plasmon resonance (SPR) analysis and bicinchoninic acid assay (BCA) [219-226].

Fibrinogen adsorption assay:

Fibrinogen adsorption in our work had been evaluated using Enzyme Immunosorbent Assay (EIA) [227,228]. The EIA method allows us to determine both the identity and quantity of many substances in bodily fluids or tissues. This method can be used to detect specific hormones, enzymes, viruses, bacteria, fungi, toxic substances, parasites, cancer-linked markers on cells, pharmaceutical substances, etc. This method can also detect antibodies directed against micro-organisms or autoimmune-antibodies.

Calculations

A standard plot was drawn using the absorbance data from 316L stainless steel controls for various concentrations of fibrinogen. The fibrinogen adsorption on coated stainless steel samples were carried out by incubating the samples in solution with a fibrinogen concentration of 100ng/ml. This concentration was chosen to make sure that the concentrations do not exceed the saturation limit, so that the spectrophotometer could distinguish the absorbance intensity. The absorbance measurements for the coated steel samples were fitted in the corresponding standard chart done on the same day and the concentration of fibrinogen was calculated by extrapolation. The fibrinogen binding data were reported in terms of percentage binding with respect to plain 316L stainless steel. The fibrinogen adsorption measurement on both stainless steel controls and coated substrates were done on three different days, for three different sets, and the standard plot was drawn for each

day. Three different fibrinogen adsorption data, in percentage binding, on the coated samples were then averaged.

The average weight of five different 316L stainless steel controls with a known surface area of approximately 0.8 cm^2 (nearly constant), with a fixed shape, was measured. The weight/surface area was calculated to get a conversion factor. By measuring the weight of the samples, the exact area can be calculated. For the rest of the experiments, the weight of the samples was divided by this conversion factor to get the area in cm^2. The conversion factor was found to be 0.1566. This step was done to simplify the area calculation by measuring the weight.

Measurement 1

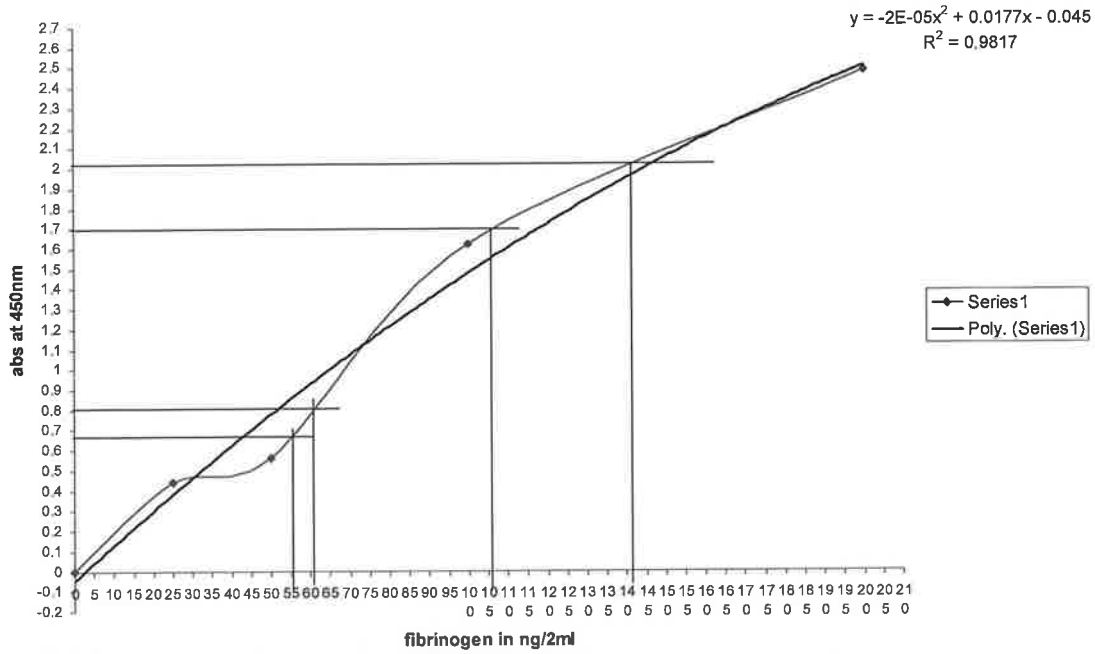

Figure 63 Standard plot 1, for 316L stainless steel controls against concentration of fibrinogen in ng/2ml and absorbance

The abscissa in standard plot corresponds to fibrinogen concentration in the solution. Since 2 ml was used for all the tests, to make sure that the entire steel surface was convered, the abscissa was in ng/2ml.

	abs	weight	cm2	ng	ng/cm2	% bound
HMDSO	1.68	0.1226	0.782886	106	135.3964	67.69821
SiO	0.656	0.1108	0.707535	56	79.14801	39.57401
TiO	2.005	0.1036	0.661558	142	214.6448	107.3224
SiO-TiO	0.803	0.0973	0.621328	61	98.17677	49.08839

Table 7 Calculation of percentage fibrinogen bound, from absorbance, by extrapolating the standard plot 1

Measurement 2

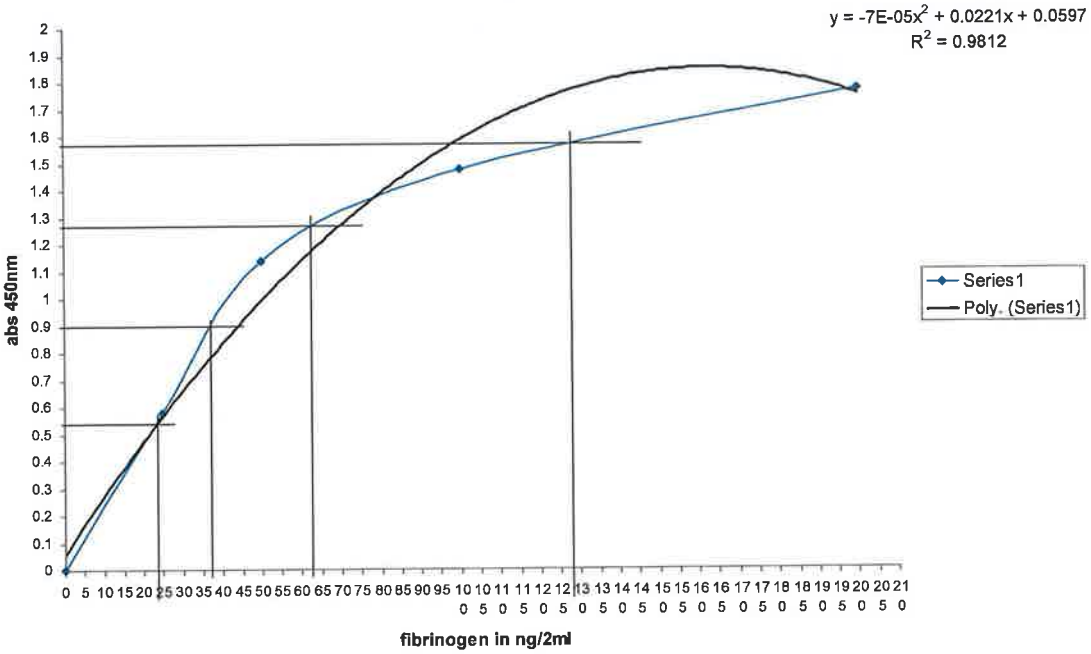

Figure 64, standard plot 2, for 316L stainless steel controls against concentration of fibrinogen in ng/2ml and absorbance

	abs	weight	cm2	ng	ng/cm2	% bound
HMDSO	0.896	0.1057	0.674968	37	54.81741	27.4087
SiO	0.541	0.1167	0.745211	24	32.20566	16.10283
TiO	1.577	0.1002	0.639847	127	198.485	99.24251
SiO-TiO	1.262	0.1135	0.724777	63	86.92335	43.46167

Table 8 Calculation of percentage fibrinogen bound, from absorbance, by extrapolating the standard plot 2

Measurement 3

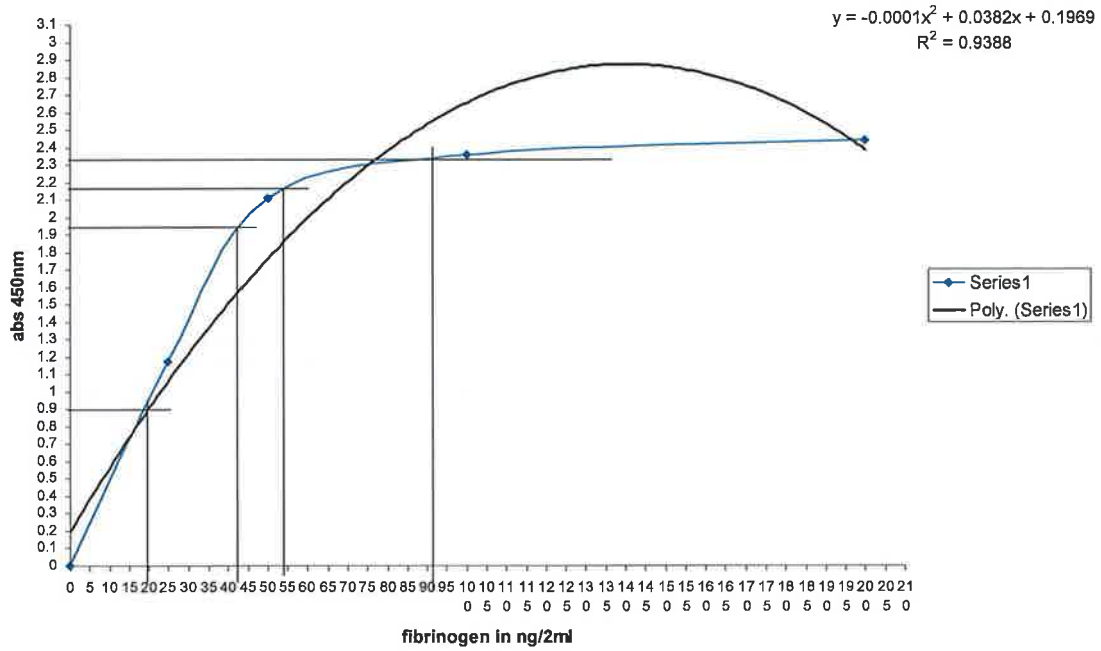

Figure 65, standard plot 3, for 316L stainless steel controls against concentration of fibrinogen in ng/ 2ml and absorbance

	abs	weight	cm2	ng	ng/cm2	% bound
HMDSO	1.938	0.1083	0.691571	43	62.17729	31.08864
SiO	0.904	0.1111	0.709451	20	28.19082	14.09541
TiO	2.322	0.1012	0.646232	92	142.3636	71.18182
SiO-TiO	2.18	0.0985	0.628991	54	85.85178	42.92589

Table 9, Calculation of percentage fibrinogen bound, from absorbance, by extrapolating the standard plot 3

Average

	Day 1	Day 2	Day 3	Average	Std dev	Std error
TiO	107.32	99.24	71.18	92.58	18.96817	10.95128
SiOTiO	49.09	43.46	42.93	45.16	3.413781	1.970947
SiO	39.57	16.1	14.1	23.25667	14.16311	8.177074
SiOCH	67.7	27.41	31.09	42.06667	22.27524	12.86062

Table 10, Percentage fibrinogen bound on three different measurements and its average

5.5.1 Fibrinogen adsorption

The fibrinogen adsorption was highest on low bandgap (3.3 eV), hydrophilic (24°) TiO_x films with a percentage binding of 93% relative to 316L stainless steel, followed by hydrophobic (105°), and high bandgap SiOCH film with a percentage binding of 42% relative to 316L stainless steel. The adsorption on hydrophilic (38°), high bandgap (3.8 eV) silicon-titanium mixed oxide coating, with a fibrinogen binding of 45%, was very close to that of SiOCH films. SiO_x films with a contact angle of 60° and bandgap 9 eV had the least adsorption of 23.3%.

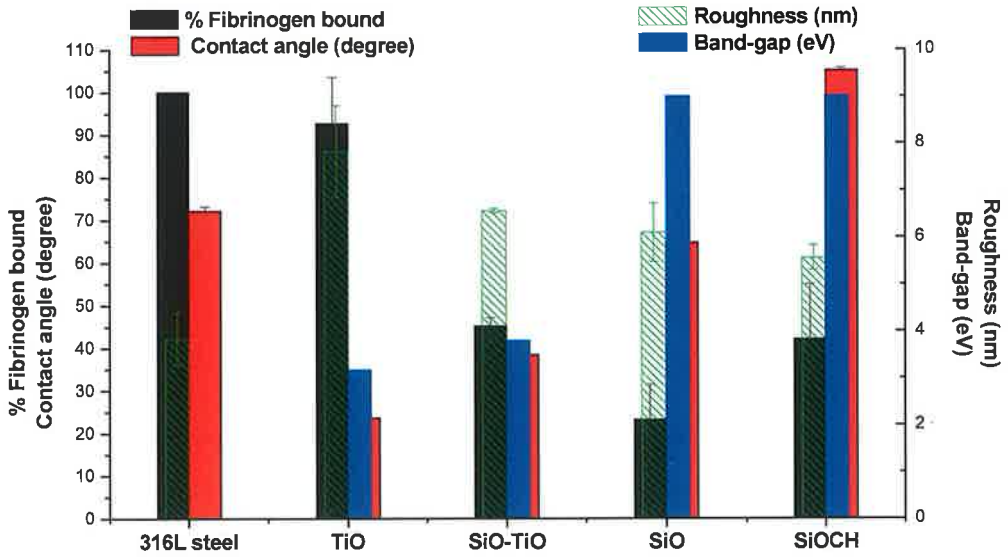

Figure 66 Fibrinogen adsorption data of silicon and titanium based coatings

From the figure 66, it is clear that as the hydrophobicity increases from TiO to SiOCH, the protein adsorption decreases and then increases for highly hydrophobic SiOCH film. It is expected that the fibrinogen adsorption be minimum at hydrophilic surface and the adsorption increase with increase in hydrophobicity. The reason for the observed high adsorption at hydrophilic TiO_x film is because of the low bandgap of TiO_x film. The bandgap effect overcomes the hydrophilicity (24°) of the film and hence the fibrinogen adsorption was high on TiO_x film. The surface roughness data shows that untreated 316L stainless steel is the smoothest of all the surfaces, with a RMS roughness of 3.8 nm, and

the fibrinogen adsorption on steel is the maximum of all, ie., all other coatings show lower percentage of fibrinogen binding relative to 316L stainless steel. Untreated 316L stainless steel with a contact angle of 72° and being a metallic surface should adsorb more amount of fibrinogen than hydrophilic (24°) titanium dioxide coating. As expected titanium dioxide coatings exhibited a fibrinogen binding of 93% relative to steel. However, some data on the replicates showed that the fibrinogen binding was higher than 100% ie., the binding was more than that of 316L stainless steel. This could either be due to the experimental error or due to the surface characteristics of the coating. A comparatively higher surface roughness of 7.8 nm for titanium dioxide coatings could possibly have contributed to the fibrinogen adsorption that led to an increased adsorption. Rechendorff et al., demonstrated that for a roughness increase from 2.9 nm to 7.1 nm, there was 24% increase in fibrinogen adsorption and further increase in roughness to 32 nm increased the fibrinogen adsorption to a significantly higher value of 70% [229]. Hence, surface roughness alone could not have contributed for such a high fibrinogen adsorption. Hence, in the case of titanium di oxide coatings, the fibrinogen adsorption similar to that of untreated 316L stainless steel is caused due to low bandgap (3.17 eV) and possibly due to higher surface roughness of 7.8 nm.

The fibrinogen adsorption in silicon dioxide was 23%, with a roughness value of 6.1 nm, relative to 316L stainless steel with a roughness of 3.8 nm. Also, the surface roughness of silicon dioxide (6.1 nm) lies in between that of SiOCH (5.6 nm) and SiOTiO (6.6 nm), whereas the fibrinogen adsorption on silicon dioxide was the lowest of all. It is very clear from this data that the effect of surface roughness in nanometer scale close to 6nm is less significant and the surface chemistry plays a significant role in governing the fibrinogen adsorption. This behaviour was in agreement with Walivaara et al., who demonstrated that for titanium dioxide coatings the fibrinogen adsorption was dependent on wettability for surfaces with RMS roughness less than 1 nm and for roughness greater than 5nm there was no good correlation between the surface wettability and fibrinogen adsorption [230].

The water contact angle was increased to 38° for SiO-TiO, the bandgap also increased to 3.8 eV and hence the adsorption (45%) was less than that of TiO_x (93%). With a further increase of water contact angle to 60° for SiO_x film, the bandgap was 9 eV and the fibrinogen binding was 23%. Since the bandgap was high enough, the fibrinogen adsorption was reduced significantly. But with a further rise of water contact angle to 105° for SiOCH film, the fibrinogen adsorption (42%) increased than silicon dioxide. In this case, even though the bandgap was high enough; the hydrophobicity was overcome by the bandgap effect. Since the hydrophobic surfaces tend to adsorb more fibrinogen the SiOCH surface had adsorbed a high amount of fibrinogen.

5.6 Summary

Cytotoxicity and cell proliferation studies were carried out using rat aortic smooth muscle cells, for silicon based $SiO_xC_yH_z$ and SiO_x coating deposited on 316L stainless steel. Fibrinogen adsorption of $SiO_xC_yH_z$, SiO_x, TiO_x, and SiO-TiO coatings deposited on 316L stainless steel was measured using enzyme immunosorbent assay.

- Cytotoxicity tests carried out on $SiO_xC_yH_z$ and SiO_x coating showed that the films did not adversely affect the growth of rat aortic smooth muscle cells
- Cell proliferation study on $SiO_xC_yH_z$ and SiO_x coating showed that the cell proliferation was higher on hydrophobic $SiO_xC_yH_z$ coating and lower on hydrophilic SiO_x coating
- Fibrinogen adsorption was highest on low bandgap (3.17 eV), hydrophilic (24°) TiO_x films with 93% relative to that of 316L stainless steel, followed by SiO-TiO films with intermediate value water contact angle of 38° and bandgap 3.8 eV showed a fibrinogen binding of 45%, hydrophobic (105°), and high bandgap SiOCH film with 42%. SiO_x with a contact angle of 60° and bandgap 9 eV had the least adsorption of 23% relative to that of steel.
- Lower fibrinogen binding on SiO_x was due to both the high bandgap and low water contact angle.

- High adsorption on hydrophilic TiO_x film was probably due to the low bandgap that caused electron transfer between fibrinogen and TiO_x surface.

- Surface roughness of TiO_x films could possibly have contributed to an increased fibrinogen adsorption. However, surface roughness of silicon dioxide did not have any influence on the fibrinogen adsorption. Since the roughness of SiOCH and SiO-TiO films were 0.5nm below and above that of silicon dioxide, the surface roughness was less likely to have influenced the fibrinogen adsorption behaviour of SiOCH and SiOTiO films, to a statistically significant quantity.

- High adsorption on hydrophobic $SiO_xC_yH_z$ was due to its hydrophobicity

- SiO-TiO film that was hypothesised to have lower adsorption due to its lower water contact angle than SiOx and higher bandgap than TiO_x showed a comparatively higher adsorption than SiO_x and lower than TiO_x.

- A combination of bandgap and wettability of the surface played a significant role in governing the fibrinogen adsorption behaviour and both had to be optimised to minimise the fibrinogen binding.

6. CONCLUSIONS

The primary objective of this work was to deposit silicon and titanium based coatings with a range of surface characteristics through a thorough understanding of the influence of process parameters on the film properties, analyse the surface related factors that govern the fibrinogen adsorption and minimise the fibrinogen adsorption by depositing films with tailored surface characteristics. For this purpose, four different kinds of coatings, with a range of surface characteristics, were deposited by PECVD. Polymer-like $SiO_xC_yH_z$ film, silica-like SiO_x film, titanium dioxide (TiO_2) and silicon-titanium mixed oxide (SiO-TiO) coatings had been deposited.

6.1 Surface chemical and mechanical properties

The initial approach was to analyse the influence of plasma process parameters including oxygen to HMDSO flow ratio, RF power, and position of substrate on the floating and powered electrode, on the surface characteristics of the silicon based coatings. It was observed that the oxygen to HMDSO flow ratio and RF power influenced the chemical structure and the mechanical characteristics of the film to a significant extent. Hydrocarbon rich plasmas with low or no oxygen flow led to the formation of a soft (1.6 GPa nano hardness), polymer-like (hydrocarbon rich), hydrophobic (CA 106°) SiOCH film with a refractive index of 1.842 and density 1.59 $g.cm^{-3}$. The observed low hardness, high hydrophobicity and high refractive index were due to the fact that the film was hydrocarbon rich. Whereas, oxygen rich plasmas with high oxygen:HMDSO flow ratio led to the formation of a hard (~7 GPa nano hardness), silica-like, less hydrophobic (CA 60°) SiO_x film with a refractive index of 1.487 and a density of 2.31 $g.cm^{-3}$.

The films deposited at oxygen to HMDSO ratio of 10:1, at varying RF powers showed that the film characteristics strongly depend on the RF power. At a low RF

power of 50W, the water contact angle of 10:1 (oxygen:HMDSO) films were around 80°, it then decreased gradually with increase in RF power reaching a value of 65° at 450W. At 50W, the refractive index and film density were 1.47 and 1.487 $g.cm^{-3}$ respectively and at 450W, the refractive index was 1.55 and the density 2.499 $g.cm^{-3}$. The increase in refractive index is because of the increase in density, which in turn arises due to the formation of a sub-stoichiometric Si rich SiO_x film at 450 W. The nano hardness results of the powered electrode deposited films show a linear increase with increase in RF power indicating the formation of hydrocarbon less Si-O-Si network that is confirmed by FTIR spectroscopy, whereas the floating potential deposited films did not show any variation in nano hardness with the RF power. The powered electrode deposited films showed a higher wettability and a superior mechanical property than the floating electrode deposited films. The optical bandgap of SiO_x films from the literature was found to be 9 eV and a minimum stable contact angle of 60° was achieved with 500 sccm oxygen and 15 sccm HMDSO flow rates. The UV-Vis spectrum of SiOCH film appeared similar to that of SiO_x film and hence the bandgap is around the same as SiO_x film.

The titanium dioxide coatings were characterised by varying the oxygen flow rate at fixed TIP flow and also by studying the effect of RF power at fixed oxygen and TIP flows. The water contact angle decreased initially with increase in oxygen:TIP flow ratio that was similar to HMDSO based coatings but after a certain oxygen:HMDSO flow ratio the water contact angle remained the same. With RF power, the water contact angle decreased initially and then increased. An optimum oxygen flow of 500 sccm and RF power of 250 W produced hydrophilic TiO_x films with a water contact angle of 24°. The bandgap of TiOx film calculated by using Tauc plot was estimated to be 3.17 eV.

The bandgap of SiO_x is 9 eV and that of TiO_x is 3.17 eV and the water contact angle of SiO_x is 60° and that of TiO_x is 24°. The silicon-titanium mixed oxide coatings were deposited with an objective of getting an intermediate value of both bandgap and wettability. The oxygen, HMDSO and TIP flow ratios were varied to optimise

the mixed oxide coating. An optimum water contact angle of 38° was obtained. The bandgap value calculated from Tauc plot was found to be 3.8 eV.

The adhesion strength measurement of the $SiO_xC_yH_z$ and SiO_x films to 316L stainless steel substrates showed that polymer-like films had poor adhesion than silica-like SiO_x films. The SiO_x films are then exposed to biological media to check its stability; it was observed that the films flaked off after exposing to biological media. Hence there was a need to increase the adhesion strength of the film to the medical grade stainless steel. Plasma pre-treatment procedures were carried out with argon, oxygen, argon and oxygen mixture plasmas at various pre-treatment time and RF power. An optimum pre-treatment time and RF power of 3 min and 250W respectively were found to increase the adhesion strength to a significant extent. SiO_x films were used as an adhesion layer for depositing $SiO_xC_yH_z$ films. The adhesion increased considerably for titanium dioxide coatings and mixed oxide coatings, after an argon + oxygen mixture plasma pre-treatment. A pre-treatment time of 3 minutes was found to be optimum similar to that of SiO_x film. But the adhesion strength of mixed oxide coatings remained much lower than that of SiO_x and TiO_x for all pre-treatment times.

The stability of the films were tested by immersing the samples in various physiological solutions at 37 +/- 1^0 C for 24 hours and also steam sterilized at 121° C and 15 psi pressure for about 30 minutes. The films were then observed through optical and scanning electron microscope, the mixed oxide coatings peeled even after plasma pre-treatment. A SiO_x coating was used as an adhesion layer and the film stability improved considerably with no peeling.

6.2 Fibrinogen adsorption

The fibrinogen adsorption was highest on low bandgap (3.17 eV), hydrophilic (24°) TiOx films with a percentage binding of 93% relative to 316L stainless steel, hydrophobic (105°), and high bandgap SiOCH film showed a percentage binding of 42% relative to 316L stainless steel. SiO_x with a contact angle of 60° and bandgap 9 eV had the least adsorption of 23.3%.

The hydrophobic $SiO_xC_yH_z$ film was expected to have high fibrinogen binding caused due to its hydrophobicity, since the fibrinogen binding on hydrophobic surface would be higher than on the hydrophilic surface [231,232,233]. Lower fibrinogen binding on SiO_x was caused due to both the high bandgap and low water contact angle. Though the TiO_x film was highly hydrophilic with a water contact angle of 24°, the fibrinogen adsorption was significantly higher than expected. This high amount was probably due to the low bandgap of TiO_x films (3.17 eV) that caused electron transfer between fibrinogen and TiO_x surface resulting in more fibrinogen binding.

Since the fibrinogen adsorption was lower on high bandgap SiO_x, with relatively high water contact angle of 60° than that of TiO_x film with low bandgap (3.17 eV) and low water contact angle (24°), it was hypothesised that by increasing the bandgap higher than that of TiO_x while retaining the hydrophilicity of the surface, the fibrinogen adsorption can be minimised. SiO-TiO films with intermediate value water contact angle and bandgap showed a fibrinogen binding of 45%. The water contact angle of SiO-TiO film was 38° and hence there should have been a much lower fibrinogen binding on SiO-TiO than that of SiO_x (23.3%) with a contact angle of 60°. The observed high fibrinogen adsorption was again probably due to the bandgap effect. The bandgap was not high enough to lower the fibrinogen adsorption even though the wettability was high. In the case of SiO_x with 9 eV and SiO-TiO with 3.8 eV, the high bandgap of SiO_x resulted in low binding. But in the case of SiOCH with contact angle 106°and SiO_x with contact angle 60°, though the bandgap was same the wettability played a crucial role in bringing down the fibrinogen binding.

A comparatively higher surface roughness of 7.8 nm for titanium dioxide coatings could possibly have contributed to the fibrinogen adsorption that led to an increased adsorption. However, surface roughness of silicon dioxide did not have any influence on the fibrinogen adsorption. The fibrinogen adsorption in silicon dioxide was 23%, with a roughness value of 6.1 nm, relative to 316L stainless steel with a roughness of 3.8 nm. Also, the surface roughness of silicon dioxide (6.1 nm) lies in between that of SiOCH (5.6 nm) and SiOTiO (6.6 nm), whereas the fibrinogen adsorption on

silicon dioxide was the lowest of all. It was very clear from this data that the effect of surface roughness in nanometer scale close to 6nm was less significant and the surface chemistry played a significant role in governing the fibrinogen adsorption.

Hence it was concluded that the combination of bandgap and wettability of the surface played a significant role in deciding the fibrinogen adsorption and both had to be optimised to minimise the fibrinogen binding.

7 FUTURE WORK

What's missing

The titanium isopropoxide was let in into the chamber through a needle valve and the flow rate of titanium isopropoxide is unknown. A heated mass flow controller has to be used in order to find the exact flow rate of titanium isopropoxide.

The adhesion strength of the film to 316L stainless steel has been increased by plasma pre-treatment but it is not clear if the adhesion strength is strong enough to withstand the expansion of coated stent. An examination has to be done on coated stainless steel stents to check for the cracking and or peeling after expansion of the stent.

An advancement of this work would be to do the competitive protein adsorption and fibrinogen adsorption from a mixed protein solution would give more information regarding the protein adsorption characteristics of the coating. Cytotoxicity, cell proliferation and cell adhesion tests for titanium oxide and silicon-titanium mixed oxide coatings has to be carried out to get a complete picture of the cell proliferation characteristics of all the coatings

Future directions

The drug holding and elution capability study of the coating could be the next step that would give an idea if the coating as such can be used as a thrombo-resistant, non inflammatory biocompatible, drug holding matrix for drug eluting stents. If the drug elution rate is high because of absence of pores in the coating, a porous oxide based coating could act as a drug holding matrix for drug eluting stents. Hence the work can be focussed to have a biocompatible thrombo-resistant base coating with a porous coating on top to enable drug loading for slow drug elution. PECVD can again be used to deposit a porous coating by choosing a cyclic polymer for plasma polymerization and then annealing the coating to evaporate the cyclic structure that will result in the formation of a porous coating.

REFERENCES

1 Vroman L., Adams A. L., Klings M., Fisher G. C., Munoz P. C. and Solensky R. P. (1977) Reactions of formed elements of blood with plasma proteins at interfaces. Annals of the New York Academy of Science 283, 65

2 Lissy Paul and Chandra P. Sharma. Preferential adsorption of albumin onto a polymer surface: An understanding. Journal of Colloid and Interface Science Volume 84, Issue 2 , December 1981, Pages 546-549

3 Th. Groth, E.J. Campbell , K. Herrmann and B. Seifert. Application of enzyme immunoassays for testing haemocompatibility of biomedical polymers. Biomoteriols 16 (1995) 1009-1015

4 Ratner B, Hoffman A, Schoen F, Lemons J, eds. An introduction to materials in medicine. San Diego, London, Boston, New York, Sydney, Tokyo, Toronto: Academic Press, 1996.

5 Horbett T. Principles underlying the role of adsorbed plasma proteins in blood interactions with foreign materials. Cardiovasc Pathol 1993;2:137S–48S

6 Nimeri G, Lassen B, Golander CG, Nilsson U, Elwing H. Adsorption of fibrinogen and someother proteins from blood plasma at a variety of solid surfaces. J Biomater Sci Polym Edn 1994; 18: 573-83

7 Kaiyong Cai, Marion Frant, Jörg Bossert, Gerhard Hildebrand, Klaus Liefeith, Klaus D. Jandt. Surface functionalized titanium thinfilms: Zeta-potential, protein adsorption and cell proliferation

8 Vroman L, Adams AL. Identification of rapid changes at plasma-solid interfaces J Biomed Mater Res 1969;3:43

9 Bo Lassen, Martin Malmsten. Competitive Protein Adsorption at Plasma Polymer Surfaces. Journal of Colloid and Interface Science 186 (1997) 9-16

10 Kandice Kottke-Marchant, James M. Anderson, Yoshihiro Umemura and Roger E. Marchant. Effect of albumin coating on the in vitro blood compatibility of Dacron arterial prostheses. Biomaterials 10 (1989) 147-155

11 Sevastianov VI. Role of protein adsorption in blood compatibility of polymers. Crit Rev Biocompatibil 1988;4:109-30

12 J. – H. Elam and M. Elam. Surface modification of intravenous catheters to reduce local tissue reactions. Biomaterials 14 (1993) 861-864

13 Ghada Nimeri, Lena Ohman, Hans Elwing, Jonas Wettero, Torbjorn Bengtsson. The influence of plasma proteins and platelets on oxygen radical production and F-actin distribution in neutrophils adhering to polymer surfaces. Biomaterials 23 (2002) 1785-1795

14 Hakan Nygren, Magnus Braide and Christin Karlsson. Protein-platelet and platelet-leukocyte interaction at materials in contact with human blood. J. Vac. Sci. Technol. A 13(5), 1995

15 Jirouskova M, Evangelista J, Suttnar J, Holada K, Trnkova B. Platelet adhesion to fibrinogen, fibrin monomer and fibrin protofibrils in flowing blood. The effect of fibrinogen immobilization and fibrin formation. Thromb Haemostasis 78 (1997) 1125-31

16 Denis Labarre. Improving Blood-Compatibility of Polymeric Surfaces. Trends Biomater. Artif. Organs, 2001;15:1-3

17 Chen Yongli, Zhang Xiufang, Gong yandao, Zhao Nanming, Zeng Tingying, Song Xinqi. Conformational changes of fibrinogen adsorption onto hydroxyapatite and titanium oxide nanoparticles. Journal of Colloid and Interface Science 1999;214:38-45

18 Martin Malmsten. Ellipsometry studies of the effects of surface hydrophobicity on protein adsorption. Colloids and Surfaces B: Biointerfaces 3 (1995) 297-308

19 K. Wannenberger, S. Welin-Klintstrom, T. Arnebrant,. Activity and Adsorption of Lipase from Humicola lanuginosa on Surfaces with Different Wettabilities. Langmuir 1997; 13:784-790

20 B. Jonacha, D. Hegemann, C. Oehr, H. Brunner, F. Rupp, J. Geis-Gerstorfer. Adsorption of protein on plasma-polysiloxane layers of different surface energies. Surface and Coatings Technology 2001;142-144:1051-1055

21 Hakan Nygren. Initial reactions of whole blood with hydrophilic and hydrophobic titanium surfaces. Colloids and Surfaces B: Biointerfaces 6 (1996) 329- 333

22 Hans Elwing, Stefan Welin, Agneta Askendahl and Ingemar Lundström. Adsorption of fibrinogen as a measure of the distribution of methyl groups on silicon surfaces. J. Colloid Interface Sci 123, 306 (1988)

23 S. Welin-Klintström, M. Lestelius, B. Liedberg, P. Tengvall. Comparison between wettability gradients made on gold and on Si/SiO2 substrates. Colloids and Surfaces B: Biointerfaces 15 (1999) 81-87

24 Baurschmidt P, Schaldach M. The electrochemical aspects of the thrombogenicity of a material. J Bioeng 1977;1:261-78

25 Armin Bolz, PhD., Michael Amon, MS., Cem Ozbek, MD.,Bernd Heublein, MD., Max Schaldach, MD, PhD. Coating of Cardiovascular Stents with a Semiconductor to Improve Their Hemocompatibility. Tex Heart Inst J 1996;23:162-6

26 Stephan Windecker, MD; Isabella Mayer, MD; Gabriella De Pasquale, BA; Willibald Maier, MD; Olaf Dirsch, MD; Philip De Groot, MD; Ya-Ping Wu, PhD; Georg Noll, MD; Boris Leskosek, BA; Bernhard Meier, MD; Otto M. Hess, M. Stent Coating With Titanium-Nitride-Oxide for Reduction of Neointimal Hyperplasia. Circulation 2001;104:928-933

27 Bolz A, Schaldach M. Artificial Heart Valves: Improved Blood Compatibility by PECVD a-SiC:H Coating. Artif Organs 1990;14:260-269

28 J.Y. Chen, Y.X. Leng, X.B. Tian, L.P. Wang, N. Huang, P.K. Chu, P. Yang. Antithrombogenic investigation of surface energy and optical bandgap and hemocompatibility mechanism of $Ti(Ta^{+5})O_2$ thin films. Biomaterials 23 (2002) 2545-2552

29 N. Huang, P. Yang, Y.X. Leng, J.Y. Chen, H. Sun, J. Wang, G.J. Wang, P.D. Ding, T.F. Xi, Y. Leng. Hemocompatibility of titanium oxide films. Biomaterials 24 (2003) 2177-2187

30 David Antoniucci, MD, Giovanni M. Santoro, MD, Leonardo Bolognese, MD, Renato Valenti, MD, Maurizio Trapani, MD, Pier Filippo Fazzini, MD. A Clinical Trial Comparing Primary Stenting of the Infarct-Related Artery With Optimal Primary Angioplasty for Acute Myocardial Infarction. J Am Coll Cardiol 1998;31:1234 –9

31 David L. Fischman, Martin B. Leon, Donald S. Baim, Richard A. Schatz, Michael P. Savage, Ian Penn, Katherine Detre, Lisa Veltri, Donald Ricci, Masakiyo Nobuyoshi, Michael Cleman, Richard Heuser, David Almond, Paul S. Teirstein, R. David Fish, Antonio Colombo, Jeffrey Brinker, Jeffrey Moses, Alex Shaknovich, John Hirshfeld, Stephen Bailey, Stephen Ellis, Randal Rake, Sheldon Goldberg. A Randomized Comparison of Coronary-Stent Placement and Balloon Angioplasty in the Treatment of Coronary Artery Disease
N Engl J Med 1994; 331: 496-501

32 Patrick W. Serruys, Peter de Jaegere, Ferdinand Kiemeneij, Carlos Macaya, Wolfgang Rutsch, Guy Heyndrickx, Hakan Emanuelsson, Jean Marco, Victor Legrand, Pierre Materne, Jorge Belardi, Ulrich Sigwart, Antonio Colombo, Jean Jacques Goy, Paul van den Heuvel, Juan Delcan, Marie-angele Morel. A Comparison of Balloon-Expandable-Stent Implantation with Balloon Angioplasty in Patients with Coronary Artery Disease
N Engl J Med 1994; 331: 489-495

33 Stefano Sdringola, MD, Abid Assali, MD, H. Vernon Anderson, MD, and Richard W. Smalling , MD, PhD. Current Interventional Cardiology Reports 2000; 2:285-292

34 Andrew J. Carter, DO; Douglas Scott, MD; John R. Laird, MD; Lynn Bailer; Julie A. Kovach, MD; Timothy G. Hoopes, MD; Karen Pierce; Kevin Heath; Kathy Hess; Andrew Farb, MD; Renu Virmani, MD. Progressive vascular remodelling and reduced neointimal formation after placement of a thermoelastic self-expanding nitinol stent in an experimental model. Cathererization and Cardiovascular Diagnosis 1998;44:193-201

35 Robert D. Winslow, M.D., Samin K. Sharma, M.D., Michael C. Kim, M.D. Restenosis and Drug-Eluting Stents. The Mount Sinai Journal Of Medicine 2005;Vol. 72 :81-89 2005

36 R. Hoffmann1 and G. S. Mintz. Coronary in-stent restenosis — predictors, treatment and prevention. European Heart Journal (2000) 21, 1739–1749

37 Scott NA, Robinson KA, Nunes GL, et al. Comparison of the thrombogenicity of stainless steel and tantalum coronary stents. Am Heart J 1995;129:866–872

38 P. W. Serruys, K. J. Beatt and W. J. Van Der Giessen. Stenting of coronary arteries. Are we the sorcerer's apprentice? European Heart Journal (1989) 10, 774-782

39 Peter Wenaweser, Christoph Rey, Franz R. Eberli, Mario Togni, David Tüller, Stefan Locher, Andrea Remondino, Christian Seiler, Otto M. Hess, Bernhard Meier and Stephan Windecker. Stent thrombosis following bare-metal stent implantation: success of emergency percutaneous coronary intervention and predictors of adverse outcome. European Heart Journal (2005) 26, 1180–1187

40 Herrmann R, Schmidmaier G, Markl B, Resch A, Hahnel I, Stemberger A, Alt E. Antithrombogenic coating of stents using a biodegradable drug delivery technology. Thromb Haemost. 1999;82(1):51-7

41 Sutton CS, Consigny PM, Thakur M. Thrombogenicity of intravascular stent wires. Circulation 1994;90:I-9

42 Megumi Taniuchi, MD, PhD; Howard I. Kurz, MD; John M. Lasala, MD, PhD. Randomized Comparison of Ticlopidine and Clopidogrel After Intracoronary Stent Implantation in a Broad Patient Population. *Circulation.* 2001;104:539

43 Christian Mueller, MD, Helmut Roskamm, MD, FACC, Franz-Josef Neumann, MD, FACC, Patrick Hunziker, MD, Stephan Marsch, MD, PhD, André Perruchoud, MD and Heinz J. Buettner, MD. A randomized comparison of clopidogrel and aspirin versus ticlopidine and aspirin after the placement of coronary artery stents. J Am Coll Cardiol, 2003; 41:969-973

44 Donald E. Cutlip, MD; Donald S. Baim, MD; Kalon K.L. Ho, MD, MSc; Jeffrey J. Popma, MD; Alexandra J. Lansky, MD; David J. Cohen, MD; Joseph P. Carrozza, Jr, MD; Manish S. Chauhan, MD; Orlando Rodriguez, MD; Richard E. Kuntz, MD, MSc. Stent Thrombosis in the Modern Era, A Pooled Analysis of Multicenter Coronary Stent Clinical Trials. Circulation 2001; 103:1967-1971

45 Michel E. Bertrand, MD; Hans-Jürgen Rupprecht, MD; Philip Urban, MD; Anthony H. Gershlick, MD. Double-Blind Study of the Safety of Clopidogrel With and Without a Loading Dose in

Combination With Aspirin Compared With Ticlopidine in Combination With Aspirin After Coronary Stenting. *Circulation.* 2000;102:624

46 Robert D. Winslow, M.D; Samin K. Sharma, M.D; Michael C. Kim, M.D. Restenosis and Drug-Eluting Stents. The Mount Sinai Journal of Medicine 2005;72:81-89

47 Ian Menown, MD; Rob Lowe, MD; Ian Penn, MD. Passive Stent Coatings in the Drug-Eluting Era. J Invasive Cardiol. 2005; 17 (4): 222-228

48 Schwartz R.S. Pathophysiology of restenosis : Interaction of thrombosis, hyperplasia, and/or remodelling. Annual Symposium: Transcatheter Cardiovascular Therapeutics No9, Washington, DC , ETATS-UNIS (24/09/1997) 1998, vol. 81, no 7A (12 ref.), pp. 14E-17E

49 RS Schwartz, KC Huber, JG Murphy, WD Edwards, AR Camrud, RE Vlietstra, and DR Holmes. Restenosis and the proportional neointimal response to coronary artery injury: results in a porcine model. J Am Coll Cardiol, 1992; 19:267-274

50 Campbell Rogers, MD; Elazer R. Edelman, MD, PhD. Endovascular Stent Design Dictates Experimental Restenosis and Thrombosis. *Circulation.* 1995;91:2995-3001

51 Joseph M. Garasic, Elazer R. Edelman, James C. Squire, Philip Seifert, Michael S. Williams and Campbell Rogers. Stent and Artery Geometry Determine Intimal Thickening Independent of Arterial Injury. Circulation 2000;101;812-818

52 Dougal R. McClean, MD, Neal L. Eigler, MD. Stent Design: Implications for Restenosis. Rev Cardiovasc Med. 2002;3(suppl 5): S16-S22

53 Magdi M. El-Omar, MBBS, MRCP, George Dangas, MD, PhD, FACC, Ioannis Lakovou, MD, and Roxana Mehran, MD, FACC. Update on In-stent Restenosis. Current Interventional Cardiology 2001; 3: 296-305

54 Tavernaraki, Kyriaki1; N. Brountzos, Elias. Vascular Wall Responses to Angioplasty and Stenting: Endothelial Injury, Neointimal Hyperplasia and the Process of Restenosis. Vascular Disease Prevention, Volume 3, Number 3, August 2006, pp. 211-215

55 Yunzhi Yang, Renee Cavin, Joo L Ong. Protein adsorption on titanium surfaces and their effect on osteoblast attachment. Journal of Biomedical Materials Research 67 (2003) 344-349

56 Th. Groth, E.J. Campbell , K. Herrmann and B. Seifert. Application of enzyme immunoassays for testing haemocompatibility of biomedical polymers. Biomoteriols 16 (1995) 1009-1015

57 Alexander Welle, Michael Grunze,Dsidra Tur. Plasma protein adsorption and platelet adhesion on poly[bis(trifluoroethoxy)phosphazene] and reference material surfaces. Journal of Colloid and Interface Science 197, (1998) 263-274

58 JC Palmaz, OJ Garcia, RA Schatz, CR Rees, T Roeren, GM Richter, G Noeldge, GA Gardiner Jr, GJ Becker and C Walker. Placement of balloon-expandable intraluminal stents in iliac arteries: first 171 procedures. Radiology, Vol 174, 969-975

59 Ulrich Sigwart, MD, Philip Urban, MD, Svein Golf, MD, Urs Kaufmann, MD, Christian Imbert, Adam Fischer, MD, and Lukas Kappenberger, MD. Emergency Stenting for Acute Occlusion After Coronary Balloon Angioplasty. Circulation 1988;78:1121-1127

60 Tim A. Fischell, MD. Polymer Coatings for Stents. Can We Judge a Stent by its Cover? Circulation 1996; 94: 1494-1495

61 Joerg Lahann, Doris Klee, Wilhelm Pluester, Hartwig Hoecker. Bioactive immobilization of r-hirudin on CVD coated metallic implant devices

62 Juan Luis Ortega-Vinuesa, Pentti Tengvall, Ingemar Lundström. Aggregation of HSA, IgG and Fibrinogen on methylated silicon surfaces. Journal of Colloind and Interface Science 1998;207:228-239

63 R.J. Green, M.C. Davies, C.J. Roberts, S.J.B. Tendler. Competitive protein adsorption as observed by surface plasmon resonance. Biomaterials 1999;20:385-391

64 P. Yang, N. Huang, Y.X. Leng, J.Y. Chen, H. Sun, J. Wang, G.J. Wan. Inhibition of adherent platelet activation produced by Ti-O thin film fabricated by PIII. Surface and Coatings Technology 2004;186:265-269

65 Anne Gry Hemmersam, Morten Foss, Jacques Chevallier, Flemming Besenbacher. Adsorption of fibrinogen on tantalum oxide, titanium oxide and gold studied by the QCM-D technique. Colloids and Surfaces B: Biointerfaces 2005;43:208-215

66 O. Joshi, H.J. Lee, J. McGuire, P. Finneran, K.E. Bird. Protein concentration and adsorption time effects on fibrinogen adsorption at heparinized silica interfaces. Colloids and Surfaces B: Biointerfaces 50 (2006) 26-35

67 Tomohiko Yoshioka, Kanji Tsuru, Satoshi Hayakawa, Akiyoshi Osaka. Preparation of organotitanium molecular layers for biomedical applications. Materials Science and Engineering C 24 (2004) 901 – 905

68 Andrade JD. Surface and interfacial aspects of biomedical polymers.
New York, NY: Plenum Press, 1985

69 Baurschmidt P, Schaldach M. The electrochemical aspects of the thrombogenicity of a material. J Bioeng 1977;1:261-78

70 Armin Bolz, PhD., Michael Amon, MS., Cem Ozbek, MD.,Bernd Heublein, MD., Max Schaldach, MD, PhD. Coating of Cardiovascular Stents with a Semiconductor to Improve Their Hemocompatibility. Tex Heart Inst J 1996;23:162-6

71 N. Huang, P. Yang, Y.X. Leng, J.Y. Chen, H. Sun, J. Wang, G.J. Wang, P.D. Ding, T.F. Xi, Y. Leng. Hemocompatibility of titanium oxide films. Biomaterials 24 (2003) 2177-2187

72 Stephan Windecker, MD; Isabella Mayer, MD; Gabriella De Pasquale, BA; Willibald Maier, MD; Olaf Dirsch, MD; Philip De Groot, MD; Ya-Ping Wu, PhD; Georg Noll, MD; Boris Leskosek, BA; Bernhard Meier, MD; Otto M. Hess, M. Stent Coating With Titanium-Nitride-Oxide for Reduction of Neointimal Hyperplasia. Circulation 2001;104:928-933

73 Bernd Heublein, MD; Cem Özbek, MD; Klaus Pethig, MD. Silicon Carbide Coated Stents: Clinical Experience in Coronary Lesions With Increased Thrombotic Risk. J Endovasc Surg 1998;5:32-41

74 Chen Yongli, Zhang Xiufang, Gong Yandao, Zhao Nanming, Zeng Tingying, Song Xinqi. Conformational changes of fibrinogen adsorption onto hydroxyapatite and titanium oxide nanoparticles. Journal of Colloid and Interface Science 214 (1999) 38-45

75 Kaiyong Cai, Marion Frant, Jörg Bossert, Gerhard Hildebrand, Klaus Liefeith, Klaus D. Jandt. Surface functionalized titanium thin films: Zeta –potential, protein adsorption and cell proliferation. Colloids and Surfaces B: Biointerfaces 50 (2006) 1-8

76 Juan Luis Ortega-Vinuesa, Pentti Tengvall, Ingemar Lundström. Aggregation of HSA, IgG, and Fibrinogen on Methylated Silicon Surfaces. Journal of Colloid and Interface Science 207, 228-239 (1998)

77 Marie Wahlgren, Stefan Welin-Klinström, Thomas Arnebrant, Agneta Askendal, Hans Elwing. Competition between fibrinogen and a non-ionic surfactant in adsorption to a wettability gradient surface. Colloids and Surfaces B: Biointerfaces 4 (1995) 23-31

78 Bo Lassen, Martin Malmsten. Competitive Protein Adsorption at Plasma Polymer Surfaces. Journal of Colloid and Interface Science 186 (1997) 9-16

79 Wen J. Ma, Andrew J. Ruys, Rebecca S. Mason, Phil J. Martin, Avi Bendavid, Zongwen Liu, Mihail Ionescu and Hala Zreiqat. Biomaterials 28(2007) 1620-1628

80 Kaiyong Cai, Jorg Bossert, Klaus D. Jandt. Colloids and Surfaces B : Biointerfaces 49 (2006) 136-144

81 Paolo Cacciafesta, Keith R. Hallam, Adrian C. Watkinson, Geoff C. Allen, Mervyn J. Miles, Klaus D. Jandt. Surface Science 491 (2001) 405-420

82 T. Hasebe, T. Ishimaru, A. Kamijo, Y. Yoshimoto, T. Yoshimura, S. Yohena, H. Kodama, A. Hotta, K. Takahashi, T. Suzuki. Diamond and Related Materials. Article in press

83 B. Wälivaara, B.O. Aronsson, M. Rodahl, J. Lausmaa, P. Tengvall. Titanium with different oxides: *in vitro* studies of protein adsorption and contact activation. Biomaterials 15 (1994) 827-834

84 K. Rechendorff, M.B. Hovgaard, M. Foss, V.P. Zhdanov, F. Besenbacher. Enhancement of protein adsorption induced by surface roughness. Langmuir 22 (2006) 10885-10888

85 Serruys PW, De Jaegere P, Kiemeneiji F, et al. A comparison of balloon expandable-stent implantation with balloon angioplasty in patients with coronary artery disease. N Engl J Med 1994;331:489-95

86 Richard A. Schatz, MD; Donald S. Baim, MD; Martin Leon, MD; Stephen G. Ellis, MD; Sheldon Goldberg, MD; John W. Hirshfeld, MD; Michael W. Cleman, MD; Henry S. Cabin, MD; Craig Walker, MD; Jody Stagg, MD; Maurice Buchbinder, MD; Paul S. Teirstein, MD; Eric J. Topol, MD; Michael Savage, MD; Jose A. Perez, MD; R. Charles Curry, MD; Hall Whitworth, MD; J. Eduardo Sousa, MD; Fermin Tio, MD; Yaron Almagor, MD; Regina Ponder, BS; Ian M. Penn, MD; Brad Leonard, MD; Sally L. Levine, RN, MEd; R. David Fish, MD; and Julio C. Palmaz, MD. Clinical Experience With the Palmaz-Schatz Coronary Stent
Initial Results of a Multicenter Study. Circulation 1991;83:148-161

87 Klemens H. Barth, MD; Renu Virmani, MD; Jens Froelich, MD; Toshiaki Takeda, MD; Steven V. Lossef, MD; Joseph Newsome, DVM; Rusell Jones, PT; David Lindisch, CVRT. Paired Comparison of Vascular Wall Reactions to Palmaz Stents, Strecker Tantalum Stents, and Wallstents in Canine Iliac and Femoral Arteries. Circulation 1996;93:2161-2169

88 Albert Schömig, M.D., Franz-Josef Neumann, M.D., Adnan Kastrati, M.D., Helmut Schühlen, M.D., Rudolf Blasini, M.D., Martin Hadamitzky, M.D., Hanna Walter, M.D., Eva-Maria Zitzmann-Roth, M.D., Gert Richardt, M.D., Eckhard Alt, M.D., Claus Schmitt, M.D., and Kurt Ulm, Ph.D. A Randomized Comparison of Antiplatelet and Anticoagulant Therapy after the Placement of Coronary-Artery Stents. N Engl J Med 1994:334:1084-89

89 Urban P, Macaya C, Rupprecht HJ, Kiemeneij F, Emanuelsson H, Fontanelli A, Pieper M, Wesseling T, Sagnard L. Randomized evaluation of anticoagulation versus antiplatelet therapy after coronary stent implantation in high-risk patients: the multicenter aspirin and ticlopidine trial after intracoronary stenting (MATTIS). *Circulation* 1998;98:2126–2132

90 Bertrand ME, Rupprecht HJ, Urban P, Gershlick AH, Investigators FT. Double-blind study of the safety of clopidogrel with and without a loading dose in combination with aspirin compared with ticlopidine in combination with aspirin after coronary stenting: the clopidogrel aspirin stent international cooperative study (CLASSICS). *Circulation* 2000;102:624–629

91 Olivier F. Bertrand, MD, Rajender Sipehia, PHD, Rosaire Mongrain, PHD, Joseprode's, MD, Jean-Claude Tardif, MD, Luc Bilodeau, MD, Gilles Cote, MD, FACC, Martial G. Bourassa, MD, FACC. Biocompatibility Aspects of New Stent Technology. JACC Vol. 32, No. 3 September 1998:562–71

92 Stokes K. Biodegradation. Cardiovasc Pathol 1993;2:111S–9S

93 Tim A. Fischell, MD. Polymer Coatings for Stents. Can we judge a stent by its cover? Circulation 1996;94:1494-1495

94 Mohan N. Babapulle, MD; Mark J. Eisenberg, MD, MPH. Coated Stents for the Prevention of Restenosis: Part 1

95 Tao Peng, Paul Gibula, Kang-de Yao and Mattheus F.A. Goosen. Role of Polymers in improving the results of stenting in coronary arteries. Biomaterials 1996,17, 685-694

96 Stephen Windecker, MD; Isabella Mayer, MD; Gabriella De Pasquale, BA; Willibald Maier, MD; Olaf Dirsch, MD; Philip De Groot, MD; Ya-Ping Wu, PhD; Georg Noll, MD; Boris Leskosek, BA; Bernhard Meier, MD; Otto M. Hess, MD. Stent Coating With Titanium-Nitride-Oxide for Reduction of Neointimal Hyperplasia. Circulation 2001; 104:928-933

97 Mohan N. Babapulle, MD; Mark J. Eisenberg, MD MPH. Coated Stents for the Prevention of Restenosis: Part II. Circulation 2002; 106:2859-2866

98 Willem J. Van der Giessen, MD, PhD; A. Michael Lincoff, MD; Robert S. Schwartz, MD; Heleen M.M. van Beusekom, PhD; Patrick W. Serruys, MD, PhD; David R. Holmes, Jr, MD; Stephen G. Ellis, MD; Eric J. Topol, MD. Marked Inflammatory sequelae to Implantation of Biodegradable and Nonbiodegradable Polymers in Porcine Coronary Arteries. Circulation 1996; 94: 1690-1697

99 Armin Bolz, PhD; Michael Amon, MS; Cem Ozbek, MD; Bernd Heublein, MD; Max Schaldach, MD, PhD. Coating of Cardiovascular Stents with a Semiconductor to Improve Their Hemocompatibility. Tex Heart Inst J 1996;23:162-6

100 Bernd Heublein, MD; Cem Özbek, MD; Klaus Pethig, MD. Silicon Carbide Coated Stents: Clinical Experience in Coronary Lesions With Increased Thrombotic Risk. J Endovasc Surg 1998;5:32-41

101 Cem Özbek, MD *, Armin Heisel, MD, Bernhard Groß, MD, Wolfgang Bay, MD, Hermann Schieffer, MD. Coronary implantation of silicone-carbide-coated Palmaz-Schatz stents in patients with high risk of stent thrombosis without oral anticoagulation. Catheterization and Cardiovascular Diagnosis, 1998; 14:71-78

102 Uldis Kalnins , Andrejs Erglis , Iveta Dinne , Indulis Kumsars , Sanda Jegere. Clinical outcomes of silicon carbide coated stents in patients with coronary artery disease. Med Sci Monit, 2002; 8(2): PI16-20

103 Clara Hanekamp, MD, Jacques Koolen, MD, PhD, Hans Bonnier, MD, PhD, Keith Oldroyd, MD, Menko-Jan de Boer, MD, PhD, Bernd Heublein, MD, PhD, and Cees Visser, MD, PhD. Randomized Comparison of Balloon Angioplasty Versus Silicon Carbon-Coated Stent Implantation for De Novo Lesions in Small Coronary Arteries. Am J Cardiol 2004;93:1233–1237

104 Martin Unverdorben, MD, PhD, Babett Sippel, MD, Ralf Degenhardt, PhD, Katherine Sattler, MD, Roland Fries, MD, Bernd Abt, MD, Eberhard Wagner, MD, Henning Koehler, MD, Gabriele Daemgen, MD, Manfred Scholz, MD, Hassan Ibrahim, MD, Karl-Heinz Tews, PhD, Benno Hennen,

MD, Heiner K. Berthold, MD, PhD, and Christian Vallbracht, MD. Comparison of a silicon carbide-coated stent versus a noncoated stent in human beings: The Tenax versus Nir Stent Study's long-term outcome. Am Heart J 2003;145:e17

105 Joseph G. Murphy, MD; Robert S. Schwartz, MD; William D. Edwards, MD;Allan R. Camrud, RN; Ronald E. Vlietstra,MB,ChB; and David R. Holmes Jr., MD. Percutaneous Polymeric Stents in Porcine Coronary Arteries Initial Experience With Polyethylene Terephthalate Stents. Circulation 1992;86:1596-1604

106 Rudolph Alvarado, MD , Julio C. Palmaz, MD, Oscar J. Garcia, MD, Fermin 0. Tio, MD , Chet R. Rees, MD. Evaluation of Polymer-coated Balloonexpandable Stents in Bile Ducts. Radiology 1989; 170:975-978

107 Tanigawa N, Sawada S, Kobayashi M. Reaction of the aortic wall to six metallic stent materials. Acad Radiol. 1995 May;2(5):379-84

108 Elazer R. Edelman, MD, PhD; Philip Seifert, MS; Adam Groothuis, MS; Alisa Morss, MS; Danielle Bornstein, BS; Campbell Rogers, MD. Gold-Coated NIR Stents in Porcine Coronary Arteries. *Circulation.* 2001;103:429

109 R Ohri, E Bachili, G Sur, V Monni, C Szynal, J Lenz, T Jancaric, N Simons,
T Gardener, D VanCamp, M Shen, R Radhakrishnan, A Whalen Boston Scientific Corporation, Natick, MA. Gold-coated stainless-steel stent materials elicit exaggerated cytokine levels from human monocytes—gaining biocompatibility insights with
primary monocytes, platelets, endothelial-cells and surface analysis. Cardiovascular Revascularization Medicine 7 (2006) 81–126

110 Adnan Kastrati, MD; Albert Scho¨mig, MD; Josef Dirschinger, MD; Julinda Mehilli, MD;
Nicola von Welser, MD; Ju¨rgen Pache, MD; Helmut Schu¨hlen, MD; Tassilo Schilling, MD;
Claus Schmitt, MD; Franz-Josef Neumann, MD. Increased Risk of Restenosis After Placement of Gold-Coated Stents Results of a Randomized Trial Comparing Gold-Coated With Uncoated Steel Stents in Patients With Coronary Artery Disease. Circulation. 2000;101:2478-2483

111 Glen Geremia, Mati Bakon, Luke Brennecke, Michael Haklin, and Bruce Silver. Experimental Arteriovenous Fistulas: Treatment with Silicone-Covered Metallic Stents. Am J Neuroradiol 18:271–277, 1997

112 I.K.De Scheerder, Krzysztof L. Wilczek, Eric V. Verbeken, Joke Vandorpe, Pham N. Lan, Etienne Schacht, Hilaire De Geest, Jan Piessens. Biocompatibility of polymer coated oversized metallic stents implanted in normal porcine coronary arteries. Atherosclerosis 114 (1995) 105-114

113 Hirsh J. Heparin. *N Engl J Med.* 1991;324:1565-1574

114 JR Guyton, RD Rosenberg, AW Clowes and MJ Karnovsky
Inhibition of rat arterial smooth muscle cell proliferation by heparin. In vivo
studies with anticoagulant and nonanticoagulant heparin
Circ. Res. 1980;46;625-634

115 ER Edelman and MJ Karnovsky. Contrasting effects of the intermittent and continuous administration of heparin in experimental restenosis. Circulation 1994;89;770-776

116 Peter A. Hårdhammar, MD; Heleen M.M. van Beusekom, PhD; Håkan U. Emanuelsson, MD; Sjoerd H. Hofma, MD; Per A. Albertsson, MD; Pieter D. Verdouw, PhD; Eric Boersma, MSc; Patrick W. Serruys, MD, PhD; Willem J. van der Giessen, MD, PhD. Reduction in Thrombotic Events With Heparin-Coated Palmaz-Schatz Stents in Normal Porcine Coronary Arteries. *Circulation.* 1996;93:423-430

117 Ivan De Scheerder, MD, PhD; Kai Wang, MD; Krzysztof Wilczek, MD; Dirk Meuleman, PhD; Ronald Van Amsterdam, PhD; Gerard Vogel, BS; Jan Piessens, MD, PhD; Frans Van de Werf, MD, PhD. Experimental Study of Thrombogenicity and Foreign Body Reaction Induced by Heparin-Coated Coronary Stents. *Circulation.* 1997;95:1549-1553

118 Wohrle J, Al-Khayer E, Grotzinger U. Comparison of the heparin coated vs. the uncoated Jostent: no influence on restenosis or clinical outcome. Eur Heart J. 2001;22:1808-1816

119 I. Verweire, E. Schacht, B. P. Qiang, K. Wang, I. De Scheerder. Evaluation of fuorinated polymers as coronary stent coating. J Mater Sci: Mater Med 2000;11:207-12

120 Stefan Verheye; Christos P. Markou; Mahomed Y. Salame; Barbara Wan; Spencer B. King, III; Keith A. Robinson; Nicolas A. F. Chronos; Stephen R. Hanson. Reduced Thrombus Formation by Hyaluronic Acid Coating of Endovascular Devices. *Arteriosclerosis, Thrombosis, and Vascular Biology.* 2000;20:1168

121 Chen C, Lumsden AB, Ofenloch JC, et al.Phosphorylcholine coating of ePTFE grafts reduced neointimal hyperplasia in canine model.Ann Vasc Surg 1997;11:74–9

122 Fischell, David R.; Fischell, Tim A. Antithrombogenic radioactive coating for an intravascular stent. United States Patent 5722984. 606 / 198, 600 / 3

123 A.L. Lewis, L.A. Tolhurst, P.W. Stratford. Analysis of a phosphorylcholine-based polymer coating on a coronary stent pre- and post-implantation. Biomaterials 23 (2002) 1697–1706

124 F. Z. Cui, D.J. Li. A review of investigations on biocompatibility of diamond-like carbon and carbon nitride films. Surface and Coatings Technology 131 (2000) 481-487

125 David Antoniucci, MD, Antonio Bartorelli, MD, Renato Valenti, MD, Piero Montorsi, MD, Giovanni M. Santoro, MD, Franco Fabbiocchi, MD, Leonardo Bolognese, MD, Alessandro Loaldi, MD, Maurizio Trapani, MD, Daniela Trabattoni, MD, Guia Moschi, MD, and Stefano Galli, MD. Clinical and Angiographic Outcome After Coronary Arterial Stenting With the Carbostent. Am J Cardiol 2000;85:821–825

126 Korkmaz Mehmet Emin, Tayfun Egemen, Muderrisoglu Haldun, Yildirir Aylin, Ozin Bülent, Ulucam Melek, Turan Münire. Carbon coating of stents has no effect on inflammatory response to primary stent deployment. American College of Cardiology's Annual Meeting, Atlanta , ETATS-UNIS (17/03/2002) 2002, vol. 53, no5, pp. 563-568 (25 ref.)

127 P.D. Maguire, J.A. McLaughlin, T.I.T. Okpalugo, P. Lemoine, P. Papakonstantinou, E.T. McAdams, M. Needham, A.A. Ogwu, M. Ball, G.A. Abbas. Mechanical stability, corrosion performance and bioresponse of amorphous diamond-like carbon for medical stents and guidewires. Diamond and Related Materials 14 (2005) 1277-1288

128 Martin Unverdorben, MD, PhD, Ralf Degenhardt, PhD, Peter Sick, MD, Adnan Kastrati, MD, Walter Desmet, MD, Antonio Colombo, MD, Eulegio Garcia, MD, Werner Klein, MD, Eberhard Wagner, MD, Henning Köhler, MD, Manfred Scholz, MD, Heiner K. Berthold, MD, PhD, Christian Vallbracht, MD. Evaluation of the Coroflex™ Theca-Stent for Reduction of Restenosis (ECORI). The Journal of Invasive Cardiology, 17 - Issue 4 (2005) : 199 – 202

129 I. A. Karoussos, H. Wieneke, T. Sawitowski, S. Wnendt, A. Fischer, O. Dirsch, U. Dahmen, R. Erbel. Inorganic materials as drug delivery systems in coronary artery stenting. Materialwissenschaft und Werkstofftechnik 2003;33: 738-746

130 Christian W. Hamm, MD *, Paul G. Hugenholtz, MD. Silicon carbide-coated stents in patients with acute coronary syndrome. Catheterization and Cardiovascular Interventions 2003;60:375-381

131 Martin Malmsten. Ellipsometry studies of the effects of surface hydrophobicity on protein adsorption. Colloids and Surfaces B: Biointerfaces 3 (1995) 297-308

132 J.Y. Chen. Antithrombogenic investigation of surface energy and optical bandgap and hemocompatibility mechanism of Ti(Ta+5)O2 thin films. Biomaterials 23 (2002) 2545-2552

133 Uldis Kalnins, Andrejs Erglis, Iveta Dinne, Indulis Kumsars, Sanda Jegere
Clinical outcomes of silicon carbide coated stents in patients with coronary artery disease. Med Sci Monit, 2002; 8(2): PI16-20

134 C. Bayer, P. Rudolf von Rohr, Plasma Chem. Plasma Proc. 18 . 1998 189_214

135 W.J. van Ooij, S. Eufinger, S. Guo, Plasma Chem. Plasma Proc.. 17 1997 123_154

136 J.A. Theil, J.Gl Brace, and R.W. Knoll. J. Vac. Sci. Technol. A 12(4), Jul/Aug 1994

137 Mariadriana Creatore, Fabio Palumbo, and Riccardo d'Agostino. Plasmas and Polymers, Vol. 7, No. 3, September 2002

138 K. Aumaille, C. Vallee, A. Granier, A. Gouller, F. Gaboriau, G. Turban. Thin Solid Films 359 (2000) 188-196

139 Nilson C. da Cruz, Elidiane C. Rangel, Jianjun Wang, Benedito C. Trasferetti, Celso U. Davanzo, Sandra G.C. Castro, Mario A.B. de Moraes. Surface and Coatings Technology 126 (2000) 123-130

140 Jui-Che Lin and S.L. Cooper. Biomaterials 16 (1995) 1017-1023

141 D.J. Li, F.Z. Cui, H.Q. Gu, J. Zhao. Applied Surface Science 126 (1998) 1-10

142 Tohru Hayakawa, Masao Yoshinari, Kimiya Nemoto. Biomaterials 25 (2004) 119-127

143 Brian Chapman. Glow Discharge Processes. A Wiley-Interscience publication. ISBN 0-471-07828-X

144 J Reece Roth. Industrial Plasma Engineering. Institute of Physics Publishing Ltd. ISBN 0-7503-0317-4

145 Brian Chapman. Glow Discharge Processes. A Wiley-Interscience publication. ISBN 0-471-07828-X

146 F. Chen. Plasma Diagnostic Techniques. R.H. Huddlestone, S.L. Leonard eds, Academic Press, New York 1965.

147 R. Mahlberg, H.E.-M. Niemi, F. Denes, R.M. Rowell. International Journal of Adhesion and Adhesives 18 (1998) 283-297

148 G. Socrates. Infrared and Raman Characteristic Group Frequencies. Chichester : Wiley, 2004

149 J.A. Theil, J. G. Brace, R. W. Knoll. Carbon content of silicon oxide films deposited by room temperature plasma enhanced chemical vapor deposition of hexamethyldisiloxane and oxygen. J. Vac. Sci. Technol. A 12 (4) 1994

150 C. Vautrin-Ul, C. Boisse-Laporte, N. Benissad, A. Chausse, P. Leprince, R. Messina. Plasma-polymerized coatings using HMDSO precursor for iron protection. Progress in Organic Coatings 38 (2000) 9-15

151 Mariadriana Creatore, Fabio Palumbo, Riccardo d'Agostino. Deposition of SiOx films from hexamethyldisiloxane/oxygen radiofrequency glow discharges:process optimization by plasma diagnostics. Plasmas and Polymers, vol 7, No. 3 (2002) 291-310

152 J. A. Theil, D.V. Tsu, M.W. Watkins, S.S. Kim, G. Lucovsky. Local bonding environments of Si-OH groups in SiO2 deposited by remote plasma enhanced chemical vapour deposition and incorporated by postdeposition exposure to water vapour. J. Vac. Sci. Technol. A 8 (3) 1990

153 Nur Selamoglu, John A. Mucha, Dale E. Ibbotson, Daniel L. Flamm. Silicon oxide deposition from tetraethoxysilane in a radio frequency downstream reactor: Mechanisms and step coverage. J. Vac. Sci. Technol. B 7 (6) 1989

154 N. Benissad, K. Aumaille, A. Granier, A.Goullet. Thin Solid Films 384 (2001) 230-235

155 G. Borvon, A. Goullet, X. Mellhaoui, N. Charrouf, A. Granier. Electrical properties of low-dielectric-constant films prepared by PECVD in O2/CH4/HMDSO. Materials Science in Semiconductor Processing 5 (2003) 279-284

156 C. Vallee, A. Goullet, F. Nicolazo, A. Granier, G. Turban. In situ ellipsometry and infrared analysis of PECVD SiO2 films deposited in an O2/TEOS helicon reactor. Journal of Non-Crystalline Solids 216 (1997) 48-54

157 Stephanie Roualdes, Nadine Hovnanian, Arie Van der Lee, Rene Berjoan, Jean Durand. Organic/inorganic thin films deposited from diethoxydimethylsilane by plasma enhanced chemical vapor deposition. Journal of Non-Crystalline Solids 248 (1999) 235-246

158 C. Vallee, A. Goullet, A. Granier, A. Van der Lee, J. Durand, C. Marliere. Inorganic to organic crossover in thin films deposited from O2/TEOS plasmas. Journal of Non-Crystalline Solids 272 (2000) 163-173

159 E.Bapin, Ph. Rudolf von Rohr. Deposition of SiO2 films from different organosilicon/O2 plasmas under continuous wave and pulsed modes. Surface and Coatings Technology 142-144 (2001) 649-654

160 E.Ba Rudolf von Rohr. Deposition of SiO2 films from different organosilicon/O2 plasmas under continuous wave and pulsed modes. Surface and Coatings Technology 142-144 (2001) 649-654

161 S. Spiga, G. Tallarida, A. Borghesi, A. Sassella, G. De Santi. Annealing effects on silicon-rich oxide films studied by spectroscopic ellipsometry. Thin Solid Films 325 (1998) 36-41

162 Yizhou Song, Takeshi Sakurai, Koichi Kishimoto, Kazuhiko Maruta, Shigeharu Matsumoto, Kazuo Kikuchi. Optical and structural properties of low-temperature PECVD ETMS SiOx thin films. Thin Solid Films 334 (1998) 92-97

163 Yasumi Yamada, Takahiro Harada, Haruo Uyama, Takanori Murata, Hisakazu Nozoye. Low-temperature deposition of optical films by oxygen radical beam-assisted evaporation. Thin Solid Films 377-378 (2000) 92-96

164 R. Mahlberg, H.E.-M. Niemi, F. Denes, R.M. Rowell. International Journal of Adhesion and Adhesives 18 (1998) 283-297

165 F. Benitez, E. Martinez, J. Esteve. Thin Solid Films 377-378 (2000) 109-114

166 Dirk Hegemann, Herwig Brunner, Christian Oehr. Nuclear Instruments and Methods in Physics Research B 208 (2003) 281-286

167 Thomas R. Gengenbach, Hans J. Griesser. Post-deposition ageing reactions differ markedly between plasma polymers deposited from siloxane and silazane monomers. Polymer 40 (1999) 5079-5094

168 F. Benitez, E. Martinez, J. Esteve. Thin Solid Films 377-378 (2000) 109-114

169 R. Mahlberg, H.E.-M. Niemi, F. Denes, R.M. Rowell. Effect of oxygen and hexamethyldisiloxane plasma on morphology, wettability and adhesion properties of polypropylene and lignocellulosics. International Journal of Adhesion and Adhesives 18 (1998) 283-297

170 J. Behnisch, J. Tyczkowski, M. Gazicki, I. Pela, A. Holländer, R. Ledzion. Formation of hydrophobic layers on biologically degradable polymeric foils by plasma polymerization. Surface and Coatings Technology 98 (1998) 872-874

171 D.K. Owens and R.C. Wendt. Estimation of the surface free energy of polymers, J.Appl.Polym. Sci., 13 (1969) 1741-47

172 Oliver, W.C. and Pharr, G.M., Journal of Materials Research, Vol. 7, No. 6, p. 1564, 1992

173 F. Benitez, E. Martinez, J. Esteve. Improvement of hardness in plasma polymerized hexamethyldisiloxane coatings by silica-like surface modification. Thin Solid Films 377-378 (2000) 109-114

174 Jacques I. Pankove. Optical processes in semiconductors. Englewood cliffs, London: Prentice-Hall, 1971

175 N. F. Mott and E. A. Davis. Electronic processes in non-crystalline materials. Oxford University Press, 1979

176 P.P.K. Shishodia, R.M. Mehra. Effect of oblique deposition on optical and electrical properties of As2S3 and As2Se3. Journal of Optoelectronics and Advanced Materials, 3 (2001) 319-322

177 Sadanand V. Deshpande, Erdogan Gulari, Steven W. Brown, Stephen C. Rand. Optical properties of silicon nitride films deposited by hot filament chemical vapor deposition. J. Appl. Phys. 77 (1995) 6534-41

178 K. Takahashi, M. B. Seman, K. Hirose and T. Hattori. Penetration of electronic states from silicon substrate into silicon oxide. Applied Surface Science 190, (2002) 56-59

179 Nilson C. da Cruz, Elidane C. Rangel, Jianjun Wang, Benedito C. Trasferetti, Celso U. Davanzo, Sandra G.C. Castro, Mario A.B. de Moraes. Properties of titanium oxide films obtained by PECVD. Surface and Coatings Technology 126 (2000) 123-130

180 Never Kaliwoh, Jun-Ying Zhang, Ian W. Boyd. Titanium dioxide films prepared by photo-induced sol-gel processing using 172 nm excimer lamps. Surface and Coatings Technology 125 (2000) 424-427

181 Role of terminal OH groups on the electrical and hydrophilic properties of hydro-oxygenated amorphous TiOx:OH thin films. Journal of Applied Physics, Vol 90, 7, 3391-3395

182 Synthesis of titania-silica materials by sol-gel. Rubia F.S. Lenza, Wander L. Vasconcelos. Materials Research, Vol. 5, No. 4, 497-502, 2002.

183 Morphology and crystalline phase study of electrospun TiO2-SiO2 nanofibres. Bin Ding, Hakyong Kim, Chulki Kim, Myungseob Khil and Soojin Park. Nanotechnology 14 (2003) 532 – 537
184 A. Larbot, I. Laaziz, J. Marignan, J.F. Quinson. J. Non-Crystall. Solids 147-148 (1992) 157

185 Synthesis and characterization of poly(methyl acrylate-co-itaconic anhydride)/TiO2 hybrid materials via sol-gel process. Hai Hu Qin, Jian Hua Dong, Kun Yuan Qiu, Yen Wei. Journal of Applied Polymer Science, Vol. 78, 1763-1768 (2000)

186 Wenxiu Que, Z. Sun, Y. Zhou, Y.L. Lam, Y.C.Chan, C.H. Kam. Optical and mechanical properties of TiO2/SiO2/organically modified silane composite films prepared by sol-gel processing. Thin Solid Films 359 (2000) 177- 183

187 Properties of titanium oxide films obtained b PECVD. Nilson C. da Cz, Elidiane C. Rangel, Jianjun Wang, Benedito C. Trasferetti, Celso U. Davanzo, Sandra G.C. Castro, Mario A.B. de Moraes. Surface and Coatings Technology 126 (2000) 123-130

188 G.A. Battiston, R. Gerbasi, A. Gregori, M. Porchia, S. Cattarin, G.A. Rizzi. PECVD of amorphous TiO2 thinfilms: effect of growth temperature and plasma gas composition. Thin Solid Films 371 (2000) 126 – 131

189 G. K. Boschloo, A. Goossens, and J. Schoonman. Photoelectrochemical Study of Thin Anatase TiO2 Films Prepared by Metallorganic Chemical Vapor Deposition
J. Electrochem. Soc., Volume 144, Issue 4, pp. 1311-1317 (April 1997)

190 Feng Zhang, Xianghui Wang, Changrong Li, Huimin Wang, Lizhi Chen, Xianghuai Liu. Rutile type titanium oxide films synthesised by filtered arc deposition. Surface and Coatings Technology 110 (1998) 136-139

191 G. Socrates. Infrared and Raman Characteristic Group Frequencies. Chichester : Wiley, 2004

192 Si-TiO2 interface evolution at prolonged annealing in low vacuum or N2O ambient. V.G. Erkov, S.F. Devyatova, E.L. Molodstova, T.V. Malsteva, U.A. Yanovskii. Applied Surface Scienve 166 (2000) 51-56

193 Optical and mechanical properties of TiO2/SiO2/organically modified silane composite films prepared by sol-gel processing. Wenxiu Que, Z. Sun, Y. Zhou, Y.L. Lam, Y.C.Chan, C.H. Kam. Thin Solid Films 359 (2000) 177- 183

194 Titania-silica as catalysts: molecular structural characteristics and physica-chemical properties. Xingtao Gao, Israel E. Wachs. Catalysis Today 51 (1999) 233- 254

195 Synthesis of titania-silica materials by sol-gel. Rubia F.S. Lenza, Wander L. Vasconcelos. Materials Research, Vol. 5, No. 4, 497-502, 2002

196 Synthesis of titania-silica materials by sol-gel. Rubia F.S. Lenza, Wander L. Vasconcelos. Materials Research, Vol. 5, No. 4, 497-502, 2002.

197 Hafedh Kochkar and Francois Figueras. Synthesis of hydrophobic TiO2-SiO2 mixed oxides for the epoxidation of cyclohexane. Journal of catalysis, 171, 420, 1997

198 Hafedh Kochkar and Francois Figueras. Synthesis of hydrophobic TiO2-SiO2 mixed oxides for the epoxidation of cyclohexane. Journal of catalysis, 171, 420, 1997

199 Masatoshi Nakamura, Koumei Makino, Lucel Sirghi, Toru Aoki, Yoshinori Hatanaka. Hyrophilic properties of hydro-oxygenated TiOx films prepared by plasma enhanced chemical vapour deposition. Surface and Coatings Technology, 160-170, 699, 2003.

200 G. Lassaletta, A. Fernandez, J. P. Espinos, and A. R. Gonzalez-Elipe. Spectroscopic Characterization of Quantum-Sized Ti02 Supported on Silica: Influence of Size and TiO2-SiO2 Interface Composition. J. Phys. Chem. 1995,99, 1484-1490

201 Xingtao Gao, Israel E. Wachs. Titania-Silica as catalysts: molecular structural characteristics and physica-chemical properties. Catalysis Today 51 (1999) 233-254

202 H. Kiyono, S. Shimada, K. Sugawara, A. Christensen. TEM observation of oxide scale formed on TiC single crystals with different faces. Solid State Ionics 160 (2003) 373-380

203 R. N. Viswanath, A. Chandra Bose, S. Ramasamy. Preparations and characterizations of nanostructured TiO_2 and TiO_2-Si(Ti)O_2 composite systems. Journal of Physics and Chemistry of Solids 62 (2001) 1991-1998

204 D. Hegemann, U. Vohrer, C. Oehr, R. Riedel. Surface and Coatings Technology 116-119 (1999) 1033-1036

205 L. Domingues, C. Oliveira, J.C.S. Fernanded, M.G.S. Ferreira. Electrochimica Acta 47 (2002) 2253-2258.

206 N. Bertrand, B. Drevillon, A. Gheorghiu, C. Senemaud, L. Martinu, J.E. Klemberg-Sapieha. J. Vac. Sci. Technol. A 16(1) 1998, 6-12

207 A. M. Peters, M. Nastasi. J. Vac. Sci. Technol. A 19(6) 2001, 2773-2778.

208 M. Haidopoulos, S. Turgeon, G. Laroche, D. Mantovani. Surface and Coatings Technology 197 (2005) 278-287

209 Christine Vautrin-Ul, Francaoise Roux, Caroline Boisse-Laporte, Jean Louis Pastol and Annie Chausse. J. Mater. Chem., 2002, 12, 2318-2324

210 Dan Y. Perera. Progress in Organic Coatings 28 (1996) 21-23.

211 M.M. Morshed, B.P. McNamara, D.C. Cameron, M.S.J. Hashmi. Surface and Coatings Technology 163-164 (2003) 541-545.

212 Dan Y. Perera. Progress in Organic Coatings 28 (1996) 21-23.

213 D. Hegemann, H. Brunner, C. Oehr. Surface and Coatings Technology 142-144 (2001) 849-855.

214 V. Bursikova. Proceedings of 1998 ICPP & 25th EPS Conf. Contr. Fusion & Plasma Physics, Praha, June 29-July 3, 1998.

215 U. Kreissig, R. Gago, M. Vinnichenko, P. Fernandez-Hidalgo, R.J. Martin-Palma, J.M. Martinez-Duart. Nuclear Instruments and Methods in Physics Research B 219-220 (2004) 908-913.

216 S.E. Rodil, R. Olivares, H. Arzate, S. Muhl. Diamond and Related Materials 12 (2003) 931-937.

217 Rodolfo Villa, Celina R. Ortiz, Stephanie Tapia, Gabriela Gonzalez, Elizabeth Trillo, Kristine M. Garza, Steve W. Stafford and Larry E. Murr. Materials Transactions, Vol.43, No.12 (2002) 2991-2994.

218 Dan Y. Perera. Progress in Organic Coatings 28 (1996) 21-23.

219 M.S. Wagner, T.A. Horbett, David G. Castner. Characterizing multicomponent adsorbed protein films using electron spectroscopy for chemical analysis, time-of-flight secondary ion mass spectrometry, and radiolabeling: capabilities and limitations. Biomaterials 24 (2003) 1897-1908

220 Hong Chen,Michael A. Brook,Heather Sheardown. Silicone elastomers for reduced protein adsorption. Biomaterials 25 (2004) 2273–2282

221 Alexander Welle, Michael Grunze,Dsidra Tur. Plasma protein adsorption and platelet adhesion on poly[bis(trifluoroethoxy)phosphazene] and reference material surfaces. Journal of Colloid and Interface Science 197, (1998) 263-274

222 Martin Malmsten, Bo Lassen. Competitive adsorption at hydrophobic surfaces from binary protein systems. Journal of Colloid and Interface Science 166 (1994) 490-498

223 H. Fitzpatrick, P. F. Luckham, S. Eriksen and K. Hammond. Use of x-ray photoelectron spectroscopy to study protein adsorption to mica surfaces. Journal of Colloid and Interface Science, Volume 149, Issue 1 , 1992, 1-9

224 Ace M. Baty, Peter A. Suci, Bonnie J. Tyler, Gill G. Geesey. Investigation of Mussel Adhesive Protein Adsorption on Polystyrene and Poly(octadecyl methacrylate) Using Angle Dependent XPS, ATR-FTIR, and AFM. Journal of Colloid and Interface Science 177, 307 –315 (1996)

225 R.J. Green, M.C. Davies, C.J. Roberts, S.J.B. Tendler. Competitive protein adsorption as observed by surface plasmon resonance. Biomaterials 20 (1999) 385-391

226 Kaiyong Cai, Marion Frant, Jörg Bossert, Gerhard Hildebrand, Klaus Liefeith, Klaus D. Jandt. Surface functionalized titanium thin films: Zeta –potential, protein adsorption and cell proliferation. Colloids and Surfaces B: Biointerfaces 50 (2006) 1-8

227 Th. Groth, E.J. Campbell , K. Herrmann and B. Seifert. Application of enzyme immunoassays for testing haemocompatibility of biomedical polymers. Biomaterials 16 (1995) 1009-1015

228 Mike Otto, Arno Franzen, Torsten Hansen, Charles James Kirkpatrick. Modification of human platelet adhesion on biomaterial surfaces by protein preadsorption under static and flow conditions. Journal of Materials Science: Materials in Medicine 15 (2004) 35-42

229 K. Rechendorff, M.B. Hovgaard, M. Foss, V.P. Zhdanov, F. Besenbacher. Enhancement of protein adsorption induced by surface roughness. Langmuir 22 (2006) 10885-10888

230 B. Wälivaara, B.O. Aronsson, M. Rodahl, J. Lausmaa, P. Tengvall. Titanium with different oxides: *in vitro* studies of protein adsorption and contact activation. Biomaterials 15 (1994) 827-834

231 Juan Luis Ortega-Vinuesa, Pentti Tengvall, Ingemar Lundström. Aggregation of HSA, IgG, and Fibrinogen on Methylated Silicon Surfaces. Journal of Colloid and Interface Science 207, 228-239 (1998

232 Martin Malmsten. Ellipsometry studies of the effects of surface hydrophobicity on protein adsorption. Colloids and Surfaces B: Biointerfaces 3 (1995) 297-308

233 S. Welin-Klintström, M. Lestelius, B. Liedberg, P. Tengvall. Comparison between wettability gradients made on gold and on Si/SiO2 substrates. Colloids and Surfaces B: Biointerfaces 15 (1999) 81-87

PUBLICATIONS

1. G. Ram Prasad, Stephen Daniels, D.C. Cameron, B.P. McNamara, Elizabeth Tully, R.O'Kennedy. PECVD of biocompatible coatings on 316L stainless steel. **Surface and Coatings Technology 200 (2005) 1031-1035**

2. G.Ram Prasad, E. Tully , S. M. Daniels, D. C. Cameron and R. O'Kennedy. Adhesion improvement of plasma polymerized HMDSO films on 316L steel by plasma pre-treatment and layering. **Plasma Polymers and Related Materials**, Eds. M. Mutlu, G Dinescu, R Förch, J M Martin-Martinez and J Vyskocil, Hacettepe University Press, ISBN 975-491-194-0, p. 115, 2005

3. G. Ram Prasad, Stephen Daniels, David C. Cameron. A Comparative Study of Characteristics of $SiO_xC_yH_z$, TiO_x and SiO-TiO Oxide Based Biocompatible Coatings. **Plasma Processes and Polymers** (Accepted)

4. G. Ram Prasad, Stephen Daniels, D. C. Cameron. Variation in Surface Characteristics of $SiO_xC_yH_z$ Thin Films Deposited at Floating Potential and on Powered Electrode by PECVD. **Thin Solid Films** (Submitted)

5. G. Ram Prasad, M. Mohan Kumar, Paul Barham, Niall Barron, M. Clynes, Stephen Daniels, D.C. Cameron. Influence of Surface Characteristics of PECVD Deposited Silicon and Titanium Based Coatings on Fibrinogen Adsorption. **Biomaterials** (Submitted)

6. G. Ram Prasad, M. Mohan Kumar, E. Tully, Stephen Daniels, D.C.Cameron, R.O'Kennedy. The adhesion strength and sterilization stability analysis of Silicon and titanium based coatings for biomedical applications. **Journal of Biomedical Materials Research** (Submitted)